論文 / 著書情報
Article / Book Information

題目(和文)	
Title(English)	Development of Antibody-based Fluorogenic Probe for p53 that Allows Live-cell Imaging and Sorting
著者(和文)	DAI YANCEN
Author(English)	Yancen Dai
出典(和文)	学位:博士(工学), 学位授与機関:東京工業大学, 報告番号:甲第12231号, 授与年月日:2022年9月22日, 学位の種別:課程博士, 審査員:上田 宏,久堀 徹,中村 浩之,木村 宏,田中 祐圭,北口 哲也
Citation(English)	Degree:Doctor (Engineering), Conferring organization: Tokyo Institute of Technology, Report number:甲第12231号, Conferred date:2022/9/22, Degree Type:Course doctor, Examiner:,,,,,
学位種別(和文)	博士論文
Type(English)	Doctoral Thesis

令和四年度

博士論文

Development of Antibody-based Fluorogenic Probe for p53 that Allows Live-cell Imaging and Sorting

主指導教員　上田　宏　教授

副指導教員　北口　哲也　准教授

東京工業大学生命理工学院

生命理工学系　ライフエンジニアリングコース

戴（ダイ）　艷岑（ヤンセン）

2022

Ph.D. Dissertation

Development of Antibody-based Fluorogenic Probe for p53 that Allows Live-cell Imaging and Sorting

Academic Supervisor (main): **Hiroshi Ueda**

Academic Supervisor (sub): **Tetsuya Kitaguchi**

Yancen DAI

Human Centered Science and Biomedical Engineering

Graduate School of Life Science and Technology

Tokyo Institute of Technology

Table of contents

Abbreviations

ABA	4-azidobenzoic acid
ACT	adoptive cell therapy
BLI	bio-layer interferometry
C11	C11 mutant
CBB	coomassie brilliant blue
cfu	cloning-forming unit
DIC	differential interference contrast
DIF	direct immunofluorescence
DMSO	dimethyl sulfoxide
ds-DNA	double-strand DNA
DTT	dithiothreitol
ELISA	enzyme-linked immunosorbent assay
F.I.	fluorescence intensity
F/P ratio	fluorescent dye to protein ratio
Fab	antigen-binding fragment
FACS	fluorescence-activated cell sorter
FCM	Flow cytometry
FP	fluorescent protein
IF	immunofluorescence
IgG	immunoglobin G
IPTG	isopropyl β-d-thiogalactopyranoside
LOD	limit of detection
MD	molecular dynamics
MDM2	mouse double minute 2
Nb	nanobody
PCR	polymerase chain reaction
PET	photo-induced electron transfer
pfu	plaque-forming unit

POIs	proteins of interest
Q-body	quenchbody
QY	quantum yield
RMSD	root-mean-square deviation
RMSF	root-mean-square fluctuation
RT	room temperature
RP-HPLC	reversed-phase high-performance liquid chromatography
S/B ratio	signal-to-back-ground ratio
scFv	single-chain variable fragment
SDS-PAGE	sodium dodecyl sulfate–polyacrylamide gel electrophoresis
SEM	standard error of the mean
SrtA 7+	sortase A 7+ mutant
TAMRA	carboxytetramethylrhodamine
TCEP-HCl	tris (2-carboxyethyl) phosphine -hydrochloride
UAA	unnatural amino acid
VH	antibody heavy chain variable region
VL	antibody light chain variable region
WT	the wild-type

Chapter 1. Introduction

1.1 Antibody applications in detection

Antibodies are immunoglobulin proteins produced by the immune system in response to the presence of foreign substances. It can recognize and bind corresponding antigens with high specificity and affinity. Therefore, antibodies have been regarded as valuable reagents for the detection of various molecules in fundamental biological studies as well as diseases diagnostics and therapeutics (Fidalgo et al., 2022; Poehlein et al., 2022; Xie et al., 2012). The immunoglobin G (IgG) derived from mammals (e.g., humans, mice, and rabbits) is the most commonly used antibody. IgG (≈ 150 kDa) (Scheme 1-1) is a homodimer consisting of two heavy (H) and two light (L) chains. Normally, the antibodies possess high affinity and specifically bind to their corresponding targets. Besides, antibodies are stable and resistant to misfolding and degradation. Benefiting from these characteristics, various antibody-based tools have been developed and widely used in the detection, such as enzyme-linked immunosorbent assay (ELISA) (Konstantinou, 2017; Peterson, 1981; Shah and Maghsoudlou, 2016), immunofluorescence assay (IF) (Hicks, 1984; Im et al., 2019; Tan et al., 2020), and genetically encoded antibody-based intrabody (Baidya et al., 2020; Trimmer, 2022).

The ELISA assay relies on the enzyme-linked antibodies with the high binding ability to the corresponding antigens to detect a target analyte (Lin, 2015a, b). The analyte could be small molecules such as hormones (Ongaro et al., 2021; Yang et al., 2021), macromolecules such as proteins (Aydin, 2015; Martínez-Sernández et al., 2016), and viruses (Ong et al., 2021; Spackman and Killian, 2020). It is the most commonly used method for quantitative and/or qualitative detection of an analyte in solutions. For the visualization and localization of proteins of interest (POIs) in cells or tissues, there is another antibody-based assay, called IF staining assay (Chhabra et al., 2012; Diercks et al., 2017; Francisco-Cruz et al., 2020; Odell and Cook, 2013) in which the fluorescent dye labeled antibodies specifically bind to a specific target antigen and the fluorescent microscope is used to observe the fluorescent signals appear in the location of the target antigens.

Most importantly the antibody-based probes are also able to visualization of the target molecules that locate in living cells or in vivo. Because the antigen-binding fragments with smaller molecular weight and size can be engineered as intrabody to visualize intracellular POIs, such as the antibody IgG-derived antigen-binding fragment (Fab) (≈ 50 kDa) and single-chain variable fragment (scFv) (≈ 25 kDa). Besides conventional antibody IgG, a new class of antibodies, called heavy chain antibody, which misses the light chain was originally identified in camels (Hamers-Casterman et al., 1993). The heavy chain antibody-derived fragments, VHH [the variable heavy chain of the heavy chain antibody, also termed nanobody (Nb)], were widely used in the development of intrabody due to their low molecular weight (≈ 15 kDa), high stability, and small size (≈ 2.5 nm in diameter, ≈ 4 nm in length) (Wagner and Rothbauer, 2021). An intrabody sensor could be an antibody fragment fused with a fluorescent protein (FP) or labeled with a fluorescent dye that is functional within the cell and to label an intracellular POI.

The antibody-based biosensors are powerful tools that not only can be used for

fundamental biological research but also are widely applied to food safety inspection, environment contaminants detection, illegal drug detection, and disease diagnostics and therapeutics.

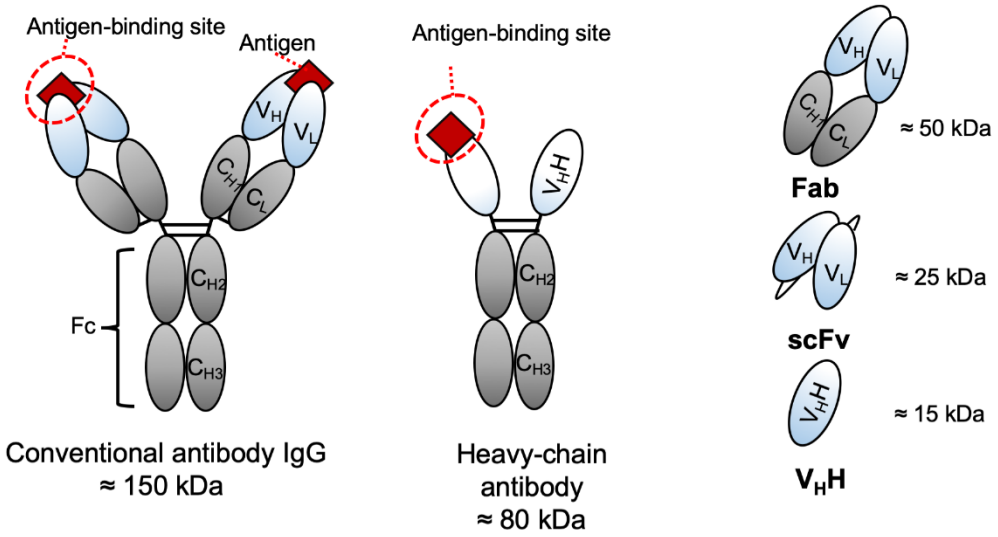

Scheme 1-1. Schematics of conventional antibody IgG, heavy chain antibody, and corresponding antigen-binding fragments.

1.2 Live-cell imaging probes for intracellular targets

Visualization of intracellular POIs in living cells is valuable for understanding the biological principles of cellular homeostasis, dysfunction, and protein dynamics. Fluorescent labeling of the endogenous POI has been regarded as a crucial approach for these purposes. Over the past decades, numerous technologies for the fluorescent labeling of endogenous POIs in living cells have been developed. As shown in Scheme 1-2, according to the publications, I classified them into the following three categories: **I**) **directly genetically encoded fluorescence labeling of POI** [the gene of the POI is directly fused with a fluorescent reporter gene (Chudakov et al., 2010; He et al., 2019; Thorn, 2017), a protein tag gene for fluorescent dye labeling (e.g., SNAP-tag, Halo-tag, and CLIP-tag) (Dean and Palmer, 2014; Liu et al., 2014), or an unnatural amino acid (UAA) for fluorescent dye labeling (e.g., TCO and BCN) (Elia, 2021; Galeta et al., 2020)]; **II**) **indirectly genetically encoded probes** [the antibody fragment (e.g., scFv and nanobody) or ligand that can bind the POI is fused with FP or fluorescent dye labeling tag (e.g., protein-tag or UAA) is expressed endogenously) (Hebbrecht et al., 2020; Ovechkina et al., 2021)]; and **III) extrinsic intrabody probes** (the probe is constructed extrinsically, then delivered into cells to target the POI) (Klein et al., 2018; Liu et al., 2020).

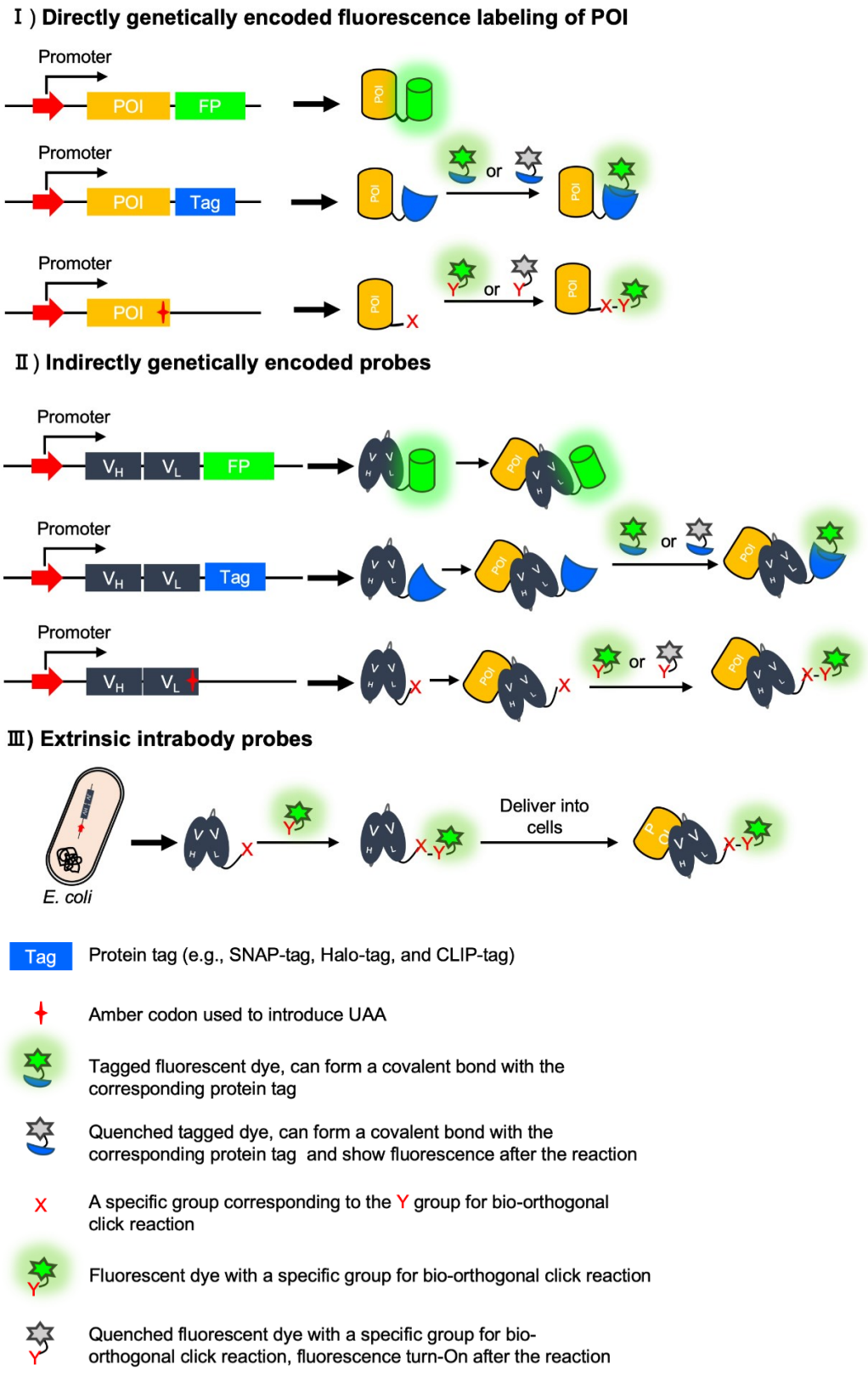

Scheme 1-2. Schematic illustration of the probes for the visualization of endogenous POIs in living cells. The principle of category **I** probes which directly genetical engineer the POI.

The POI fused with the FP, protein tag, or introduced with UAA is expressed in situ. For the category **II** probes, the mechanism of producing probes is similar to that of **I**. The difference is that the engineering is indirectly performed in the ligand (e.g., scFv or nanobody) which can bind the POI instead of directly conducted in the POI. Although DNA plasmid transfection is necessary, it no needs genome manipulations in the cells. In the category **III** probes, the *Escherichia coli* (*E. coli*) or other protein expression system is utilized to largely express recombinant proteins, followed by fluorescent dye labeling and purification, the prepared probes can be delivered into the live cells for imaging of the intracellular target.

Although the probing sensors in the former two categories (**I** and **II**) are widely used in the imaging of intracellular POIs in living cells and in vivo, almost all of them were considered to be time-consuming imaging methods because it usually takes one to two days for protein expression, and the fluorescence of these probes are always in an "On" state, which makes them difficult for dynamics imaging. To the best of my knowledge, although a new generation of fluobody (Wongso et al., 2017), called flashbody (Scheme 1-3), where a circularly permuted GFP flanked with variable region of heavy (VH) and light (VL) chains showed fluorescence enhancement upon antigen-binding allowing to visualize dynamic changes of the target protein, the technology is not widely applicable due to extreme difficulty in the development of a new flashbody. Since the first released of this technology in 2017, despite the constant efforts of the developer, there is no new flashbody reported. Besides there is a chemical molecule that is cell-permeable and turn-on fluorescence upon binding to estrogen receptor) (Yang et al., 2018) contains all the above features, but it is not widely applicable to other targets.

The fluorescent-labeled scFv or nanobody is termed fluobody (Scheme 1-3) (Barakat et al., 2022; Herce et al., 2017). The fluobody could be the antibody fragment fused with the fluorescent protein or labeled with the fluorescent dye. To avoid genetic manipulation of the cells, the extrinsic fluorescent dye-labeled fluobody has been used for live-cell imaging (Herce et al., 2017). The extrinsic fluobody can be pre-prepared and stored for later utilization as a ready-to-use reagent. As the extrinsic probes are cell-membrane impermeable, they have to be delivered into the cells for intracellular labeling. However, most of the traditional extrinsic probes are similar to the genetically encoded probes which always show fluorescent irrespective of the presence of the corresponding targets. In proof-of-concept experiments, these probes were capable of detecting highly expressed targets, albeit with relatively low signal-to-background (S/B) ratios. However, their sensitivity for the detection of less abundant clinically relevant targets is compromised because of an intracellular excess of unbound or non-specific probes. This excess can reduce the S/B ratio and confound the identification of target proteins since the probes are always "On".

Here, in this study, I employed new technology, termed Quenchbody (Q-body) (Scheme 1-3) (Abe et al., 2011), to prepare the extrinsic probes. Based on the principle of the Q-body technology, it is a fluorescence switchable immunosensor that shows antigen-dependent fluorescence enhancement. That means it will generate a low background signal even without removing unbound Q-bodies in intracellular target imaging. Because the unbound

Q-body is in an "Off" state. In Section 1.3, the details of the Q-body technology will be described.

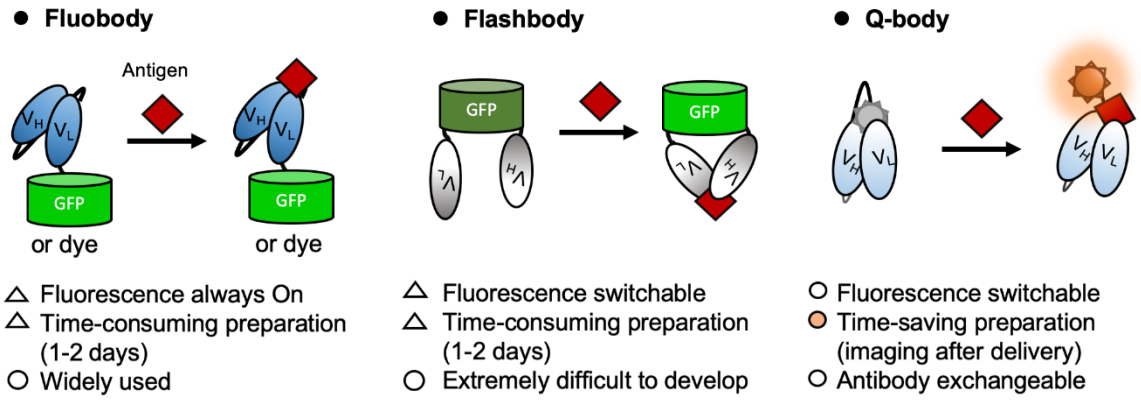

Scheme 1-3. Schematics of antibody-based probes, fluobody, flashbody, and Q-body. And their possible pros and cons in imaging of intracellular POIs in living cells in comparison with Q-body.

1.3 Quenchbody fluorescent immunosensor

The Q-body (Scheme 1-4) is a newly developed homogeneous fluorescent immunosensor using antibody fragments as an affinity agent with signal-On fluorescent readout (Abe et al., 2011). The Q-body is constructed through a site-specific fluorescent dye(s)-labeling on one of (or both) the N-termini of the antibody fragment with length-optimized peptide linkers. The labeled dye(s) are quenched by intrinsic tryptophan residues of the antibody fragment through photo-induced electron transfer (PET) and/or dye-dye interactions (H-dimer) (Abe et al., 2014; Abe et al., 2011), and light up after a conformational change triggered by antigen-binding. The antibody fragments can be synthesized and simultaneously labeled with fluorophore-conjugated amino acids using cell-free protein synthesis (Abe et al., 2011; Jeong et al., 2013), or recombinantly expressed by *E. coli* (Jeong et al., 2016) followed by dye-labeling through thiol-maleimide reaction (Jeong et al., 2016), transamination reaction (Dong et al., 2016) or coiled-coil hetero-assembly (Yasuda et al., 2021).

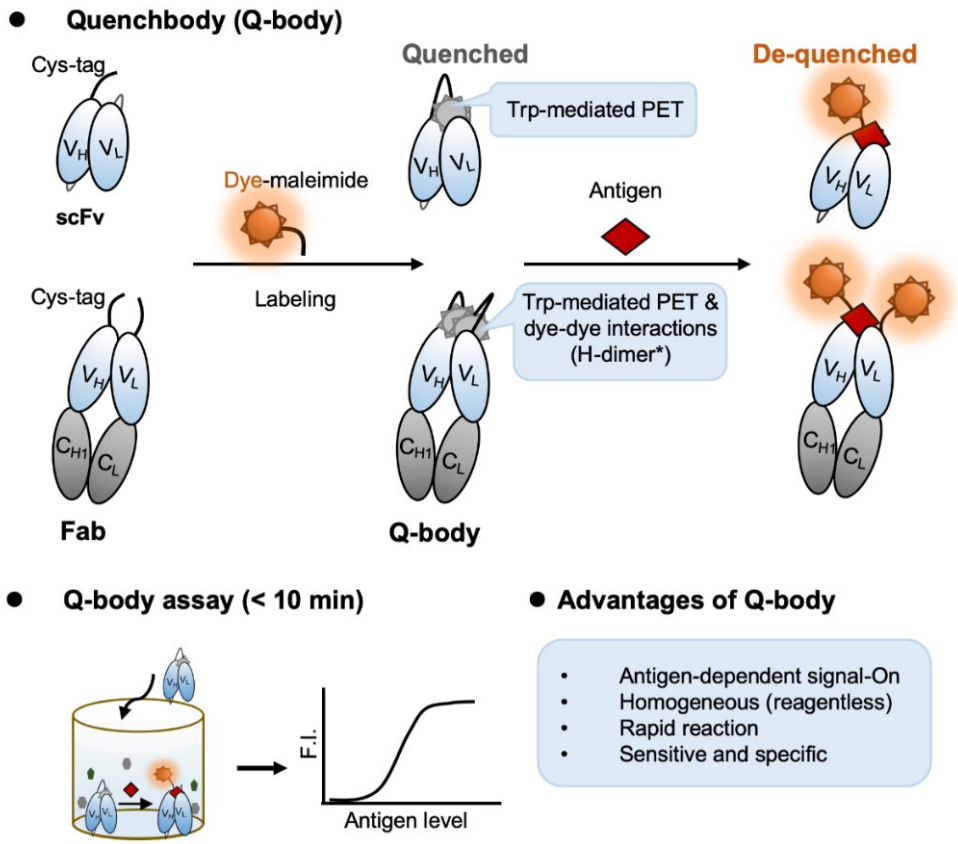

Scheme 1-4. Schematics of Q-body technology and Q-body assay. PET, photo-induced electron transfer.

Benefiting from the antibody fragment as the affinity agent, a wide range of the analytes could be detected by the Q-body probes, including small molecules and proteins. To date, more than ten Q-bodies made of Nb, scFv, or Fab against antigens ranging from small molecules [such as narcotics (Abe et al., 2014), chemotherapy drugs (Inoue et al., 2020), and pesticides (Zhao et al., 2018)] to proteins [such as bone Gla protein (Abe et al., 2011), TNF-alpha (Li et al., 2021), influenza virus hemagglutinin (Jeong et al., 2018), claudins (Jeong et al., 2017), and HER2 (Dong et al., 2020)], and protein phosphorylation (Jeong et al., 2013) have been developed. The developed Q-body immunosensors have been successfully employed for the detection of targets on the live-cell surface (Scheme 1-5). Despite the applications for in vitro target detection or cell-surface imaging, the visualization of intracellular target in living cells has not been achieved yet. Given the reversible binding between the antibody and the antigen, the signal of the Q-body may be also reversible, which will allow the Q-body to work in continuous monitoring of analytes or intercellular dynamics imaging for living cells.

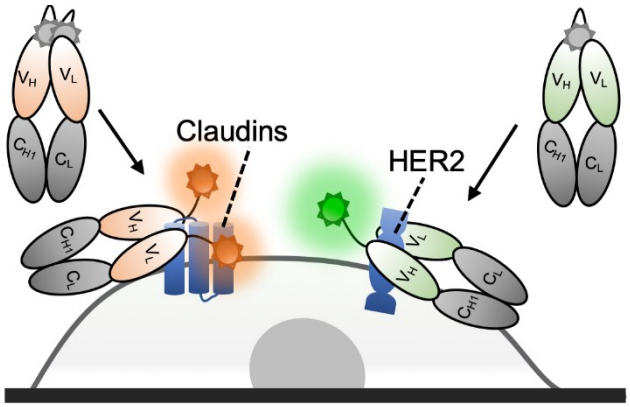

Scheme 1-5. Schematics of Q-bodies for the visualization of cell surface cancer markers, claudins and HER2.

1.4 Intracellular antigen-specific live-cell sorting

Cell therapy involves the delivery of a specific cell type, such as stem, progenitor, primary and/or genetically modified, and antigen-specific cells, into a damaged organ or tissue to facilitate their regeneration (Raffin et al., 2020; Serr et al., 2021). Isolation of a specific cell type, such as intracellular antigen-specific live cells, remains challenging due to the shortage of intracellular available biosensors. Currently, to screen a cell type with an intracellular bona fide marker, people usually take a lot of time and cost to find out several corresponding cell surface markers and then use them to identify the cell type and isolate them by fluorescence-activated cell sorting. The major issue with this strategy is that sometimes a specific cell type can be very difficult to definitively identify based on their cell surface antigen expression patterns alone. Because all of the cell surface markers may not be specific for them, and this will make the transplantation of cells identified in this way relatively risky, as some of the same antigens are expressed by potentially damaging similar cells (Giganti et al., 2021).

For instance, isolation of regulatory T cells (Tregs) for cell therapies. The therapeutic potential of an immuno-suppressive subset of Tregs has been proved in various preclinical models, including graft-versus-host diseases, type 1 diabetes, solid organ transplantation, etc. (Giganti et al., 2021; Motwani et al., 2020; Pilat and Sprent, 2020). To make the adoptive cell therapy (ACT) feasible for clinical treatment, it is critical to isolate pure Tregs. The Tregs could be identified by some cell surface markers (including $CD4^+$, $CD25^+$, and $CD127^{low/-}$) (Marek-Trzonkowska et al., 2014), however, the surface biomarkers are also expressed on some potentially damaging-activated T cells, which makes the successful selection rate low (Baeten et al., 2022). The gold standard way of identifying Treg cells is to stain for the transcription factor FOXP3. FOXP3 has been acknowledged as one of the most reliable biomarkers for Tregs (Deng et al., 2022; Fontenot et al., 2003; Hori et al., 2003). However, this requires that cells are fixed and permeabilized to allow antibody passage through into the nucleus, and besides being a labor-intensive process, it also kills the Treg cells. Thus, confirming the identity of true Treg cells by FOXP3 staining is currently incompatible with their subsequent sorting and transfer for immunotherapy. Unfortunately, labeling intracellular protein renders cells inviable because most of the probes are not able

to access live cells efficiently. Even though some new technologies such as liposome-mediated membrane trafficking and electroporation can deliver probes into live cells, the inability to wash out unbound conventional fluorophore-labeled immunoprobe generally gives a high level of background fluorescence as they don't necessarily facilitate nuclear delivery and even if they do, the inability to wash out unbound antibody by these methods means that there is a high level of background fluorescence that can easily confound resultant data interpretation.

As mentioned above, I believe the Q-body technology may overcome the current issue. Because the unbound Q-bodies are quenched. It means that this major hurdle for washing off unbound probes could be effectively overcome. The Q-body only shows fluorescence enhancement in the presence of the corresponding antigen and the fluorescence intensity of the cell reflects the expression levels of the target antigen.

1.5 Tumor suppressor protein p53

The tumor suppressor protein, p53, is a key transcription factor that acts as a crucial suppressor during improper cell proliferation via induction of DNA repair, cell cycle arrest, and apoptosis under cellular stress (Hernández Borrero and El-Deiry, 2021; Marei et al., 2021). p53 plays a pivotal role in controlling tumorigenesis, cell division, and apoptosis. In normal cells and tissues, p53 is maintained at low levels by mouse double minute 2 homolog (MDM2), an E3 ubiquitin-protein ligase that targets p53 for proteasomal degradation. Cellular stress signals result in p53 stabilization by post-translational modifications, such as phosphorylation of Ser-20 (Chehab et al., 1999) and/or inhibition of the MDM2-p53 interaction (Chene, 2003). In cancer tissues or cells, overexpression of p53 has been frequently observed. Besides, p53 is found mutated in approximately 50% of human malignancies. Therefore, mutant p53 oncoproteins are recognized as a sensor of cancer-related cellular stress because the mutant p53 assists in reprogramming cell metabolism and enhances cancer cell survival under harsh microenvironments (Mantovani et al., 2019).

The expression level of p53 and the mutation profile of the p53 gene have been used as important criteria for cancer diagnostics (Fadare et al., 2018; Köbel and Kang, 2021; Que et al., 2018). And it has been used as a target for cancer therapeutics (Hernández Borrero and El-Deiry, 2021; Marei et al., 2021). A review regarding targeting p53 for the development of anti-cancer drugs has been published (Bouchet et al., 2006). p53 is a double-edged sword. There are strategies aimed at active p53 to induce cell cycle arrest for normal cell survival and to promote cell apoptosis for killing cancer cell.

For the former strategies, restoring the wide-type property of the mutant p53 using antibodies could be employed. For example, intracellularly expressed single chain Fv fragment of an antibody, ME1, against the common epitope of mutant p53 could abrogate the mutant p53-mediated "gain of function" which restores the wide-type function of the mutant p53 (Orgad et al., 2005). For the latter strategy, as p53 can facilitate apoptosis to prevent tumorigenesis, small-molecule MDM2 antagonists, such as nutlin-3a that interact with MDM2 to inhibit the MDM2-mediated p53 degradation is developed to upregulate p53

in wide-type p53 tumor leading to facilitate arrest or apoptosis of the tumor cells (Huang et al., 2009; Villalonga-Planells et al., 2011).

1.6 Approaches for the detection of endogenous p53

Up to now, various strategies have been reported for the detection of endogenous p53, such as ELISA assay (Jagelska et al., 2002), immunohistochemistry approaches (Gaballah and Tawfik, 2010), genetically encoded immunofluorescence probes (Doubrovin et al., 2001), double-stranded -DNA (ds-DNA) modified electrode (Wang and El-Deiry, 2003), and a combination of gold nanoparticles and fluorescent dye-antibody conjugation sensor (Qian et al., 2016). The most common method is ELISA assay, which is sensitive but only available for measuring the total p53 and is not able to localize the p53 expression pattern. Even though some of these methods, such as immunohistochemistry and intrinsic immunofluorescence probes, are good at visualizing and localizing p53, the non-switchable characteristic of these probes makes them difficult to monitor the dynamic changes of intracellular p53. Besides, bioluminescent protein-fragment complementation pair has been reported to real-time imaging of p53 translocation from cytosol to mitochondria which may allow to screen novel p53 inhibitors in a high-throughput manner (Noda et al., 2017). However, this strategy needs transfect multiple expression vectors into cells which is time-consuming.

1.7 Overview of this study

Visualization and localization of POIs in cells or tissues using antibody-based probes are critically important for fundamental biological studies and/or clinical diagnostics. The traditional immunoprobes used for this purpose are normally the antibody which is unspecific labeled with fluorophores or fused with fluorescent proteins. These probes always show fluorescence irrespective of the presence of antigen (non-switchable). Therefore, multiple washing steps are necessary for removing unbound or non-specific probes to improve the S/B ratio. It is simple and efficient to increase the S/B ratio by washing off excess probes in fixed cells or tissue sections staining assay. However, it is extremely difficult to reduce that in the visualization of the intracellular POIs in living cells using the same method. Because these probes are cell-membrane impermeable, once they are delivered into the cytosol, it is hardly removed by washing which is the most common and effective approach used for this purpose.

Q-body is an antibody fragment, such as scFv and Fab, which is site-specifically labeled with the fluorescent dye(s) at their N-terminal. The fluorescent signals can be switched on by the binding of the corresponding antigen and then turned off after dissociation. This study aims to investigate the feasibility and applicability of the Q-body technology in monitoring the dynamics of intracellular targets and isolating intracellular antigen-specific live cells.

In this study, an intracellular protein p53 (a cancer marker) was used as a target and the corresponding monoclonal antibody, DO-1, was used to construct Q-bodies. In Chapter 2, to prepare enough amount of protein for the Q-body preparation, a mutant DO-1 (C11) with higher secretory productivity was selected from its consensus mutagenesis library by phage

display. And the molecule dynamics (MD) simulation of WT_ and C11_scFv was performed, it showed that the residues in C11 are less fluctuation than that in WT, indicating C11_scFv is more stable than WT_scFv. In Chapter 3, then a double-labeled C11_Fab Q-body with high sensitivity (LOD = 0.72 nM), response (maximum response = 27-fold), and specificity (respond to human p53 peptide) was successfully constructed.

In Chapter 4, to verify the specificity and sensitivity of this Q-body in the visualization of endogenous p53 protein, wash-free imaging of p53 in fixed human and mouse cell lines was performed, compared with traditional immunoprobe (C11_scFv-TAMRA, a representative of a traditional IF probe that shows no signal switching function because TAMRA was labeled at the C-terminus of the light chain far from the antigen-binding site), the C11_Fab Q-body displays an antigen-dependent signal on fixed human cancer cells which either harbors WT p53 or mutant p53 and shows a higher S/B ratio than the traditional IF probe. Besides, this Q-body showed no fluorescent enhancement in mouse cells, indicating that the C11_Fab Q-body specifically recognizes human p53.

Visualization of the intracellular POI, especially monitoring their dynamics in living cells using the currently available probes is still challenging due to the cell membrane impermeable and non-switchable of these probes. Having established that the C11_Fab Q-body displays antigen-dependent signal turn-On in fixed cell imaging (Chapter 4), its applicability to live-cell imaging was evaluated in Chapter 5. The ability of visualization of both WT and mutant p53 in living cells was evaluated followed by delivery of the C11_Fab Q-body into the cytosol using electroporation. It showed fluorescence enhancement in the p53 expression cells irrespective of mutation types of p53 in comparison to p53-negative cells, indicating that Q-body shows antigen-dependent fluorescence enhancement in the complex intracellular environment of live cells. To further evaluate whether the C11_Fab Q-body is stable for a longer period and shows p53 level-dependent fluorescence changes in living cells, time-lapse confocal microscopy was performed under the treatment of nutlin-3a (increase p53) and cisplatin (decrease p53). The fluorescent signals fluctuated p53 levels dependently. While in p53-negative cells, the signals were almost unchanged and kept at a low level. These data indicate that the Q-body is stable enough for long-term live-cell imaging and enables visualization of p53 dynamics in live cells. These pilot studies demonstrate that Q-body technology can be utilized to localize intracellular POIs in viable cells, but also allows visualization of the dynamic changes in intracellular targets in living cells.

In Chapter 6, to investigate the feasibility of applying this technology to intracellular antigen-specific live-cell sorting, a proof-of-concept experiment was performed using FACS. The ratio of p53-positive cells was enriched 14-fold from 6.9% (before sorting) to 94% (after sorting) indicating that the application of Q-body technology in intracellular antigen-specific live-cell sorting is possible.

Overall, this study provides the first evidence of the feasibility and applicability of Q-body probes for the live-cell imaging of intrinsically intracellular proteins and opens a novel avenue for research and diagnostic applications on intracellular target-based live-cell sorting

(Scheme 1-6).

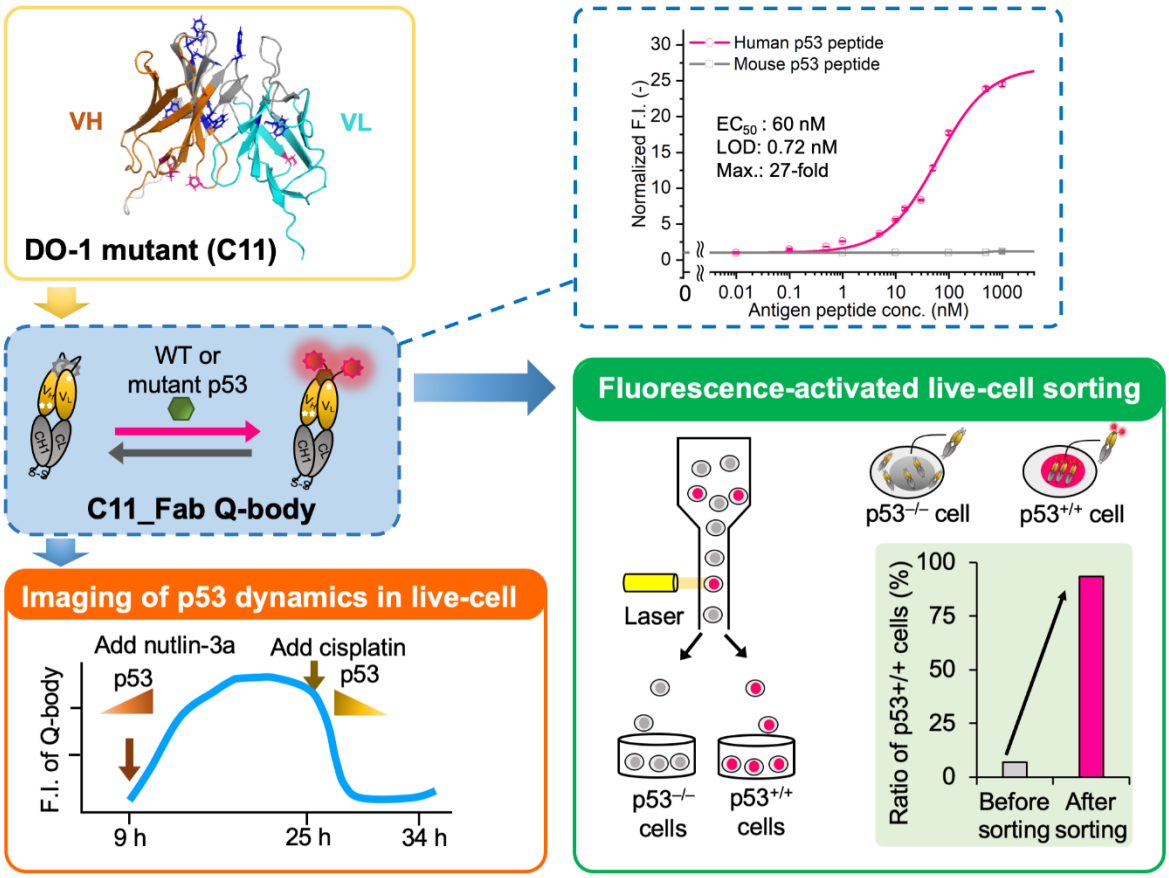

Scheme 1-6. Main achievement of this study. A fluorescent immunosensor that illuminates tumor biomarker p53 in living cells was developed based on the Q-body technology. The technology was further applied to the live cell monitoring of p53 levels, and live cell sorting based on p53 expression.

1.8 References

Abe, R., Jeong, H.J., Arakawa, D., Dong, J., Ohashi, H., Kaigome, R., Saiki, F., Yamane, K., Takagi, H., and Ueda, H. (2014). Ultra Q-bodies: quench-based antibody probes that utilize dye-dye interactions with enhanced antigen-dependent fluorescence. Sci Rep *4*, 4640.

Abe, R., Ohashi, H., Iijima, I., Ihara, M., Takagi, H., Hohsaka, T., and Ueda, H. (2011). "Quenchbodies": Quench-Based Antibody Probes That Show Antigen-Dependent Fluorescence. Journal of the American Chemical Society *133*, 17386-17394.

Aydin, S. (2015). A short history, principles, and types of ELISA, and our laboratory experience with peptide/protein analyses using ELISA. Peptides *72*, 4-15.

Baeten, P., Van Zeebroeck, L., Kleinewietfeld, M., Hellings, N., and Broux, B. (2022). Improving the Efficacy of Regulatory T Cell Therapy. Clin Rev Allergy Immunol *62*, 363-381.

Baidya, M., Kumari, P., Dwivedi-Agnihotri, H., Pandey, S., Sokrat, B., Sposini, S., Chaturvedi, M., Srivastava, A., Roy, D., Hanyaloglu, A.C.*, et al.* (2020). Genetically encoded intrabody sensors report the interaction and trafficking of beta-arrestin 1 upon activation of G-protein-coupled receptors. J Biol Chem *295*, 10153-10167.

Barakat, S., Berksöz, M., Zahedimaram, P., Piepoli, S., and Erman, B. (2022). Nanobodies as molecular imaging probes. Free Radic Biol Med *182*, 260-275.

Bouchet, B.P., de Fromentel, C.C., Puisieux, A., and Galmarini, C.M. (2006). p53 as a target for anti-cancer drug development. Critical Reviews in Oncology Hematology *58*, 190-207.

Chehab, N.H., Malikzay, A., Stavridi, E.S., and Halazonetis, T.D. (1999). Phosphorylation of Ser-20 mediates stabilization of human p53 in response to DNA damage. *96*, 13777-13782.

Chene, P. (2003). Inhibiting the p53-MDM2 interaction: an important target for cancer therapy. Nat Rev Cancer *3*, 102-109.

Chhabra, S., Minz, R.W., and Saikia, B. (2012). Immunofluorescence in dermatology. Indian J Dermatol Venereol Leprol *78*, 677-691.

Chudakov, D.M., Matz, M.V., Lukyanov, S., and Lukyanov, K.A. (2010). Fluorescent proteins and their applications in imaging living cells and tissues. Physiol Rev *90*, 1103-1163.

Dean, K.M., and Palmer, A.E. (2014). Advances in fluorescence labeling strategies for dynamic cellular imaging. Nat Chem Biol *10*, 512-523.

Deng, B., Zhang, W., Zhu, Y., Li, Y., Li, D., and Li, B. (2022). FOXP3(+) regulatory T cells and age-related diseases. FEBS J *289*, 319-335.

Diercks, G.F., Pas, H.H., and Jonkman, M.F. (2017). Immunofluorescence of Autoimmune Bullous Diseases. Surg Pathol Clin *10*, 505-512.

Dong, J., Jeong, H.J., and Ueda, H. (2016). Preparation of Quenchbodies by protein transamination reaction. J Biosci Bioeng *122*, 125-130.

Dong, J., Oka, Y., Jeong, H.J., Ohmuro-Matsuyama, Y., and Ueda, H. (2020). Detection and destruction of HER2-positive cancer cells by Ultra Quenchbody-siRNA complex. Biotechnol Bioeng *117*, 1259-1269.

Doubrovin, M., Ponomarev, V., Beresten, T., Balatoni, J., Bornmann, W., Finn, R., Humm, J., Larson, S., Sadelain, M., Blasberg, R.*, et al.* (2001). Imaging transcriptional regulation of p53-dependent genes with positron emission tomography in vivo. Proc Natl Acad Sci U S A *98*, 9300-9305.

Elia, N. (2021). Using unnatural amino acids to selectively label proteins for cellular imaging: a cell biologist viewpoint. Febs j *288*, 1107-1117.

Fadare, O., Roma, A.A., Parkash, V., Zheng, W., and Walavalkar, V. (2018). Does a p53 "Wild-type" Immunophenotype Exclude a Diagnosis of Endometrial Serous Carcinoma? Adv Anat Pathol *25*, 61-70.

Fidalgo, C., Mendes, A., Cunha, R., and Rodrigues, F. (2022). Diagnosis of Statin-Induced Necrotizing Myopathy: Contribution of Anti-HMGCR Antibodies. Acta Medica Portuguesa *35*, 584-587.

Fontenot, J.D., Gavin, M.A., and Rudensky, A.Y. (2003). Foxp3 programs the development and function of CD4+CD25+ regulatory T cells. Nat Immunol *4*, 330-336.

Francisco-Cruz, A., Parra, E.R., Tetzlaff, M.T., and Wistuba, I.I.J.B.f.I.o.C. (2020). Multiplex immunofluorescence assays. 467-495.

Gaballah, E.T., and Tawfik, M.A. (2010). Immunohistochemical analysis of P53 protein in odontogenic cysts. Saudi Dent J *22*, 167-170.

Galeta, J., Dzijak, R., Obořil, J., Dračínský, M., and Vrabel, M. (2020). A Systematic Study of Coumarin-Tetrazine Light-Up Probes for Bioorthogonal Fluorescence Imaging. Chemistry *26*, 9945-9953.

Giganti, G., Atif, M., Mohseni, Y., Mastronicola, D., Grageda, N., Povoleri, G.A., Miyara, M., and Scottà, C. (2021). Treg cell therapy: How cell heterogeneity can make the difference. Eur J Immunol *51*, 39-55.

Hamers-Casterman, C., Atarhouch, T., Muyldermans, S., Robinson, G., Hamers, C., Songa, E.B., Bendahman, N., and Hamers, R. (1993). Naturally occurring antibodies devoid of light chains. Nature *363*, 446-448.

He, L., Binari, R., Huang, J., Falo-Sanjuan, J., and Perrimon, N. (2019). In vivo study of gene expression with an enhanced dual-color fluorescent transcriptional timer. Elife *8*.

Hebbrecht, T., Liu, J., Zwaenepoel, O., Boddin, G., Van Leene, C., Decoene, K., Madder, A., Braeckmans, K., and Gettemans, J. (2020). Nanobody click chemistry for convenient site-specific fluorescent labelling, single step immunocytochemistry and delivery into living cells by photoporation and live cell imaging. New Biotechnology *59*, 33-43.

Herce, H.D., Schumacher, D., Schneider, A.F.L., Ludwig, A.K., Mann, F.A., Fillies, M., Kasper, M.A., Reinke, S., Krause, E., Leonhardt, H.*, et al.* (2017). Cell-permeable nanobodies for targeted immunolabelling and antigen manipulation in living cells. Nat Chem *9*, 762-771.

Hernández Borrero, L.J., and El-Deiry, W.S. (2021). Tumor suppressor p53: Biology, signaling pathways, and therapeutic targeting. Biochim Biophys Acta Rev Cancer *1876*, 188556.

Hicks, J.M. (1984). Fluorescence immunoassay. Hum Pathol *15*, 112-116.

Hori, S., Nomura, T., and Sakaguchi, S. (2003). Control of regulatory T cell development by the transcription factor Foxp3. Science *299*, 1057-1061.

Huang, B., Deo, D., Xia, M., and Vassilev, L.T. (2009). Pharmacologic p53 activation blocks cell cycle progression but fails to induce senescence in epithelial cancer cells. Mol Cancer Res *7*, 1497-1509.

Im, K., Mareninov, S., Diaz, M.F.P., and Yong, W.H. (2019). An Introduction to Performing Immunofluorescence Staining. Methods Mol Biol *1897*, 299-311.

Inoue, A., Ohmuro-Matsuyama, Y., Kitaguchi, T., and Ueda, H. (2020). Creation of a Nanobody-Based Fluorescent Immunosensor Mini Q-body for Rapid Signal-On Detection of Small Hapten Methotrexate. ACS Sens *5*, 3457-3464.

Jagelska, E., Brazda, V., Pospisilova, S., Vojtesek, B., and Palecek, E. (2002). New ELISA technique for analysis of p53 protein/DNA binding properties. Journal of Immunological Methods *267*, 227-235.

Jeong, H.-J., Kojima, T., Dong, J., Ohashi, H., and Ueda, H. (2016). One-pot construction of Quenchbodies using antibody-binding proteins. Analytical Methods *8*, 7774-7779.

Jeong, H.J., Dong, J., and Ueda, H. (2018). Single-Step Detection of the Influenza Virus Hemagglutinin Using Bacterially-Produced Quenchbodies. Sensors (Basel) *19*.

Jeong, H.J., Kawamura, T., Iida, M., Kawahigashi, Y., Takigawa, M., Ohmuro-Matsuyama, Y., Chung, C.I., Dong, J., Kondoh, M., and Ueda, H. (2017). Development of a Quenchbody for the Detection and Imaging of the Cancer-Related Tight-Junction-Associated Membrane Protein Claudin. Anal Chem *89*, 10783-10789.

Jeong, H.J., Ohmuro-Matsuyama, Y., Ohashi, H., Ohsawa, F., Tatsu, Y., Inagaki, M., and Ueda, H. (2013). Detection of vimentin serine phosphorylation by multicolor Quenchbodies. Biosens Bioelectron *40*, 17-23.

Klein, A., Hank, S., Raulf, A., Joest, E.F., Tissen, F., Heilemann, M., Wieneke, R., and Tampé, R. (2018). Live-cell labeling of endogenous proteins with nanometer precision by transduced nanobodies. Chem Sci *9*, 7835-7842.

Köbel, M., and Kang, E.Y. (2021). The Many Uses of p53 Immunohistochemistry in Gynecological Pathology: Proceedings of the ISGyP Companion Society Session at the 2020 USCAP Annual9 Meeting. Int J Gynecol Pathol *40*, 32-40.

Konstantinou, G.N. (2017). Enzyme-Linked Immunosorbent Assay (ELISA). Methods Mol Biol *1592*, 79-94.

Li, H., Li, X., Chen, L., Li, B., Dong, H., Liu, H., Yang, X., Ueda, H., and Dong, J. (2021). Quench-Release-Based Fluorescent Immunosensor for the Rapid Detection of Tumor Necrosis Factor alpha. ACS Omega *6*, 31009-31016.

Lin, A.V. (2015a). Direct ELISA. Methods Mol Biol *1318*, 61-67.

Lin, A.V. (2015b). Indirect ELISA. Methods Mol Biol *1318*, 51-59.

Liu, J., Fraire, J.C., De Smedt, S.C., Xiong, R., and Braeckmans, K. (2020). Intracellular Labeling with Extrinsic Probes: Delivery Strategies and Applications. Small *16*, e2000146.

Liu, T.K., Hsieh, P.Y., Zhuang, Y.D., Hsia, C.Y., Huang, C.L., Lai, H.P., Lin, H.S., Chen, I.C., Hsu, H.Y., and Tan, K.T. (2014). A rapid SNAP-tag fluorogenic probe based on an environment-sensitive fluorophore for no-wash live cell imaging. ACS Chem Biol *9*, 2359-2365.

Mantovani, F., Collavin, L., and Del Sal, G. (2019). Mutant p53 as a guardian of the cancer cell. Cell Death and Differentiation *26*, 199-212.

Marei, H.E., Althani, A., Afifi, N., Hasan, A., Caceci, T., Pozzoli, G., Morrione, A., Giordano, A., and Cenciarelli, C. (2021). p53 signaling in cancer progression and therapy. Cancer Cell Int *21*, 703.

Marek-Trzonkowska, N., Mysliwiec, M., Dobyszuk, A., Grabowska, M., Derkowska, I., Juscinska, J., Owczuk, R., Szadkowska, A., Witkowski, P., Mlynarski, W.*, et al.* (2014). Therapy of type 1 diabetes with CD4(+)CD25(high)CD127-regulatory T cells prolongs survival of pancreatic islets - results of one year follow-up. Clin Immunol *153*, 23-30.

Martínez-Sernández, V., Orbegozo-Medina, R.A., Romarís, F., Paniagua, E., and Ubeira, F.M. (2016). Usefulness of ELISA Methods for Assessing LPS Interactions with Proteins and Peptides. PLoS One *11*, e0156530.

Motwani, K., Peters, L.D., Vliegen, W.H., El-Sayed, A.G., Seay, H.R., Lopez, M.C., Baker, H.V., Posgai, A.L., Brusko, M.A., Perry, D.J.*, et al.* (2020). Human Regulatory T Cells From Umbilical Cord Blood Display Increased Repertoire Diversity and Lineage Stability Relative to Adult Peripheral Blood. Front Immunol *11*, 611.

Noda, N., Awais, R., Sutton, R., Awais, M., and Ozawa, T. (2017). Dynamic monitoring of p53 translocation to mitochondria for the analysis of specific inhibitors using luciferase-fragment complementation. Biotechnol Bioeng *114*, 2818-2827.

Odell, I.D., and Cook, D. (2013). Immunofluorescence techniques. J Invest Dermatol *133*, e4.

Ong, D.S.Y., Fragkou, P.C., Schweitzer, V.A., Chemaly, R.F., Moschopoulos, C.D., and Skevaki, C. (2021). How to interpret and use COVID-19 serology and immunology tests. Clin Microbiol Infect *27*, 981-986.

Ongaro, L., Alonso, C.A.I., Zhou, X., Brûlé, E., Li, Y., Schang, G., Parlow, A.F., Steyn, F., and Bernard, D.J. (2021). Development of a Highly Sensitive ELISA for Measurement of FSH in Serum, Plasma, and Whole Blood in Mice. Endocrinology *162*.

Orgad, S., Goldfinger, N., Cohen, G., Rotter, V., and Solomon, B. (2005). Single chain antibody against the common epitope of mutant p53 restores wild-type activity to mutant p53 protein. FEBS Lett *579*, 5609-5615.

Ovechkina, V.S., Zakian, S.M., Medvedev, S.P., and Valetdinova, K.R. (2021). Genetically Encoded Fluorescent Biosensors for Biomedical Applications. Biomedicines *9*.

Peterson, E.M. (1981). ELISA: a tool for the clinical microbiologist. Am J Med Technol *47*, 905-908.

Pilat, N., and Sprent, J. (2020). Treg Therapies Revisited: Tolerance Beyond Deletion. Front Immunol *11*, 622810.

Poehlein, E., Rane, M.S., Frogel, D., Kulkarni, S., Gainus, C., Profeta, A., Robertson, M., and Nash, D. (2022). Presence of SARS-CoV-2 antibodies following COVID-19 diagnosis: a longitudinal study of

patients at a major urgent care provider in New York. Diagnostic Microbiology and Infectious Disease *103*.

Qian, R., Cao, Y., and Long, Y.T. (2016). Dual-Targeting Nanovesicles for In Situ Intracellular Imaging of and Discrimination between Wild-type and Mutant p53. Angew Chem Int Ed Engl *55*, 719-723.

Que, S.K.T., Zwald, F.O., and Schmults, C.D. (2018). Cutaneous squamous cell carcinoma: Incidence, risk factors, diagnosis, and staging. J Am Acad Dermatol *78*, 237-247.

Raffin, C., Vo, L.T., and Bluestone, J.A. (2020). T(reg) cell-based therapies: challenges and perspectives. Nat Rev Immunol *20*, 158-172.

Serr, I., Drost, F., Schubert, B., and Daniel, C. (2021). Antigen-Specific Treg Therapy in Type 1 Diabetes - Challenges and Opportunities. Front Immunol *12*, 712870.

Shah, K., and Maghsoudlou, P. (2016). Enzyme-linked immunosorbent assay (ELISA): the basics. Br J Hosp Med (Lond) *77*, C98-101.

Spackman, E., and Killian, M.L. (2020). Detection of Influenza A Antibodies in Avian Samples by ELISA. Methods Mol Biol *2123*, 177-193.

Tan, W.C.C., Nerurkar, S.N., Cai, H.Y., Ng, H.H.M., Wu, D., Wee, Y.T.F., Lim, J.C.T., Yeong, J., and Lim, T.K.H. (2020). Overview of multiplex immunohistochemistry/immunofluorescence techniques in the era of cancer immunotherapy. Cancer Commun (Lond) *40*, 135-153.

Thorn, K. (2017). Genetically encoded fluorescent tags. Mol Biol Cell *28*, 848-857.

Trimmer, J.S. (2022). Genetically encoded intrabodies as high-precision tools to visualize and manipulate neuronal function. Semin Cell Dev Biol *126*, 117-124.

Villalonga-Planells, R., Coll-Mulet, L., Martínez-Soler, F., Castaño, E., Acebes, J.J., Giménez-Bonafé, P., Gil, J., and Tortosa, A. (2011). Activation of p53 by nutlin-3a induces apoptosis and cellular senescence in human glioblastoma multiforme. PLoS One *6*, e18588.

Wagner, T.R., and Rothbauer, U. (2021). Nanobodies - Little helpers unravelling intracellular signaling. Free Radic Biol Med *176*, 46-61.

Wang, W., and El-Deiry, W.S. (2003). Bioluminescent molecular imaging of endogenous and exogenous p53-mediated transcription in vitro and in vivo using an HCT116 human colon carcinoma xenograft model. Cancer Biol Ther *2*, 196-202.

Wongso, D., Dong, J., Ueda, H., and Kitaguchi, T. (2017). Flashbody: A Next Generation Fluobody with Fluorescence Intensity Enhanced by Antigen Binding. Anal Chem *89*, 6719-6725.

Xie, X.M., Richard, G., and Hall, J.C. (2012). Antibody Fragment Engineering and Applications in Diagnosis and Therapeutics. Antibodies Applications and New Developments, 225-279.

Yang, L., Meng, Q., Hu, Z., Ning, W., Zheng, J., Dong, C., and Zhou, H.-B. (2018). Estrogen receptor sensing in living cells by a high affinity turn-on fluorescent probe. Sensors and Actuators B: Chemical *272*, 589-597.

Yang, Y.Y., Wang, Y., Zhang, Y.F., Wang, F., Liang, Y.F., Yang, J.Y., Xu, Z.L., Shen, Y.D., and Wang, H. (2021). Nanobody-Based Indirect Competitive ELISA for Sensitive Detection of 19-Nortestosterone in Animal Urine. Biomolecules *11*.

Yasuda, T., Inoue, A., Kitaguchi, T., and Ueda, H. (2021). Rapid construction of fluorescence quenching-based immunosensor Q-bodies using alpha-helical coiled-coil peptides. Chem Commun (Camb) *57*, 8206-8209.

Zhao, S., Dong, J., Jeong, H.J., Okumura, K., and Ueda, H. (2018). Rapid detection of the neonicotinoid insecticide imidacloprid using a quenchbody assay. Anal Bioanal Chem *410*, 4219-4226.

Chapter 2. Improvement of anti-p53 scFv (DO-1) secretory expression

2.1 Introduction

E. coli is widely recognized as an easy, quick, cost-effective, and robust system for the expression of recombinant proteins (Francis and Page, 2010). However, it also has drawbacks. For instance, the highly reductive environment of the bacterial cytosol gives rise to the insoluble expression or misfolding of the POI that results in the reduction of the productivity or activity of this POI, especially for recombinant antibodies whose activity needs the formation of disulfide bonds. Although multiple novel *E. coli* strains, such as SHuffle® T7 Express *lysY* and BL21(DE3) allowed for the expression of disulfide bonds containing proteins in the cytoplasm and periplasm, respectively, have been developed, there are still challenging for a few antibodies to efficiently produce in *E. coli* system. They show different activities in the periplasm and cytoplasm expression system.

Finding consensus amino acids by the alignment of homogeneous sequences is a powerful approach to postulate stabilizing proteins. And the replacement of the non-conserved residues with conserved residues makes the protein more stabilizing (Michel et al., 2022). Phage display (Ledsgaard et al., 2022) is a robust tool for screening proteins with specific characteristics, such as improved thermal stability (Jung et al., 1999), or binding ability (Tsukahara et al., 2022). The combination of phage display technology and consensus mutagenesis usually allows people to screen target proteins with estimated abilities (Amin et al., 2004). The phagemid contains a pelB signal peptide right after the start codon that is employed for the secretory of the functional POI into the periplasm where is the more oxidizing environment. And the folded POI (e.g., scFv fragment) may further translocate into the culture medium (Sandomenico et al., 2020). The abundance of the POI in the culture medium indirectly reflects the secretory ability and stability of the corresponding protein which can be evaluated using ELISA assay.

The scFv DO-1 produced in the periplasm in BL21(DE3) showed higher antigen-binding activity than that produced in the cytoplasm in SHuffle® T7 Express *lysY* (data not shown). Although the periplasm is superior in producing high active scFv DO-1, its yield was too low to be used for further studies (According to the experience of antibody probe delivery assay, at least 1 μM concentration of the stock solution is necessary). Here in this chapter, a consensus mutagenesis library of DO-1 scFv was constructed and phage display bio-panning was performed to screen variants with higher secretory productivity. The seven variants with significantly improved secretory productivity were obtained.

2.2 Materials and methods

2.2.1 Materials

The pIT2-vector containing DO-1 scFv gene derived from mouse hybridoma monoclonal antibody was kindly provided by Dr. Farid J. Ghadessy in A*STAR, Singapore. Oligonucleotide primers (Table. 2-1) were synthesized by Eurofins Genomics (Tokyo, Japan). KOD-Plus-Neo PCR kit was obtained from Toyobo (Osaka, Japan). A thermal cycler called Biometra TRIO (Analytik Jena GmbH, Göttingen, Germany) was used to perform PCR. The *E. coli* strain XL10-Gold (Stratagene, La Jolla, CA) was used for DNA cloning,

TG-1 (GE healthcare) for phage display and secreted antibody ELISA. Biotinylated p53 peptide (biotin-EPPLSQETFSDLWKLLPENN-COOH) was synthesized by ABGENT. BL21(DE3) was purchased from New England Biolabs.

Other chemicals were obtained from Wako Pure Chemicals except as otherwise stated.

2.2.2 Oligonucleotides

The primers shown in Table 2-1 were used for the construction of the combinatorial consensus mutagenesis phagemid library.

Table 2-1. Primers used for the construction of combinatorial consensus mutagenesis library.

Block No.	Primer name	Sequence (5′– 3′)
Block 0	B0_0_for	CCCAGGGCCAGACTCTTTCAGAGTA
	B0_0_back	ATTGTTATTACTCGCGGCCCAGCCGGC
Block 1	B1_A_for	AGTGAAAACCCAGAGGCAGAACAAG TCAGACTGAG
	B1_0_for	AGTGAAAACCCAGAGAAAGAACAAG TCAGACTGAG
	B1_L_back	AGAGTCTGGCCCTGGGWTATTGCAGC CCTCCCAGA
Block 2	B2_P_for	TCCAGACCCTTCCCTGRAGACTGACG AATCCAGCC
	B2_0_back	TCTGGGTTTTCACTGAGCACTTCTAAT ATGGG
Block 3	B3_0_for	GATCTTGAGGAATACCTGGTTGTTGGA GGT
	B3_0_back	CAGGGAAGGGTCTGGAGTGGCTGGCA CACATTT
Block 4	B4_A_for	GCCCAAGCCATTCGAGCACAGAAATAT GTGGCACT
	B4_0_for	GCCCAAGCCATTCGAAAACAGAAATAT GTGGCACT
	B4_S_back	GGTATTCCTCAAGATCKCCAGTGTGGA CACTGCAG
Block 5	B5_S_for	GGCAGGGAGAGTGGAGATTGGGTCAT CAAAACATC
	B5_0_for	GGCAGGGAGAGTGGAATTTGGGTCAT CAAAACATC
	B5_T_back	TCGAATGGCTTGGGCCTACGGCGACTA CTGGGGCCAAGGCACCMCTCTCACAG TCTCTTCAG
Block 6	B6_0_back	TCCACTCTCCCTGCCTGTCAGTCTTGG

		AGATCAA
	B6_0_for	TGATGATGATGTGCGGCCG
Sequencing primer	M13 Rev	CAGGAAACAGCTATGAC

2.2.3 Consensus mutagenesis library design and construction

To construct a combinatorial consensus mutagenesis library, the gene sequence of a WT_scFv DO-1 was used as a query at AbYsis (http://www.abysis.org/abysis/) database to annotate the distribution frequency of each amino acid with its natural homologs. If the amino acid frequency in the framework region is less than or equal to 1%, it will be chosen as a mutation site.

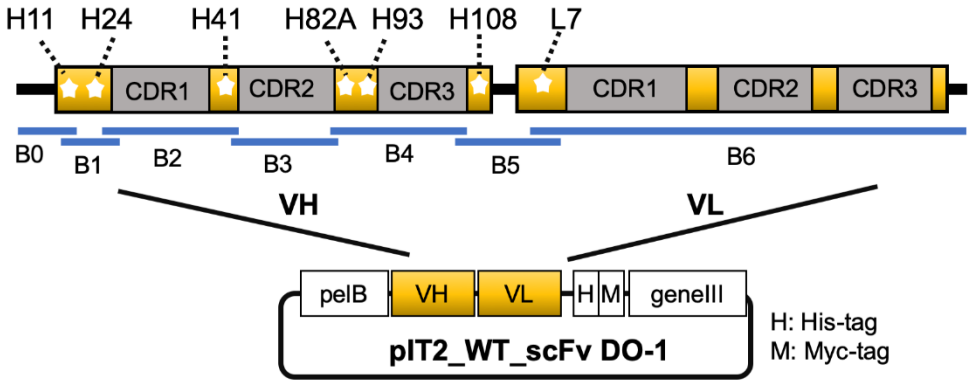

Scheme 2-1. The structure of pIT2_WT_scFv DO-1 and the location of selected mutation sites. B0 to B6 fragments indicate the blocks 0 to 6 in the PCR reaction in Table 2-1. The white star indicates the mutation sites.

The library was constructed based on the plasmid pIT2 vector, which contains a WT_scFv DO-1 encoding DNA sequence flanked by a pelB and His- and Myc-tag sequences at its N-terminus and C-terminus, respectively (Scheme 2-1). An amber (TAG) stop codon was located between the Myc-tag and phage M13 gene III. The pIT2-WT_scFv DO1 was used as a template to amplify each gene block using primers shown in Table 2-1 by PCR. In each reaction, 100 ng of pIT2-WT_scFv DO-1, 10 pmol each of primer, and 1U of KOD-Plus-Neo DNA polymerase were added in a 50 µL reaction mixture. Their PCR cycling conditions are shown in Table 2-2. All PCR reaction mixture conditions in this study were performed under the same conditions. After PCR amplification, electrophoresis was performed to analyze each PCR product. Each target band was excised for the gel purification by Wizard® SV Gel and PCR Clean-Up System (Promega, USA). The concentration of each purified fragment was measured by Nanodrop. Then overlap extension PCR was carried out to assemble Blocks 0 to 6 into intact gene fragments with multiple combinations. In overlap extension PCR, the equal molar of Blocks 0 to 6 fragments was added in a 50 µL PCR reaction mixture which contains all PCR necessary components except primers. After 15 cycles, 10 pmol of each primer, B0_0_back, and B6_0_for, were added into the PCR reaction mixture and run a further 20 cycles to amplify the entire scFv DNA fragments which contain multiple combinations of mutations. The PCR product was purified

by gel purification for ligation.

To prepare the linearized pIT2-vector, the pIT2-WT_scFv DO-1 was digested with restriction enzymes NcoI-HF and NotI-HF (New England Biolabs) at 37 ℃ overnight followed by gel purification. The purified intact Block 0–6 fragments were inserted into the linearized pIT2-vector by In-Fusion® HD Cloning Kit (Takara-Bio, Shiga, Japan) to construct pIT2-scFv DO-1 combinatorial consensus mutagenesis phagemid library. The In-fusion product was transformed into XL10-Gold chemical competent cells followed by spreading on the LBA plate. To ensure the diversity of this library, over 3600 colonies [(26-fold larger than the library size (128)] were scratched from the LBA plate and cultured for miniprep of phagemid library. Then the library was sent for sequencing to confirm the mutation introduction using M13 Rev (Table 2-1) as a sequencing primer. At the same time, four monoclonals were also sent for sequencing.

Table 2-2. Conditions for PCR amplification of each DNA block.

Block No.	Fragment length (bp)	Primer name	PCR reaction mixture and cycling conditions
Block 0	64	B0_0_for	PCR reaction mixture
		B0_0_back	10× Buffer for KOD-Plus-Neo: 5 μL
Block 1	72	B1_A_for	2 mM dNTPs 5 μL
		B1_0_for	25 mM MgSO4 3 μL
		B1_L_back	10 pmol/μl Primer for 1 μL
Block 2	71	B2_P_for	10 pmol/μl Primer back 1 μL
		B2_0_back	Template DNA (100 ng) 1 μL
Block 3	125	B3_0_for	PCR grade water 33 μL
		B3_0_back	KOD -Plus- Neo (1.0 U/μL) 1 μL
Block 4	72	B4_A_for_hu	Total reaction volume 50 μL
		B4_0_for_hu	PCR cycling condition
		B4_S_back	Pre-denaturation: 94 ℃, 2 min
Block 5	141	B5_S_for	Denaturation: 98 ℃, 10 Sec.
		B5_0_for	Annealing: X ℃, 30 Sec. } 30 cycles
		B5_T_back	Extension: 68 ℃, 15 Sec. }
Block 6	342	B6_0_back	4 ℃: ∝
		B6_0_for	For Block 1, X=57. For Block 0, and 2–6, X=60

2.2.4 Phage display bio-panning

2.2.4.1 Amplification of *E. coli* TG1 containing phagemid library

The overview of the phage display shows in Scheme 2-2. The above-prepared phagemid library was transformed into *E. coli* TG1 chemical competent cells and grown on a 2× TY plate (containing 1.5 g Bacto-Agar, 0.8 g NaCl, 1 g Tryptone, 0.5 g Yeast Extract in 100 mL distilled water). To improve the amount and diversity of the phagemid library, two repeat

transformations were performed and the transformants on the 2× TY plate were collected. The collected transformants were then grown in 18 mL 2× TYAG medium (1.6 g Tryptone, 1 g Yeast Extract, and 0.5 g NaCl in 100 mL distilled water 100 μg/mL ampicillin and 1% glucose) at 37 ℃ with 200 rpm shaking. After the OD_{600} of the culture reached 0.4, 10 mL cultures were transferred into a 200 mL flask containing 50 mL fresh 2× TYAG (containing 1% glucose) and cultured for a further 4 h shaking at 37 ℃. Then the cells were spun down at 10,800 *g* for 10 min and were resuspended in 3 mL of 2× TY containing 15% glycerol. The suspension cells were aliquoted to 6 tubes (each 500 μL) and stored at -80 ℃. The remaining 8 mL cells were used for phage display bio-panning.

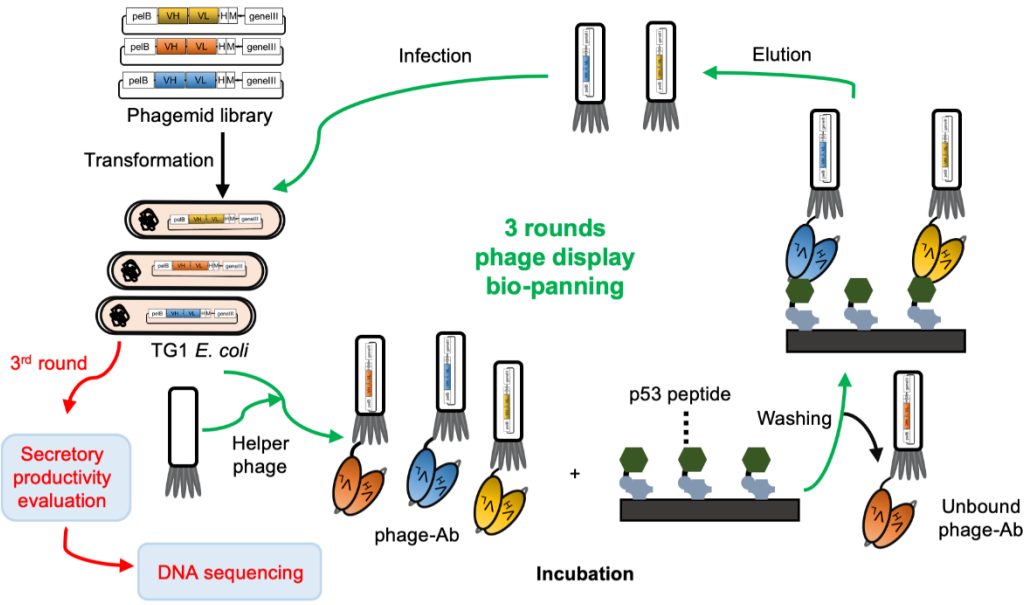

Scheme 2-2. The schematic of the phage display bio-panning.

2.2.4.2 Preparation of phage display library

The remaining 8 mL cells from 2.2.4.1 were inoculated into a 50 mL tube containing 10 mL fresh 2× TYAG medium (containing 1% glucose) and continue to culture it until its OD_{600} reached 0.4. Around 1.6×10^{11} helper phages were added and incubated at a 37 ℃ incubator for 30 min without shaking to infect TG1 cells. The infected cells were centrifuged at 3,800 rpm for 10 min and resuspended in 16 mL of 2 × TYAKG (containing 0.1% glucose). Next, the suspension was shaken at 30 ℃ overnight to produce antibody-displaying phage (phage-Ab). To precipitate phage-Ab, the overnight culture was spun at 3,800 rpm for 30 min and the supernatant (16 mL) was collected in a new tube. Then 4 mL PEG/NaCl (20% polyethylene glycol 6000, 2.5 M NaCl) was added to the supernatant, mixed thoroughly, and set for 1 h on ice. The mixture was divided into two 15 mL tubes and centrifuged at 10,000 *g* for 30 min. After pouring away the supernatant, the sample tubes were spun briefly and the remaining dregs of PEG/NaCl were aspirated off. The pellets were then resuspended in 1 mL PBS and transferred into a 1.5 mL microcentrifuge tube. The sample-containing tube was centrifuged at 12,000 *g* for 10 min to remove the remaining bacterial debris. The phage-Ab (supernatant) was stored at 4 ℃ for short-term storage for phage display bio-panning or

in PBS with 15% glycerol for longer-term storage at −80 ℃.

2.2.4.3 Titration of the phage-Ab library

To titer the phage-Ab library, as shown in Table 2-3, 2 μL phage-Ab library was diluted in 1998 μL (dilution factor 10^3) 2× TY medium, then 2 μL of this was further diluted in 198 μL 2× TY and so on to prepare 10^{-3}, 10^{-5}, 10^{-7}, 10^{-8}, 10^{-9} dilutions in total. After preparing these dilutions, 10 μL of the 10^{-7} and 10^{-8} dilutions were transferred into two different 1.5 mL Eppendorf tubes containing 10 μL log phase TG1 and 80 μL 2× TY. To infect the TG1 with phage-Ab, these phage-Ab/TG1 mixtures were incubated at 37 ℃ for 30 min. Subsequently, each mixture was spread on a 2× TYAG plate (containing 1% glucose) and grown overnight at 37 ℃. The colony number on each plate was used to calculate the titer (cfu/mL ≈ pfu/mL) of the infected cells according to the formula: cfu/mL (≈ pfu/mL) = [(# colonies on the plate) × dilution factor]/ (0.01 mL).

Table 2-3. Dilution method for the titration of phage-Ab library.

	2× TY medium	Dilution factor
2 μL undiluted phage-Ab library	+ 1998 μL	10^3
2 μL 10^{-3} dilution	+ 198 μL	10^5
2 μL 10^{-5} dilution	+ 198 μL	10^7
2 μL 10^{-7} dilution	+ 90 μL	10^8
2 μL 10^{-8} dilution	+ 90 μL	10^9

2.2.4.4 Bio-panning and phage rescue

After preparing the phage-Ab library and confirming its concentration, to select the mutants which bind with the DO-1 epitope peptide (human p53 peptide: biotin-EPPLSQETF*SDLWKL*LPENN-COOH, ABGENT), three rounds of phage display bio-panning were performed on 96-well polystyrene microplate. Firstly, three wells of the 96-well plate were coated with 100 μL/well 10 μg/mL streptavidin diluted in PBS and set at 4 ℃ overnight. Followed by washing with 200 μL/well PBST (PBS containing 0.05% Tween-20) three times and shaking out the excess PBST, these wells were treated with 2 μg/mL (100 μL/well) biotinylated human p53 peptide diluted in PBS at room temperature (RT) for 2 h to immobilize p53 peptide. Next, wells were blocked with 200 μL/well 2% MPBS (2% skim milk in PBS) at RT for 2 h. After washing with PBST, 2×10^{10} phages diluted in 600 μL 2% MPBS were added into wells (100 μL/well). The plate was first incubated at RT for 1 h with gentle shaking and then stood on the bench for one hour. The unbound or non-specific bound phage-Abs were then washed off with PBST three times. The remaining phages were eluted

by adding 100 μL/well 1 mg/mL trypsin-PBS [10 μL of 10 mg/mL trypsin stock solution (in 50 mM Tris-HCl, pH 7.4, 1 mM $CaCl_2$ and stored at −20 °C) added to 90 μL PBS] and shaking at RT for 10 min. The eluted phages were collected into a new 1.5 mL tube. After titration as mentioned in Section 2.2.4.3. The eluted phages were used for a further round of bio-panning. Totally, three rounds of bio-panning were performed.

2.2.5 Monoclonal phage-antibody and secreted antibody ELISA

Preparation of secreted antibody. From the titration plate of the third-round output phages, 95 clones were picked up using a sterile tip and inoculated in a 96-well plate containing 100 μL/well 2× TYAG (1% glucose). The plate was shaken at 37 °C, 250 rpm for 3 h to propagate. After that, 50 μL of the culture from each well was transferred into corresponding wells of a new 2 mL 96-well plate containing 800 μL 2× TYAG (1% glucose) and shaken at 37 °C, 250 rpm until OD_{600} reached 0.4. Then the culture medium was changed to 600 μL/well of 2× TYAG (containing 0.1% glucose and 1 mM IPTG) and further cultured at a 30 °C incubator with 250 rpm shaking for overnight to produce secretory antibodies. On the second day morning, the plate was centrifuged at 1800 *g*, RT for 10 min to collect the supernatant containing secretory antibody. The secreted antibodies in the culture supernatant were added as the primary antibody in the monoclonal secreted antibody ELISA assay.

ELISA assay. For ELISA assay, a 96-well microplate (Greiner Bio-one, Tokyo, Japan) was coated with 100 μL of 10 μg/mL streptomycin in PBS at 4 °C overnight. The plate was blocked with 2% MPBS for 2 h at 25 °C, washed three times with PBST, and incubated with biotinylated human p53 peptide (2 μg/mL in 2% MPBS) at RT for 1 h. The primary antibody (phage-antibody or secreted antibody in culture supernatant) was added and set at RT for 1 h following washing the plated with PBST three times. Then the plate was washed and incubated with 100 μL/well of HRP conjugated anti-M13 [1:5000 in 2% MPBS, for monoclonal phage-antibody ELISA (Scheme 2-3)] or anti-His monoclonal antibody (1:3000 in 2% MPBS, for monoclonal secreted antibody ELISA) at RT for 1 h. The plate was rinsed with PBST three times again and treated with 100 μL/well HRP substrate solution [200 μg/mL 3,3′,5,5′-tetramethylbenzidine (TMBZ) (Sigma) and 3 μL/mL 30% H_2O_2 in 100 mM NaOAc, pH 6.0]. After 15 min incubation, 50 μL/well of 10% sulfuric acid was added to stop the reaction and an SH-1000 microplate reader (Corona Electric, Ibaraki, Japan) was used to read the absorbance of the reaction product at 450 nm with 650 nm as a control.

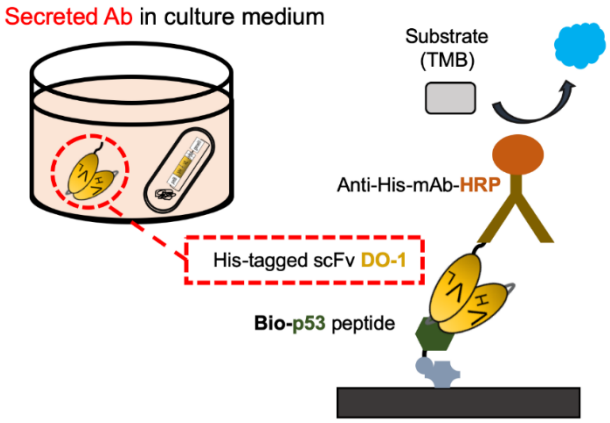

Scheme 2-3. The schematic of monoclonal secreted antibody ELISA.

2.2.6 Confirmation of sequences of selected mutants

According to ELISA results, 14 clones with higher signals were sent for sequencing using M13 Rev (Table 2-1) as a sequencing primer. The sequencing results were aligned with the WT_DO-1 sequence using SnapGene software.

2.2.7 Molecular dynamics (MD) simulation of WT and C11 scFvs

The sequences of the WT_scFv and C11_scFv DO-1 as shown below were used as input for structure prediction by AlphaFold2(Jumper et al., 2021) using multiple sequence alignments generated via MMseqs2(Mirdita et al., 2021) on Google Colaboratory. The PDB templates choice was selected during the prediction, and the Amber relax was used for clash removal. The structures predicted by model 1 of the AlphaFold2 were used for the following simulations. The MD simulations were performed as described in a published paper (Zhu et al., 2022). The differences were the holonomic constraints in the LINCS algorithm were set as all bonds, the Berendsen thermostat algorithm was set at 300 K, and the MD simulations time was 22 ns for each system. The root-mean-square deviation (RMSD) and root-mean-fluctuation (RMSF) were analyzed with GROMACS gmx-toolbox and visualized with Python (v3.7.12) library matplotlib (v3.2.2) and Microsoft Office Excel.

WT_scFv DO-1 [VH (yellow), VL (red)]

GGGTGQVTLKESGPGILQPSQTLSLTCSFSGFSLSTSNMGVGWIRQSSGKGLEWLA
G3-tag
HIWWDDDKLYNPGLKSRLTISKDTSNNQVFLKIASVDTADSATYFCFRMAWAYGD

YWGQGTPLTVSSGGGGSGGGGSGGGGSDVLMTQIPLSLPVSLGDQASISCKSSQSI
Linker
VHSNGITFLQWYLQKPGQSPKLLIYKVSKRFSGVPDRFSGTGSGTDFTLKISRVEAE

DLGVYYCFQGSHVPLTFGAGTKLELKRLEHHHHHHGSDYKDDDDK
His-tag FLAG-tag

C11_scFv DO-1 [mutation sites (italic characters)]

GGGTGQVTLKESGPGILQPSQTLSLTCSFSGFSLSTSNMGVGWIRQS*P*GKGLEWLA
G3-tag
HIWWDDDKLYNPGLKSRLTISKDTSNNQVFLKIASVDTADSATYFCFRMAWAYGD

YWGQGT*T*LTVSSGGGGSGGGGSGGGGSDVLMTQ*I*PLSLPVSLGDQASISCKSSQSI
Linker
VHSNGITFLQWYLQKPGQSPKLLIYKVSKRFSGVPDRFSGTGSGTDFTLKISRVEAE

DLGVYYCFQGSHVPLTFGAGTKLELKRLEHHHHHHGSDYKDDDDK
His-tag FLAG-tag

2.3 Results and discussion

2.3.1 Evaluation expression levels of G3-tagged WT_scFv DO-1

Although DO-1 scFv showed good expression in mammalian cells (Amin et al., 2004), its productivity in the *E. coli* periplasm expression system was too low to be used for Q-body preparation. The yield of G3-tagged WT_scFv DO-1 in BL21(DE3) strain using pET26 vector was calculated as 1 μg per 400 mL culture after His-tag purification. After labeling and FLAG-tag purification, the yield is even lower, only a few tens of microliters of Q-body with 0.13 μM were obtained. This concentration is way too low to be used for live-cell imaging. Although the expression level of DO-1 scFv in cytoplasm is higher than in the periplasm, the quality of protein in the former expression system is lower. For example, the DO-1 scFv expressed in cytoplasm showed a lower ELISA signal and Q-body response (data not shown). This might be because the reductive environment of the cytoplasm was not suitable for the efficient folding of the scFv DO-1.

2.3.2 Design and construction of consensus combinatorial mutagenesis library and phage display bio-panning

To obtain sufficient functional scFv DO-1 protein using an *E. coli* periplasm expression system, we constructed a combinatorial consensus mutagenesis library (Jung et al., 1999) and performed phage display selection to screen variants with both antigen-binding ability and high secretory productivity. A combinatorial consensus mutagenesis library containing seven mutation sites (the library size was estimated as 128) (Table 2-4) was constructed for phage display bio-panning (Jung et al., 1999). After three rounds of bio-panning, monoclonal secreted antibody ELSA were performed to evaluate the secretory productivity of the third-round outputs. As shown in Figure 2-1, compared with WT_scFv DO-1 (A1), 37 clones showed a higher secreted antibody ELISA signal. Next, from these clones, 14 of these 37 clones were sent for sequencing. As shown in Table 2-5, in these 14 clones, 7 clones are harboring different mutation types and were named A6, C11, H6, D10, G9, H5, and H9, respectively. Notably, in the 14 phagemids, no WT sequence was found, indicating that the screening succeeded.

Table 2-4. Mutation sites of combinatorial consensus mutagenesis library.

Kabat position [a]	Wild type a.a. (frequency) [b]		Consensus a.a. (frequency) [c]	
H11	I (ATA) (<1%)	or	L(TTA) (95%)	2
H24	F (TTC) (1%)	or	A (GCC) (79%)	2
H41	S (TCA) (1%)	or	P (CCA) (87%)	2
H82A	A (GCC) (<1%)	or	S (TCC) (63%)	2
H93	F (TTT) (<1%)	or	A (GCT) (84%)	2
H108	P (CCT) (1%)	or	T (ACT) (53%)	2
L7	I (ATT) (<1%)	or	S (TCT) (64%)	2
Library size				2^7

[a] *Kabat* numbering scheme at http://www.abysis.org/abysis/. [b] The amino acid (a.a.) and distribution frequency of WT_DO-1 scFv in corresponding positions. [c] The most common amino acid and distribution frequency in corresponding positions of mouse antibody.

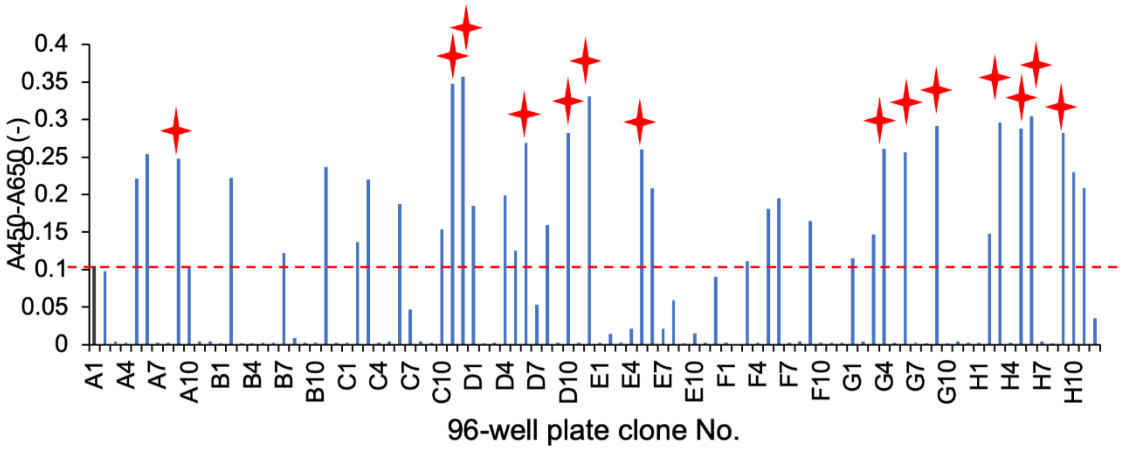

Figure 2-1. Monoclonal secreted antibody ELISA. Totally, 96 monoclones, including WT_scFv DO-1(A1), were picked up for secreted antibody ELISA assay to evaluate their secretory productivity. Fourteen clones highlighted with red stars, which showed a lower signal than WT (A1) were sent for sequencing to confirm their mutation types.

Table 2-5. Mutation sites of indicated phage display selected mutants.

Mutation type	Clone No.	Mutation site						
		H11 I→L	H24 F→A	H41 S→P	H82A A→S	H93 F→A	H108 P→T	L7 I→S
Mut.1	A6=D12=G4=G6	+	–	+	–	–	–	+
Mut.2	**C11**=D6=H3	–	–	+	–	–	+	+
Mut.3	H6=C12	–	–	+	+	–	+	+
Mut.4	D10=E5	–	–	+	–	–	–	+
Mut.5	G9	–	–	+	+	–	+	–
Mut.6	H5	+	–	+	+	–	+	+
Mut.7	H9	+	–	+	–	–	+	+

"+": mutated; "–": wild type

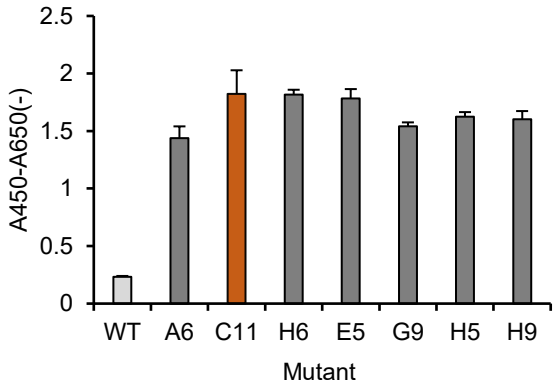

Figure 2-2. Secreted antibody ELISA assay for the detection of secretory expression ability of each mutant selected by phage display. The culture medium of each mutant, including wild type (WT), was applied as the primary antibody for the ELISA assay.

To check whether the results of the monoclonal secreted-Ab ELISA are reproducible, the secreted-Ab ELISA using the selected seven mutants was performed. As shown in Figure 2-2, signals of the seven variants increased 6–7-fold in comparison to the WT, with the C11 variant showing the highest signal. Taking together, these results indicated that the secretory productivity of WT_DO-1 scFv was improved.

2.3.3 MD simulations

MD simulations are widely applied to understand protein stability, having been used for in silico design of recombinant proteins (Dana et al., 2020; Yi et al., 2011). To understand the structural and/or stability changes for the higher ELISA signal of the mutant C11, MD simulations of the G3-WT_ and G3-C11_scFv were performed [G3 represents GGGTG amino acids employed for transpeptidase (sortase A)-mediated fluorescence dye labeling]. The structures of scFvs were predicted using AlphaFold2 Colab (Figure 2-3a). MD simulations were performed using GROMACS for 22 ns to reach a relatively stable phase

for RMSF calculation. The RMSD stabilized after the 10 ns simulation (Figure 2-4), and the 10–20 ns simulation data were used for the RMSF analysis (Figure 2-5). Fluctuation of several framework regions of the C11 mutant decreased compared to that of the WT_scFv, indicating potentially improved folding and stability of the C11 mutant.

Besides, I calculated the prevalence of mutations. As shown in Figure 2-3b, H41 (S→P), H108 (P→T), and L7 (I→S) are the most prevalent mutations. The top one variant (C11) harbors all three mutations, indicating the screening was successful.

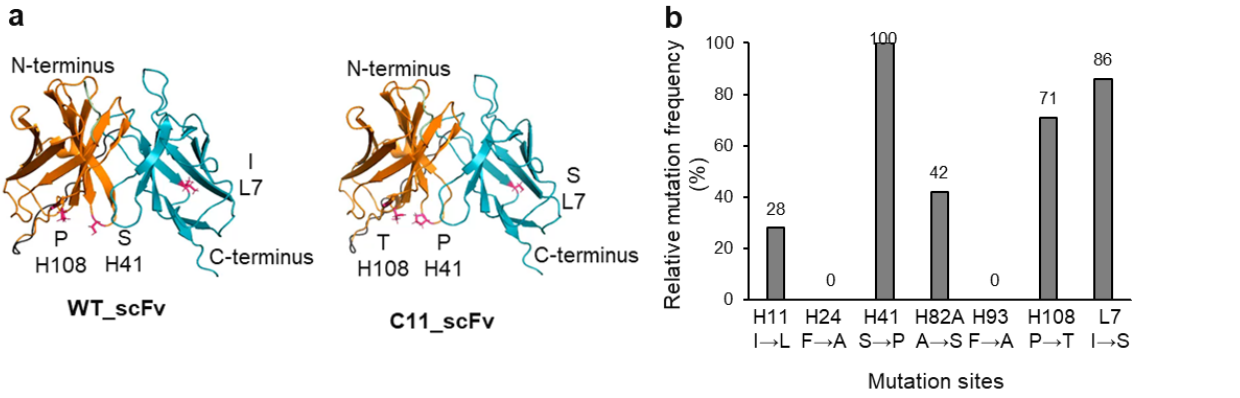

Figure 2-3. a) 3D structure of WT_ and C11_scFv DO-1 predicted by AlphaFold2. Red indicates the three mutation sites. Orange and cyan represent VH and VL chains, respectively. b) Frequency of each mutation site in the selected seven mutants. For example, S-H41-P mutation exists in all seven mutants, its relative mutation frequency is 100%.

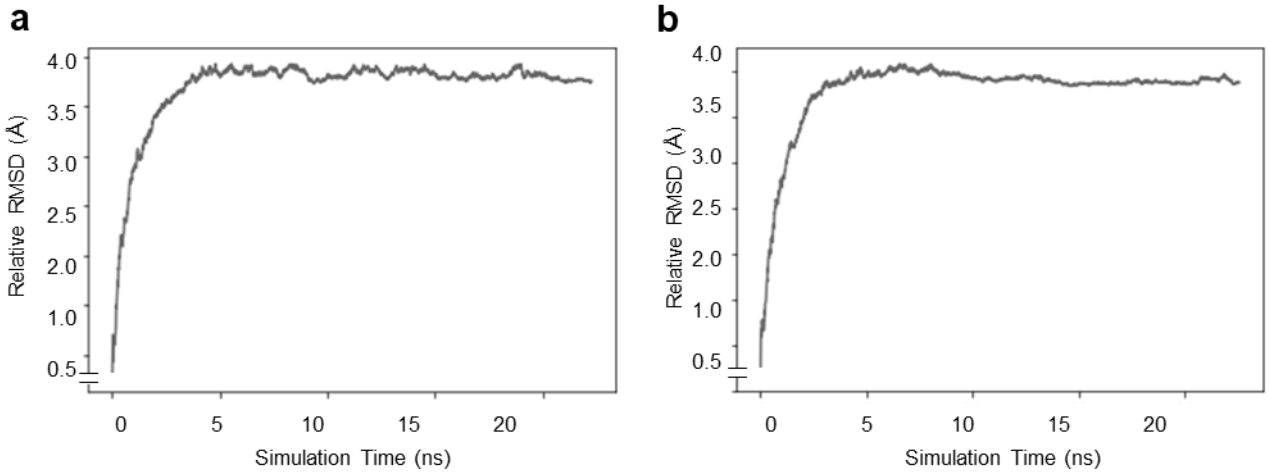

Figure 2-4. RMSD values of WT (a) and C11 (b) _scFv DO-1. RMSD, root-mean-square deviation.

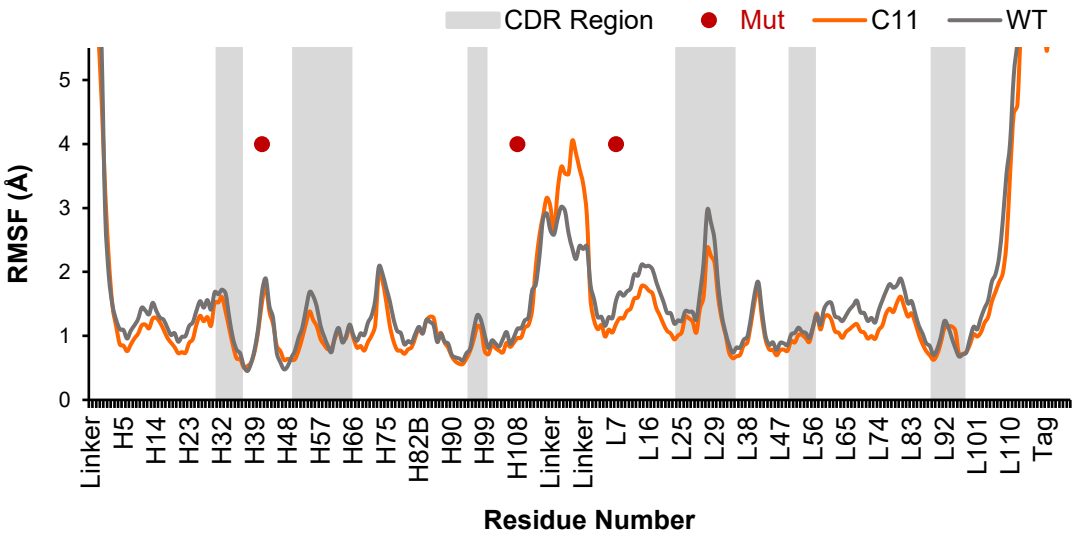

Figure 2-5. Plot showing the RMSF values of C-alpha atoms from 10–20 ns MD simulation of the WT_scFv DO-1 (light gray) and C11_scFv DO-1 (orange). Red dots indicate mutation sites. Abbreviations: RMSF, root-mean-square fluctuation; MD, molecular dynamics; Mut., mutation sites. CDR region, complementary determine region. This graph was plotted using the average RMSF of two times MD simulations.

2.4 Summary of Chapter 2

In this chapter, to improve the secretory productivity of WT_scFv DO-1, a combinatorial consensus mutagenesis library was constructed, and phage display was performed to select the variants with better secretory productivity. Firstly, an approximate 128 consensus mutagenesis phagemid library was constructed for the phage display bio-panning. From the third-round output of the phage display selection, seven variants that showed 6–7-fold higher secretory productivity in comparison to the WT, with the C11 variant showing the highest signal, were selected. The frequency of the mutation sites in the selected seven mutants was analyzed and showed proline (100%), serine (86%), and threonine (71%) are preferred amino acids for a better secretory ability. The top one mutant, C11, contains all of the three mutation sites. From the 3D structure of C11_scFv predicted by AlphaFold2, the sidechain of the three amino acids is located at the protein surface which may contribute to its higher stability leading to a better secretory ability.

2.5 References

Amin, N., Liu, A.D., Ramer, S., Aehle, W., Meijer, D., Metin, M., Wong, S., Gualfetti, P., and Schellenberger, V. (2004). Construction of stabilized proteins by combinatorial consensus mutagenesis. Protein Eng Des Sel *17*, 787-793.

Dana, H., Chalbatani, G.M., Gharagouzloo, E., Miri, S.R., Memari, F., Rasoolzadeh, R., Zinatizadeh, M.R., Zarandi, P.K., and Marmari, V. (2020). In silico Analysis, Molecular Docking, Molecular

Dynamic, Cloning, Expression and Purification of Chimeric Protein in Colorectal Cancer Treatment. Drug Des Dev Ther *14*, 309-329.

Francis, D.M., and Page, R. (2010). Strategies to optimize protein expression in E. coli. Curr Protoc Protein Sci *Chapter 5*, Unit 5 24 21-29.

Jumper, J., Evans, R., Pritzel, A., Green, T., Figurnov, M., Ronneberger, O., Tunyasuvunakool, K., Bates, R., Žídek, A., Potapenko, A.*, et al.* (2021). Highly accurate protein structure prediction with AlphaFold. Nature *596*, 583-589.

Jung, S., Honegger, A., and Pluckthun, A. (1999). Selection for improved protein stability by phage display. J Mol Biol *294*, 163-180.

Ledsgaard, L., Ljungars, A., Rimbault, C., Sorensen, C.V., Tulika, T., Wade, J., Wouters, Y., McCafferty, J., and Laustsen, A.H. (2022). Advances in antibody phage display technology. Drug Discov Today *27*, 2151-2169.

Michel, E., Cucuzza, S., Mittl, P.R.E., Zerbe, O., and Pluckthun, A. (2022). Improved Repeat Protein Stability by Combined Consensus and Computational Protein Design. Biochemistry.

Mirdita, M., Ovchinnikov, S., and Steinegger, M. (2021). ColabFold - Making protein folding accessible to all. bioRxiv, 2021.2008.2015.456425.

Sandomenico, A., Sivaccumar, J.P., and Ruvo, M. (2020). Evolution of Escherichia coli Expression System in Producing Antibody Recombinant Fragments. Int J Mol Sci *21*.

Tsukahara, N., Murakami, A., Motohashi, M., Nakayama, H., Kondo, Y., Ito, Y., Azuma, T., and Kishimoto, H. (2022). An alpaca single-domain antibody (VHH) phage-display library constructed by CDR shuffling provided high affinity VHHs against desired protein antigens. Int Immunol.

Yi, Z.L., Pei, X.Q., and Wu, Z.L. (2011). Introduction of glycine and proline residues onto protein surface increases the thermostability of endoglucanase CelA from Clostridium thermocellum. Bioresour Technol *102*, 3636-3638.

Zhu, B., Qian, C., Tang, H., Kitaguchi, T., and Ueda, H. (2022). Creating a Thermostable beta-Glucuronidase Switch for Homogeneous Immunoassay by Disruption of Conserved Salt Bridges at Diagonal Interfaces. Biochemistry.

Chapter 3. Preparation of p53 Q-bodies and evaluation of their responses in PBST

3.1 Introduction

The Quenchbody (Q-body) is a newly developed fluorescent immunosensor (Abe et al., 2011) which is a site-specific fluorescent dye(s)-labeled antibody fragment that exhibits antigen-dependent fluorescence signal enhancement. The labeled dye(s) are quenched by intrinsic tryptophan residues of the antibody fragment through photoinduced electron transfer (PET) and/or dye-dye interactions (Abe et al., 2014; Abe et al., 2011). They light up after a conformational change triggered by antigen-binding. Previously, the Q-body was made by labeling the target antibody fragment using Cys-tag mediated thiol-maleimide reaction following purification by FLAG-tag purification (Jeong et al., 2016). However, the generated thiosuccinimide product has a high possibility to be reduced in the reductive cytoplasm environment (Ravasco et al., 2019) which may give rise to the low stability of Q-body and result in high background signals in intracellular live cell imaging.

Sortase 7+ (SrtA 7+) is a variant of SrtA, showing calcium ion (Ca^{2+})-independent activity (Jeong et al., 2017), which is expected to enable calcium-free ligation without possible calcium phosphate precipitation during the labeling reaction (Theile et al., 2013). SrtA 7+ cleaves the peptide bond between threonine (T) and glycine (G) of dye-LPXTGG to yield an acyl-enzyme intermediate to form a new peptide bond between dye-LPXT and Gn (n≥3) (Scheme 3-1). The conjugation using this approach has been verified stable in intracellular environments of the living cell.

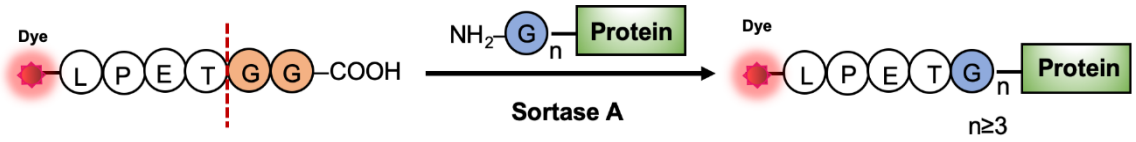

Scheme 3-1. Schematic of Sortase A labeling.

The double-labeled Q-body usually shows a better antigen-dependent response in comparison to the corresponding single-labeled Q-body, as both hydrophobic dye-dye (H-dimer) (Abe et al., 2014) and dye-antibody interactions can favor deep quenching of the dyes.

In this study, both single-labeled and double-labeled Q-bodies were prepared using SrtA 7+. Their dose-response assays against either human or mouse p53 peptides were performed. The binding kinetics of C11_Fab and its Q-body were evaluated by bio-layer interferometry assay. The labeling ratio and quantum yield of the self-quenched and the antigen-activated forms of C11_Fab Q-bodies were determined.

3.2 Materials and methods

3.2.1 Materials

TAMRA-LPETGG (ABGENT); Other chemicals were obtained from Wako Pure Chemicals except as otherwise stated.

3.2.2 Oligonucleotides

The following primers were used for the construction of plasmids.

Table 3-1. Primers used for the construction of protein expression plasmids.

Fragment name	Primer name	Primer sequence (5′ – 3′)
G3- V_HV_L (WT)-DO-1	G3-DO1(VH)-back	GGTGGAGGCACCGGTCAGGTTACTCTGAAAGAG
Or G3- V_HV_L (C11)-DO-1	VL(DO1)-Xho-for	GGTGGTGGTGCTCGAGCCGTTTCAGCTCCAGCTT
pelB-G3-tag-1	NdeI-pelB-back	AAGGAGATATACATATGAAATACCTGCTGCCGACC
	pelB-G3-for	ACCGGTGCCTCCACCGGCCATCGCCGGCTGGGC
6xHis-FLAG	His-FLAG-back	CGAGCACCACCACCACCACCACGGATCCGACTA
	T7-Terminator	TGCTAGTTATTGCTCAGCGG
G3- V_HV_L(C11)-DO-1-Cys	VH(DO1)-AgeI-back	CTCTAATGAGACCGGTCAGGTTACTCTGAAAGAGTCTGG
	VL(DO1)-Cys-Xho-for	GGTGGTGGTGCTCGAGGCAACCTCCCCGTTTCAGCTCCAGCTTG
CH1	XhoI_back	TCGAGCGCTTCCACCAAG
	CH1-Cys-for	ATGATGATGTGCGGCCGAGCAGCTTTTGGGCTCAAC
CL	Ck-back	AGCTTGAAATCAAACGTGCTGAT
	Ck-Cys-for	CCTTGTAGTCGGATCCGCCGCACTCTCCCCTGTTG
6xHis-Myc-tag	Cys-His-back	GCCGCACATCATCATCACCAT
	CH1-for	ATGATATCTCCTTCTAGATTATTATGCGG
pelB-G3-tag	pelB-overlap-back	CTAGAAGGAGATATCATCATATGAAATACCTGCTG
	pelB-for	CAAAACATCACCGGTGCCTCCACCGGCCAT
pelB-V_H-C11DO1	pelB-NdeI-Infusion-back	AAGGAGATATACATATGAAATACCTGCTG
	VH(DO1)-for	GGTGGAAGCGCTCGAGACTGTGAGAGTGGTG
V_L-C11DO1	VL(DO1)-back	ACCGGTGATGTTTTGATGACCCAA
	VL(DO1)-HindIII-for	GTTTGATTTCAAGCTTGGTCCCAGCTCCGAACGT

3.2.3 Construction of plasmids

To prepare pET26-G3-WT_scFv and -C11_scFv plasmids (Scheme 2-4a and Figure 3-1a) for generating single-labeled Q-bodies, pIT2-C11_scFv and -WT_scFv DO-1 plasmids were used as templates, G3-DO1(VH)-Back and VL(DO1)-Xho-For were used as primers to amplify G3- V_HV_L (WT)-DO1 and G3- V_HV_L (C11)-DO1 gene fragments, respectively, by polymerase chain reaction (PCR) using the KOD-plus neo kit. The pelB-G3-tag-1 signal peptide gene was amplified using NdeI-pelB-Back and pelB-G3-For as primers and using the pET26b (+) vector as a template. The 6xHis-FLAG gene was amplified from pSQ-KTM219-scFv (Abe et al., 2011) using His-FLAG-back and T7-Terminator as primers. The purified pelB and 6xHis-FLAG gene fragments were infused with G3- V_HV_L (WT)-DO1 or G3- V_HV_L (C11)-DO1 fragment, respectively, by overlapping PCR using NdeI-pelB-Back and T7-Terminator as primers. The overlapping PCR generates pelB-G3-V_HV_L(WT)-6× His-FLAG or pelB-G3-V_HV_L(C11)-6× His-FLAG gene fragments. Both gene fragments were digested with Ndel and BlpI enzymes. After digestion and purification, these two fragments were cloned into NcoI and BlpI linearized pET26b vector with Ligation High ver. II (Toyobo Biochemicals). The ligation products were transformed into *E. coli* XL10-Gold cells which were following cultured on LB agar plate containing 0.5% yeast extract, 0.5% NaCl, 1.0% tryptone, 1.5% agar, and 100 μg/mL kanamycin at 37 °C overnight. The colony PCR was performed to screen the colonies harbouring targeted plasmid with primers T7 promoter and T7 terminator using Quick Taq® HS Dye Mix (Toyobo), and positive clones were sent for sequencing to confirm the insertion of correct sequences.

To prepare a double-labeled Q-body, the pUQ-pelB-G3-C11_Fab plasmid (Scheme 2-4b and Figure 3-1a) was constructed from a previously prepared pUQ2-G3S2-29IJ6 plasmid (Abe et al., 2014) that was used to express an anti-serum albumin Fab with a Cys-tag (MSKQIEVNCNET) at the H chain and L chain N-terminus, respectively. The CH1, CL, and 6× His-Myc-tag gene fragments were amplified using pUQ2-G3S2-29IJ6 plasmid as a template, and pelB-G3-tag, pelB-V_H of C11_DO-1, and V_L of C11_DO-1 gene fragments were amplified from pET26-G3-C11_scFv plasmid, using primers as shown in Table 3-1. The six fragments were integrated into one fragment by overlap extension PCR using primer pelB-NdeI-Infusion-Back and Ck-Cys-For. The PCR product was purified and inserted into NdeI- and BamHI-linearized pUQ2 vector by an In-Fusion HD cloning kit. Transformation, plasmid preparation, and DNA sequencing were next performed to obtain the correct pUQ-pelB-G3-C11_Fab plasmid as above.

C11_Fab DO-1 sequence [VH (yellow), CH1 (green), VL (red), and CL (purple)]
Heavy chain
GGGTGQVTLKESGPGILQPSQTLSLTCSFSGFSLSTSNMGVGWIRQSPGKGLEWLA
G3-tag
HIWWDDDKLYNPGLKSRLTISKDTSNNQVFLKIASVDTADSATYFCFRMAWAYGD
YWGQGTTLTVSSASTKGPSVFPLAPSSKSTSGGTAALGCLVKDYFPEPVTVSWNSG
ALTSGVHTFPAVLQSSGLYSLSSVVTVPSSSLGTQTYICNVNHKPSNTKVDKKVEPK

SCSAAHHHHHHGAAEQKLISEEDLNGAA
His-tag Myc-tag

Light chain

GGGTGDVLMTQSPLSLPVSLGDQASISCKSSQSIVHSNGITFLQWYLQKPGQSPKL
G3-tag
LIYKVSKRFSGVPDRFSGTGSGTDFTLKISRVEAEDLGVYYCFQGSHVPLTFGAGTK
LEIKRADAAPSVFIFPPSDEQLKSGTASVVCLLNNFYPREAKVQWKVDNALQSGNS
QESVTEQDSKDSTYSLSSTLTLSKADYEKHKVYACEVTHQGLSSPVTKSFNRGECG
GSDYKDDDDK
FLAG-tag

3.2.4 Protein expression and purification

E. coli BL21(DE3) cells were transformed with each of the above-mentioned plasmids and cultured on LBK or LBA plate (LB medium containing 100 μg/mL kanamycin or 100 μg/mL ampicillin) at 37 °C overnight. A single colony was picked and grown at 37 °C in 4 mL LBK (pET26-G3-C11_scFv, pET26-G3-WT_scFv, or pET26-G3-C11_scFv-Cys) or LBA (pUQ-pelB-G3-C11_Fab) medium overnight. The cells were further cultured in 400 mL LBK or LBA medium at 37 °C until OD_{600} reached 0.6, followed by adding 0.4 mM IPTG and cultivating at 16 °C for 16–20 h. The cells were harvested by centrifugation (6000 *g* for 10 min at 4 °C). An osmotic shock method was employed to extract periplasm proteins. Firstly, the cell pellet was gently resuspended in 6 mL (3 mL solution per gram cells) 30 mM Tris-HCl, 20% sucrose, pH 8.0. The suspension was incubated on ice for 10 min and spun at RT at 8000 *g* for 10 min. After centrifugation, the supernatant was discarded and the precipitate was resuspended in 10 mL of ice-cold distilled water followed by rotating at 4 °C for 10 min and spinning at 4 °C,12000 *g*, 10 min. The supernatant was incubated with 0.2 mL pre-equilibrated TALON metal-affinity resin and rotated on a rotation wheel for 1 h at RT. The resins were collected by centrifugation and transferred into a TALON disposable gravity column. Then they were washed 5 times with 1 mL Talon buffer [50 mM sodium phosphate, 0.3 M sodium chloride (NaCl), pH 7.4]. Subsequently, nonspecifically bound proteins were removed by three washes with 0.5 mL TALON buffer containing 20 mM imidazole. After that, beads were resuspended in 0.5 mL TALON elution buffer (TALON buffer containing 500 mM imidazole) and put on ice for 10 min. The eluent was collected for further studies.

3.2.5 Fluorescent dye-labeling

SrtA 7+, a calcium-independent mutant (Jeong et al., 2017), was used to label G3-WT_ or C11_scFv or G3-C11_Fab DO-1 with TAMRA to prepare single-labeled or double-labeled Q-bodies. The use of the calcium-independent mutant is compatible with the ligation taking place in the phosphate buffer. The His-tag purified 1–2 μM scFvs or Fab were mixed with 20 μM TAMRA-LPETGG [(10 mM stock in dimethyl sufoxide (DMSO)], 2 μM SrtA 7+, and 50 mM Tris-HCl pH 8 (150 mM NaCl). The molar ratio of protein to dye was around 1:10–20. The mixture was rotated at 4 °C for 2 h avoiding light and subsequently incubated with 40 μL of pre-equilibrated anti-FLAG (DYKDDDDK)-tag M2 antibody-coated

magnetic beads (Wako, Osaka, Japan) at 4 °C overnight. The beads were washed 14 times with 200 μL PBS containing 0.1% Brij35 to remove free dyes. The bound proteins were then eluted with 200 μL 150 μg/mL 3× FLAG peptide (Lifetein) diluted in PBST (0.05% Tween20) buffer. The purified Q-bodies were added with 15% glycerol and stored at −30 °C.

3.2.6 SDS-PAGE

To evaluate the yield, purity, and concentration of proteins, SDS-PAGE (sodium dodecyl sulfate–polyacrylamide gel electrophoresis) was performed with various concentrations of BSA as references. To prepare the SDS-PAGE sample, the proteins were mixed with an equal volume of 2× SDS loading buffer [0.125 M Tris-HCl (pH 6.8), 4% (w/v) SDS, 20% (v/v) glycerol, 0.02% bromophenol blue, 0.2 M DTT (dithiothreitol)], then boil the sample mixtures in a heating block with setting to 95 °C for 5 min. After heating, the samples were briefly centrifuged and kept on ice for a few minutes. Then the samples were loaded into a 12.5% gel with the Precision Plus Protein Unstained or Dual color Standards (Bio-Rad) as a molecular weight marker and the BSA (bovine serum albumin, Bio-Rad Lab, Inc., Japan) with concentrations ranging from 200 ng/μL to 25 ng/μL per lane as references to calculate protein concentrations. After loading, the gel was set to run with a setting at 300 V, 25 mA for around 60 min. For the labeled proteins, a transilluminator was used to observe the fluorescence of the gel and make sure the labeling of fluorescent dye(s). Followed by 20 min fixation and 30 min CBB-staining, the gel was set for de-staining with distilled water containing a piece of Kimwipe paper overnight. Next, the gel photo was taken, and CS Analyzer 4 software (ATTO, Tokyo, Japan) was used to determine the concentrations of proteins using BSA as the standard. All the protein concentration analysis in this study used the same method.

3.2.7 Dose-response measurement using microplate reader

The FLAG-tag purified Q-bodies were diluted in PBST (0.05% Tween20) to prepare 1 nM of Q-body, followed by the addition of various concentrations of the antigens: human or murine p53 peptide. For each antigen concentration gradient, the same volume of antigens at different concentrations was used to ensure the same concentration of Q-body upon adding the antigen. The fluorescence intensities of the antigen and Q-body mixtures at the excitation wavelength of 545 nm were measured using a black half-well microplate (675076, Greiner Japan, Tokyo) and a CLARIOstar microplate reader (BMG Labtech Japan, Saitama, Japan). Their dose-response curves were fitted with the four-parameter logistic equation using OriginPro 2022 (Origin Software). The limit of detection (LOD) was determined based on the value of three times the standard deviation of the fluorescence intensity (F.I.) in the absence of antigen. This value plus the mean value of F.I. in the absence of antigen was used as “y” and interpolated into the following formula (four-parameter logistic) to calculate “x”. This “x” value is the LOD.

$$y = d + \frac{a - d}{\left[1 + \left(\frac{x}{c}\right)^{b}\right]}$$

3.2.8 Bio-layer interferometry (BLI) analysis

To investigate the antigen-binding affinity of C11_Fab before and after dye labeling, the BLI assays were performed on an Octet K2 system (Pall FortéBio, Fremont, CA, USA) (Ning et al., 2021). Octet® streptavidin (SA) biosensors were activated by immersing in kinetic buffer (20 mM phosphate buffer, 150 mM NaCl, 0.02% Tween20, 0.1% BSA, pH 7.4) for 10 min. The preactivated sensors were loaded with 15 μg/mL biotinylated human p53 peptide (biotin-EPPLSQETFSDLWKLLPENN-COOH, ABGENT) and equilibrated in Kinetic buffer before analysis. The unlabeled C11_Fab or its Q-body from 2.5–80 nM in two-fold dilutions in kinetic buffer were used for measurements. For each measurement of analyte concentration, the biosensors went through the following cycle: baseline measurement in the kinetic buffer for 60 s, association in the analyte for 300 s, dissociation in the kinetic buffer for 300 s, regeneration in 10 mM glycine for 10 s and washing in the kinetic buffer for 10 s for three repeats. After finishing all analyte concentrations for both sample and reference biosensors, the data were exported and analyzed in Data Analysis 11.0 (Pall FortéBio) software. Double reference subtraction and global fitting in a 1:1 binding model were used to predict the K_D values of both analytes.

3.2.9 Fluorescence spectrum measurement

The purified C11_scFv Q-body or C11_Fab Q-body was diluted in PBST containing 0.1% BSA to prepare 250 μL 1 nM of Q-body. Then the diluted Q-body was transferred into a 5 × 5 mm quartz cuvette (Starna, Atascadero, CA, USA) and a human p53 peptide was added by titration. After each addition, the fluorescence intensity was measured using a spectrofluorometer (Model FP-8500, JASCO, Tokyo, Japan) with excitation at 545 nm and emission from 565 to 640 nm. The bandwidth of excitation and emission were set as 5 nm and 10 nm, respectively. For each antigen concentration, three repeats were performed, and their mean fluorescence intensities were used to plot the fluorescence spectrum.

3.2.10 Absorbance spectrum measurement and F/P ratio calculation

The absorption spectrum of self-quenched Q-bodies and activated forms of C11_Fab Q-bodies were measured with UV-VIS Spectrophotometer (Model V-730Bio, JASCO, Tokyo, Japan) and UV-Cuvette micro (BRAND, Jena, Germany). The measurement temperature, UV/Vis bandwidth, and scanning speed were set to RT, 1 nm, and 100 nm/min, respectively. The fluorescent dye/protein (F/P) ratio of C11_Fab Q-body was calculated as following equation (Takahashi et al., 2021). The Q-body concentration was determined by SDS-PAGE as described above.

$$\frac{F}{P}\ ratio = \left(\frac{A555\ of\ Q\text{-}body}{\varepsilon 555} + \frac{A520\ of\ Q-body}{\varepsilon 520}\right) * \frac{1}{\text{Q-body concentration}}$$

Where:

A_{555}: absorption at 555 nm; A_{520}: absorption at 520 nm; ε_{555}: molar extinction coefficient (M^{-1} cm^{-1}) of the monomer TAMRA (ε_{555} = 66100); ε_{520}: molar extinction coefficient of the H-dimer TAMRA (ε_{520} = 64200) (Christie et al., 2009).

3.2.11 Measurement of fluorescence quantum yields of C11_Fab Q-body

To determine fluorescence quantum yields (QY) of the self-quenched and activated forms of C11_Fab Q-bodies, the relative fluorescence QY method was used. TAMRA-LPETGG was used as a reference dye whose absolute QY was determined using an absolute PL quantum yield spectrometer (C9920-02, Hamamatsu Photonics, Hamamatsu, Japan). Briefly, 3 mL 8.3 μM TAMRA-LPETGG in PBST (containing 0.05% Tween 20) was prepared. Its QY at an excitation wavelength of 500 nm was decided as 0.37. The fluorescence spectra of TAMRA-LPETGG, self-quenched and activated forms of C11_Fab Q-bodies from 530 to 700 nm were detected using an excitation wavelength of 500 nm by spectrofluorometer (Model FP-8500, JASCO, Tokyo, Japan). The integrated fluorescence intensity of the spectrum was calculated using OriginPro 2022 software. Single-point measurement was used to determine the QY. In this method, the QY of the unknown sample (self-quenched and activated forms of Q-bodies) was calculated using the following equation.

$$Q = Q_R \frac{I}{I_R} \frac{A_R}{A} \frac{n^2}{n^2_R}$$

Where:

Q: fluorescence quantum yield; I: integrated fluorescence intensity; A: absorption; n: refractive index of solvent; $_R$: reference dye TAMRA-LPETGG

3.3 Results and discussion

3.3.1 Preparation of single-labeled WT_scFv and C11_scFv Q-bodies

The secretory productivity of C11_scFv was improved. To understand, whether the mutation introduction affects its antigen-dependent response as a Q-body. Plasmids, pET26-G3-WT_scFv and pET26-G3-C11_scFv, were successfully constructed and were employed to express G3-tagged WT_ and C11_scFvs in the periplasm of *E. coli* strain BL21(DE3) (Figure 3-1a) for Q-body preparation. The His-tag purified G3-WT_scFv and G3_C11_scFv were labeled with TAMRA dye using a mutant of transpeptidase SrtA 7+ (Jeong et al., 2017). SrtA 7+ is a variant of SrtA, showing calcium ion (Ca^{2+})-independent activity, which is expected to enable calcium-free ligation without possible calcium phosphate precipitation during the labeling reaction. SrtA 7+ cleaves the peptide bond between threonine (T) and glycine (G) of TAMRA-LPETGG to yield an acyl enzyme intermediate. This intermediate is resolved by nucleophilic attack of a polyglycine-linked substrate (e.g., G3-C11_scFv) to form a new peptide bond between TAMRA-LPET- and G3-C11_scFv. After labeling, anti-FLAG antibody-coated beads were used to remove free dyes and obtain purified Q-bodies (Scheme 3-2). SDS-PAGE was performed to analyze FLAG-tag purified proteins. The

images of CBB-staining and fluorescence of SDS-PAGE indicated that these Q-bodies have been successfully labeled with dyes (Figures 3-1b and 3-1c).

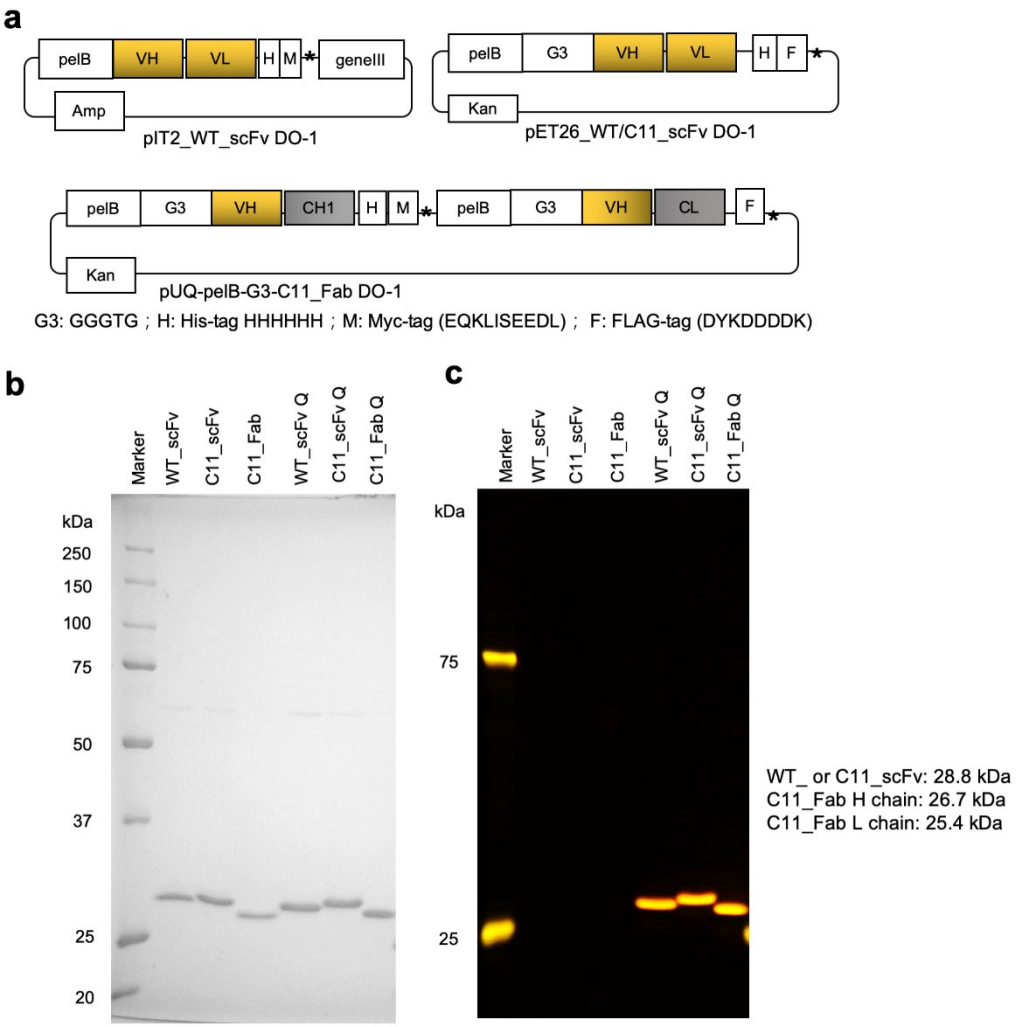

Figure 3-1. a) Scheme of plasmids used for the expression of G3-tagged WT_ or C11_scFv and C11_Fab DO-1. b-c) CBB (coomassie brilliant blue) staining (b) and fluorescence image (c) of SDS-PAGE for WT_scFv, C11_scFv, C11_Fab, and corresponding Q-bodies.

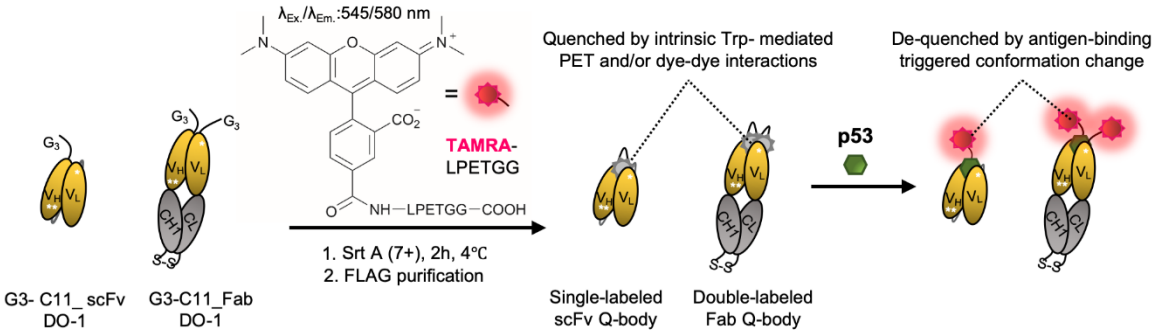

Scheme 3-2. Schematics of preparing single-labeled or double-labeled Q-bodies by transpeptidase SrtA (7+) and working image of Q-bodies with target antigen p53 peptide. Abbreviation: SrtA (7+), a mutant of Sortase A; Trp: tryptophan residues; PET: photo-induced electron transfer; Ex, excited; Em, emission. White stars represent mutation sites in the C11 mutant.

3.3.2 Evaluation of the antigen-dependent response of the WT_scFv and C11_scFv Q-bodies

After obtaining purified WT_ and C11_scFv Q-bodies, dose-response assays were performed in the presence of human p53 peptides (NH_2-EPPLSQETFSDLWKLLPENN-COOH) encoding the human p53 epitope to determine their maximum response, EC_{50}, and LOD. As presented in Figure 3-3a and 3-3c, C11_scFv (2.0-fold) and WT_scFv (1.9-fold) Q-bodies showed similar antigen-dependent responses. The EC_{50} of WT_ and C11_scFv Q-bodies were calculated as 0.78 nM and 1.6 nM, respectively. The LOD for the human p53 peptide were determined to be 0.076 nM for the WT_scFv Q-body and 0.028 nM for the C11_scFv Q-body. Although, the LOD of C11_scFv Q-body was slightly lower than that of WT_scFv Q-body, the error bar of the WT_scFv Q-body was larger than that of C11_scFv. It is hard to say both LOD has significant difference. Taking together, these data indicated that the introduction of mutations in C11 did not affect the performance of the Q-body. Therefore, the mutant, C11_scFv DO-1, was used for further improvement of antigen-dependent response.

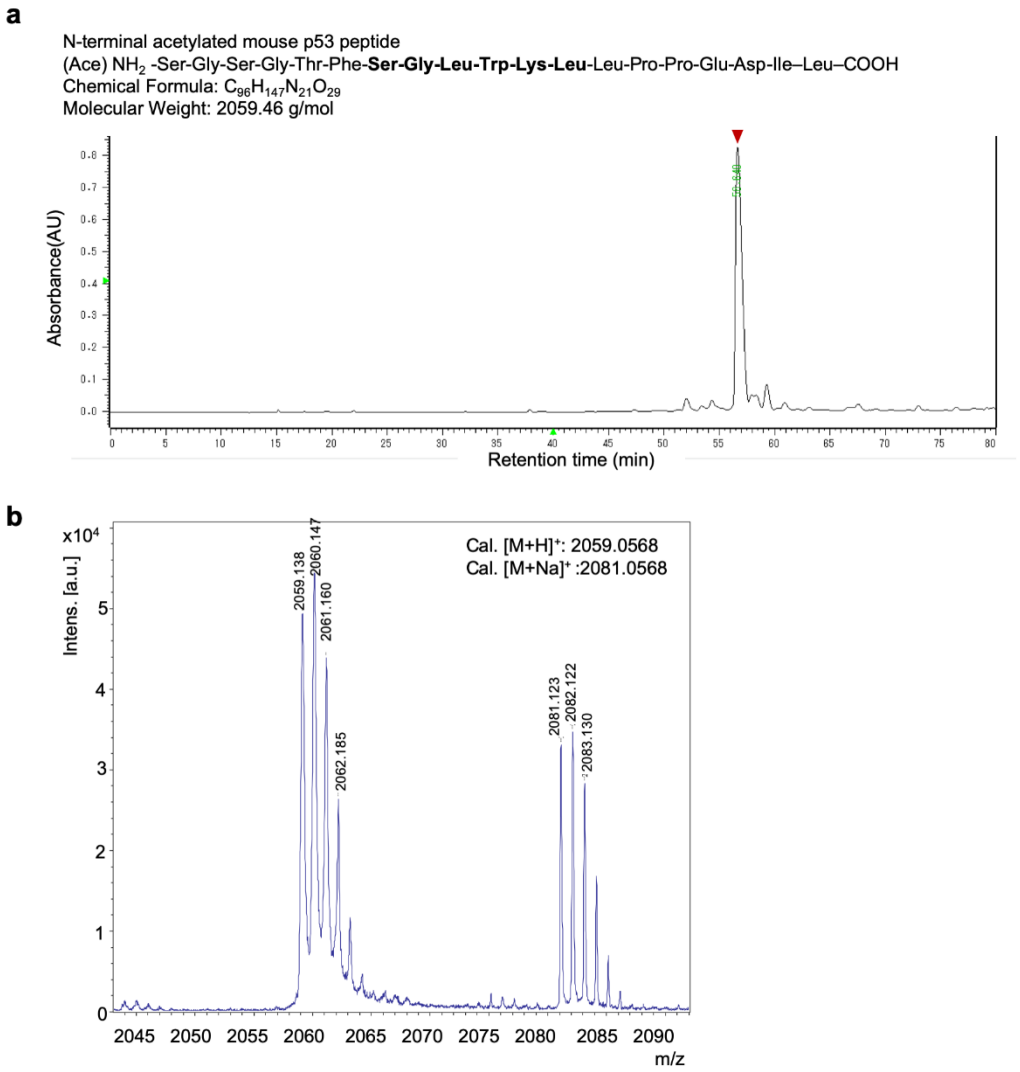

Figure 3-2. Preparation of acetylated mouse p53 peptide by Fmoc solid-phase peptide synthesis. a) Reversed-phase high-performance liquid chromatography (RP-HPLC) of the sample obtained by Fmoc peptide synthesis. Red arrowhead indicates the target peak. Column: 5C_{18}-AR-II (4.6ID × 250mm). Gradient A [H_2O containing 0.1% (v/v) TFA]: 100% (0 min) – 0% (80 min), Gradient B [CH_3CN containing 0.1% (v/v) TFA]: 0% (0 min) –100% (80 min). Flow rate: 0.6 mL/min. b) MALDI-TOF MS spectrum. Mouse p53 peptide was detected at m/z 2059.138 ($[M+H]^+$) and 2081.123 ($[M+Na]^+$).

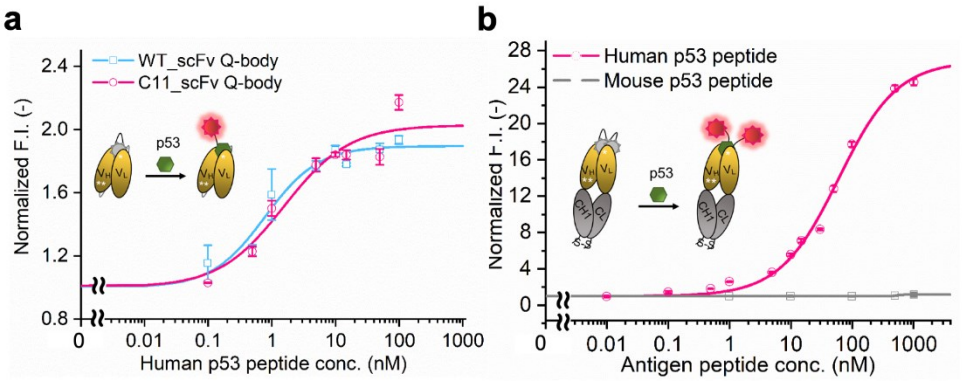

c

	WT_scFv Q-body	C11_scFv Q-body	C11_Fab Q-body
EC_{50}	0.78 nM	1.6 nM	60 nM
LOD	0.076 nM	0.028 nM	0.72 nM
Maximum response	1.9-fold	2.0-fold	27-fold

Figure 3-3. Performance of Q-bodies in PBST buffer. a) Dose-response fitting curves of single-labeled WT (blue line) and C11 (red line) _scFv Q-bodies at 1 nM concentration for human p53 peptide. b) Dose-response fitting curves of double-labeled C11_Fab Q-body at 1 nM concentration for human p53 (red line) and mouse p53 (gray line) peptides. c) EC_{50}, LOD, and the maximum response of Q-bodies. Normalized F.I.: the fluorescence intensities (F.I.) of Q-body at each antigen concentration were divided by that of antigen in the absence of antigen. Human p53 peptide: EPPLSQETFS***D***LWKLLPENN (bold characters indicate the epitope of DO-1); Mouse p53 peptide: SGSGTFS***G***LWKLLPPEDIL. The DO-1 does not recognize mouse p53 peptides because of one amino acid difference (G in the italic letter) in its epitope. Four parameters logistic equation was used for the fitting of dose-response curves. Data are shown as the mean ± SD (*n*=3).

3.3.3 Improvement of the Q-body response by making double-labeled C11_Fab Q-body

Several previous studies (Abe et al., 2014; Dong and Ueda, 2021; Ning et al., 2021) have shown that double-labeled Fabs demonstrate a more intensive turn-on response compared to the corresponding single-labeled scFv Q-bodies, as both hydrophobic dye-dye and dye-antibody interactions can favor deep quenching of the dyes. Therefore, I constructed plasmid, pUQ-pelB-G3-C11_Fab which contains two G3-tags (the one is at the N-terminus of heave chain, the other is at the N-terminus of light chain) and expressed G3-C11_Fab proteins using this plasmid. Then, I prepared the corresponding TAMRA double-labeled Fab Q-body as the same method as the preparation of the single-labeled Q-body above. Hereafter, the double-labeled Q-body was called C11_Fab Q-body (Scheme 3-1). To investigate the sensitivity, specificity, and antigen-dependent fluorescence response of the C11_Fab Q-body, fluorescence changes were measured in the presence of various concentrations of the human p53 peptide or murine p53 peptide (NH2-SGSGTFSGLWKLLPPEDIL-COOH, synthesized as shown in Figure 3-2). The mouse p53 peptide was added as a negative control to

investigate the specificity of the C11_Fab Q-body, as a single amino acid change in the mouse epitope abrogates the binding of DO-1 (Cohen et al., 1998). As shown in Figure 3-3b, a remarkable dose-dependent increase up to 27-fold in fluorescence intensity upon the addition of the human p53 peptide was observed, while negligible fluorescence improvement was observed upon adding the mouse p53 peptide. The EC_{50} and LOD of the Fab Q-body for the human p53 peptide were calculated as 60 nM and 0.72 nM, respectively (Figure 3-3c). Compared with the single-labeled scFv Q-body, the double-labeled C11_Fab Q-body showed a remarkable improvement in the maximum response and sensitivity (LOD = 0.72 nM). These results indicate that a sensitive and target-specific Q-body with a high antigen-dependent turn-on signal was developed.

3.3.4 Compare the fluorescence spectra of C11_scFv and C11_Fab Q-bodies

The basic fluorescence spectroscopy characterization of the C11_scFv and C11_Fab Q-bodies were measured using a spectrofluorometer (FP-8500). As shown in Figure 3-4, in the absence of antigen, the fluorescence intensity of the C11_scFv Q-body (F.I. ≈ 658) was higher than that of the C11_Fab Q-body (F.I. ≈ 119), suggesting that the C11_Fab possess a higher quenching efficiency in comparison to the C11_scFv. Besides, a much stronger antigen-dependent fluorescent enhancement was observed in the C11_Fab Q-body (maximum 17.7-fold) in comparison to the corresponding scFv Q-body (maximum 1.74-fold). The C11_Fab Q-body showed a 10-fold higher response than C11_scFv Q-body. These results indicate that the double labeled Q-body shows a better antigen-dependent fluorescence enhancement and deeper quenching efficiency. According to the references, the higher quenching efficiency and antigen-dependent response of the double-labeled C11_Fab Q-body are derived from the H-dimer formation of TAMRA (Abe et al., 2014; Ogawa et al., 2009).

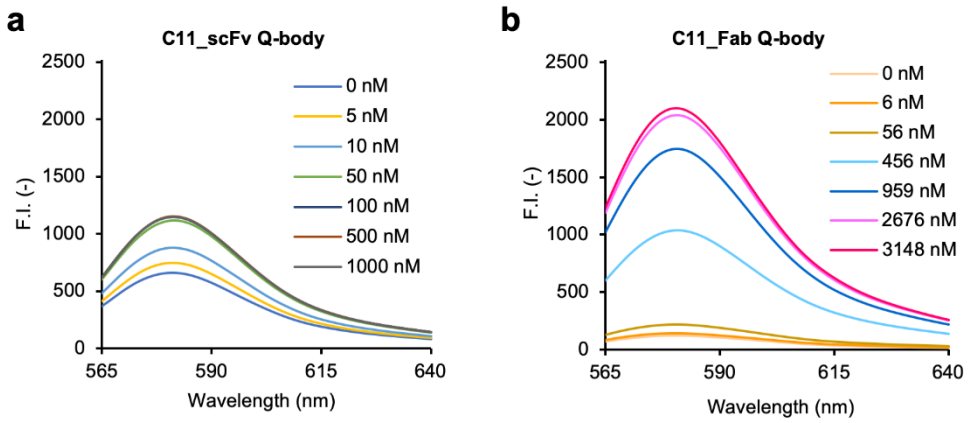

Figure 3-4. Antigen-dependent fluorescence spectra of C11_scFv and C11_Fab Q-bodies with excitation wavelength at 545 nm in the presence of different concentrations of human p53 peptide.

3.3.5 Antigen-Binding Kinetics of C11_Fab and its double-labeled Q-body

To investigate the influence of dye labeling on antigen-binding activity, the binding kinetics of C11_Fab and its Q-body were evaluated by the bio-layer interferometry assay

with immobilized biotinylated human p53 peptide. As shown in Figure 3-5, the K_D values of unlabeled C11_Fab (3.0 nM) and C11_Fab Q-body (3.3 nM) were not significantly different. This indicated minimal perturbation of the antigen-binding affinity due to the dye labeling of C11_Fab. In some extents, this result is consistent with a publication (Ning et al., 2021). In Table 1 of this publication, although the double-labeled mutant Fab Q-bodies showed lower K_D values compared with the corresponding unlabeled Fabs, its WT Fab Q-body had a similar K_D value to the corresponding unlabeled WT Fab. It indicates that the K_D value of Fab before and after labeling are antibody structure dependent.

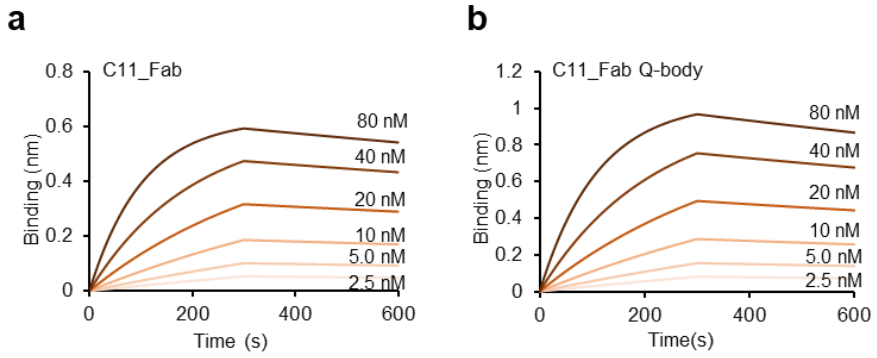

c

	K_D (nM)	k_{on} (10^5/Ms)	k_{off} (10^{-4} 1/s)	Full R^2
C11_Fab	3.03±0.11	1.10±0.007	3.33±0.12	0.985
C11_Fab Q-body	3.34±0.10	1.09±0.007	3.65±0.10	0.991

Figure 3-5. Binding of C11_Fab DO-1 to the human p53 peptide evaluated by Biolayer Interferometry. The biotinylated human p53 peptide were immobilized on a streptavidin biosensor to capture unlabeled C11_Fab or double-labeled C11_Fab Q-body. a-b) Time-dependent binding of C11 Fab (a) or corresponding Q-body (b). c) The kinetic constants, k_{on}, k_{off}, and K_D values, and the fitting parameters for the unlabeled and double-labeled C11_Fabs. Data are presented by the mean ± SD.

3.3.6 Absorbance spectrum and F/P ratio of the C11_Fab Q-body

To understand the quenching mechanism of the C11_Fab Q-body, the absorbance spectra of self-quenched and antigen-activated forms of Q-bodies were measured using a UV-VIS spectrometer. As shown in Figure 3-6, compared with the free fluorophore (TAMRA-LPETGG), the self-quenched Q-body showed two peaks with maximum absorbance at 520 nm (H-dimer) and 555 nm (monomer) (Ogawa et al., 2009), respectively. While the addition of p53 peptide led to the 520 nm peak shift and the maximum absorbance at 555 nm increased (Figure 3-6a). The results suggested that apart from Trp residues (Abe et al., 2011), H-dimer formation also contributed to the fluorescent quenching in the C11_Fab Q-body. Based on the absorbance spectra of the C11_Fab Q-body (Figure 3-6a), the fluorescent dye to protein ratio (F/P) was calculated as 190% for the self-quenched form of Q-body and 218% for the activated form of Q-body (Table 3-2). The slight increase of the F/P ratio after the addition of the antigen might be due to the environmental changes of TAMRA (exposure to solution) which generate a higher absorbance in comparison to the TAMRA in a quench state. Taking together, these results indicated that the C11_Fab was well labeled with TAMRA and

both intrinsic Trp residues and dye-dye interactions contributed to fluorescent dye quenching in Q-bodies.

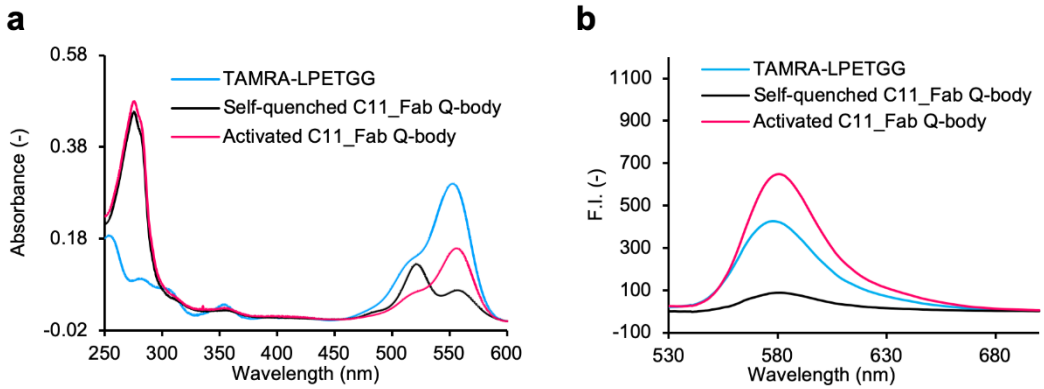

Figure 3-6. Absorbance spectra and quantum yields of self-quenched and activated forms of C11_Fab Q-bodies. a) Absorbance spectra of TAMRA-LPETGG (5 μM), self-quenched (1.56 μM) and human p53 peptide (4 μM)-activated forms of C11_Fab Q-bodies. The addition of antigen reduced the absorption at 520 nm (H-dimer TAMRA) while increased that at 555 nm (monomer TAMRA), indicating the quenching of the Q-body at least partially derived from the H-dimer formation of TAMRA. b) Fluorescence spectra of TAMRA-LPETGG, self-quenched and human p53 peptide activated forms of C11_Fab Q-bodies at an excitation wavelength of 500 nm.

Table 3-2. Fluorescent dye to protein (F/P) ratio of C11_Fab Q-body

	Self-quenched C11_Fab Q-body	Activated C11_Fab Q-body
A_{520}	0.124	0.0638
A_{555}	0.0675	0.159
Conc. of C11_Fab Q-body (μM)	1.56	1.56
F/P ratio (%)	190	218

3.3.7 Quantum yield of the C11_Fab Q-body

The QY of a fluorophore is defined as the ratio of the photons emitted to the photons absorbed after being excited by a specific light (Lakowicz, 2006). The quantum yield is proportional to the fluorescence intensity, which reflects the nature of a fluorophore. Understanding the QY of the C11_Fab Q-body between before and after the addition of the human p53 peptide could help people to know their property changes between these two states. Here, a free fluorophore, TAMRA-LPETGG, was employed as a reference to calculate the relative QY of the self-quenched and activated forms of C11_Fab Q-bodies. The absolute QY of the free dye was measured as 0.37 with excitation at 500 nm (Figure 3-7). As described in materials and methods section, the QY of the two forms of Q-bodies were

determined as 0.051 and 0.45, respectively (Figures 3-6a and 3-6b, and Table 3-3). The quantum yields increased 8.8-fold after adding antigen. This is slightly higher than the fluorescence changes (7.3-fold) shown in Figure 3-6b. The difference might result from the error during quantum yields detection because many factors, such as temperature, solvent, phase, and pH, affect the fluorescence QY.

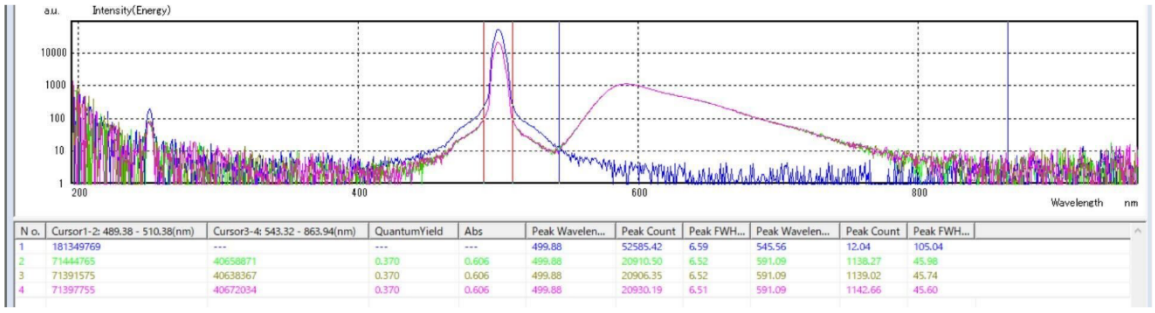

N o.	Cursor1-2: 489.38 - 510.38(nm)	Cursor3-4: 543.32 - 863.94(nm)	QuantumYield	Abs	Peak Wavelen...	Peak Count	Peak FWH...	Peak Wavelen...	Peak Count	Peak FWH...
1	181349769	---	---	---	499.88	52585.42	6.59	545.56	12.04	105.04
2	71444765	40658871	0.370	0.606	499.88	20910.50	6.52	591.09	1138.27	45.98
3	71391575	40638367	0.370	0.606	499.88	20906.35	6.52	591.09	1139.02	45.74
4	71397755	40672034	0.370	0.606	499.88	20930.19	6.51	591.09	1142.66	45.60

Figure 3-7. The raw data for the absolute quantum yield measurement of TAMRA-LPETGG (8.3 μM) in PBST (PBS containing 0.05% Tween 20, pH 7.4) at excitation wavelength of 499.88 nm (≈ 500 nm). The blue line represents the blank (PBST only). The lines in green, brown, and purple show three measurements of the same sample.

Table 3-3. Quantum yields (QY) of the self-quenched and activated forms of C11_Fab Q-bodies.

	TAMRA-LPETGG		Self-quenched C11_Fab Q-body		Activated C11_Fab Q-body	
	Absorbance ($M^{-1}cm^{-1}$)	Integrated F.I. (–)	Absorbance ($M^{-1}cm^{-1}$)	Integrated F.I. (–)	Absorbance ($M^{-1}cm^{-1}$)	Integrated F.I. (–)
Ex. 500 nm	15,650	19,797	15,650	2,753*	15,650	24,058*
QY	0.37		0.051		0.45	

* The value was adjusted to match their absorbance. For example, the absorbance and integrated F.I. of 2 nM self-quenched C11_Fab Q-body were 24,150 ($M^{-1}cm^{-1}$) and 4,235 (–), respectively. To calculate QY, its absorbance was unified as 15,650 ($M^{-1}cm^{-1}$) (the absorbance of TAMRA-LPETGG) and then the corresponding integrated F.I. was calculated as 2,753 (–) and used for the QY calculation of the self-quenched C11_Fab Q-body.

3.4 Summary of Chapter 3

In this Chapter, to construct a high-performance Q-body (high sensitivity, high response, and high specificity) for live-cell imaging, three Q-bodies were prepared. Firstly, to investigate the effect of mutation introduction in the C11 mutant, the responses of two single-labeled WT_scFv and C11_scFv Q-bodies were evaluated. According to their EC_{50} (0.78 nM vs 1.6 nM), LOD (0.028 nM vs 0.076 nM), and maximum response (2.0-fold vs 1.9-fold) against human p53 peptide, there are no big differences between these two Q-bodies.

Considering the higher secretory productivity of C11_scFv, further optimization of the C11 mutant Q-body was conducted. A double-labeled C11_Fab Q-body was prepared, which showed a remarkable increase of antigen-dependent fluorescence enhancement (27-fold) with high sensitivity (LOD = 0.72 nM) and specificity (does not respond to murine p53 peptide). Besides, the QY of the quenching and dequenching forms of C11_Fab Q-bodies was discussed. This is the first time to discuss the QY of the Q-body in the development history of the Q-body technology. In one word, a high-performance C11_Fab Q-body was successfully developed.

3.5 References

Abe, R., Jeong, H.J., Arakawa, D., Dong, J., Ohashi, H., Kaigome, R., Saiki, F., Yamane, K., Takagi, H., and Ueda, H. (2014). Ultra Q-bodies: quench-based antibody probes that utilize dye-dye interactions with enhanced antigen-dependent fluorescence. Sci Rep *4*, 4640.

Abe, R., Ohashi, H., Iijima, I., Ihara, M., Takagi, H., Hohsaka, T., and Ueda, H. (2011). "Quenchbodies": Quench-Based Antibody Probes That Show Antigen-Dependent Fluorescence. Journal of the American Chemical Society *133*, 17386-17394.

Christie, R.J., Tadiello, C.J., Chamberlain, L.M., and Grainger, D.W. (2009). Optical properties and application of a reactive and bioreducible thiol-containing tetramethylrhodamine dimer. Bioconjug Chem *20*, 476-480.

Cohen, P.A., Mani, J.C., and Lane, D.P. (1998). Characterization of a new intrabody directed against the N-terminal region of human p53. Oncogene *17*, 2445-2456.

Dong, J., and Ueda, H. (2021). Recent Advances in Quenchbody, a Fluorescent Immunosensor. Sensors (Basel) *21*.

Jeong, H.-J., Kojima, T., Dong, J., Ohashi, H., and Ueda, H. (2016). One-pot construction of Quenchbodies using antibody-binding proteins. Analytical Methods *8*, 7774-7779.

Jeong, H.J., Abhiraman, G.C., Story, C.M., Ingram, J.R., and Dougan, S.K. (2017). Generation of Ca2+-independent sortase A mutants with enhanced activity for protein and cell surface labeling. PLoS One *12*, e0189068.

Lakowicz, J.R. (2006). Principles of Fluorescence Spectroscopy Vol 3rd Edn.

Ning, X., Yasuda, T., Kitaguchi, T., and Ueda, H. (2021). Construction of Fluorescent Immunosensor Quenchbody to Detect His-Tagged Recombinant Proteins Produced in Bioprocess. Sensors (Basel) *21*.

Ogawa, M., Kosaka, N., Choyke, P.L., and Kobayashi, H. (2009). H-Type Dimer Formation of Fluorophores: A Mechanism for Activatable, in Vivo Optical Molecular Imaging. Acs Chemical Biology *4*, 535-546.

Ravasco, J., Faustino, H., Trindade, A., and Gois, P.M.P. (2019). Bioconjugation with Maleimides: A Useful Tool for Chemical Biology. Chemistry *25*, 43-59.

Takahashi, R., Yasuda, T., Ohmuro-Matsuyama, Y., and Ueda, H. (2021). BRET Q-Body: A Ratiometric Quench-based Bioluminescent Immunosensor Made of Luciferase-Dye-Antibody Fusion with Enhanced Response. Analytical Chemistry *93*, 7571-7578.

Theile, C.S., Witte, M.D., Blom, A.E.M., Kundrat, L., Ploegh, H.L., and Guimaraes, C.P. (2013). Site-specific N-terminal labeling of proteins using sortase-mediated reactions. Nature Protocols *8*, 1800-1807.

Chapter 4. Visualization of p53 in fixed cells using C11_Fab Q-body

4.1 Introduction

Immunofluorescence (IF) is a powerful technique that allows the visualization of various components in tissue sections or cells (Henchal et al., 1983). This technique relies on the use of fluorescent dyes labeled antibodies to visualize the target antigens by a fluorescent microscope. Based on whether the detection antibody directly binds to the target antigen, the IF approach is divided into two types, called direct IF (the primary antibody is directly labeled with fluorescent dye) (Zhang et al., 2022) or indirect IF (the fluorophore is labeled on the secondary antibody that recognizes the primary antibody) (Stiernstedt et al., 1985). In the standard procedures of the traditional IF assay, the sample must be blocked to avoid binding to non-target epitopes present after fixation and washing steps are necessary to remove unbound or non-specific bound antibodies. In the conventional IF assay, these two steps are necessary due to the detection antibodies which always show fluorescent signals irrespective of presenting the target epitopes.

As aforementioned, p53 is regarded as a guardian of the genome and plays pivotal roles in cancer studies, diagnostics, and therapeutics (Hernandez Borrero and El-Deiry, 2021). In normal tissues, the lifetime of p53 is short due to the MDM2 (an E3 ubiquitin ligase) mediated protein degradation (Chene, 2003). However, in tumor tissues, p53 level is upregulated. Although the IF assay for p53 could not be used to accurately diagnose most of cancers (Fadare et al., 2018), it still plays a crucial role in evaluation of the prognosis for oral squamous cell carcinoma (Cutilli et al., 2016) and basic cancer studies (Bonini et al., 2004; Timofeev et al., 2019).

In this study, to investigate if the C11_Fab Q-body is stable enough and able to visualize endogenous p53 protein, the fixed cell direct IF assay (Q-body staining assay) was performed in a time-saving manner (skip blocking and washing steps). A representative of a traditional probe (C11_scFv-TAMRA, a non-switchable probe) was employed as a control. The S/B ratios of both probes (C11_Fab Q-body and C11_scFv-TAMRA) were calculated to compare their performance in fixed cell staining assay. The corresponding western blot was performed to verify the reliability of the Q-body staining assay.

4.2 Materials and method

4.2.1 Materials

McCoy's 5A (Modified) Medium (Gibco), penicillin- streptomycin (Gibco). The other materials are the same with the previous chapter.

Other chemicals were obtained from Wako Pure Chemicals except as otherwise stated.

4.2.2 Oligonucleotides

These following two primers were used for the construction of plasmid pET26-G3-C11_scFv-Cys

VH(DO1)-AgeI-back:

5′-CTCTAATGAGACCGGTCAGGTTACTCTGAAAGAGTCTGG-3′

VL(DO1)-Cys-Xho-for:

5′-GGTGGTGGTGCTCGAGGCAACCTCCCCGTTTCAGCTCCAGCTTG-3′

4.2.3 Preparation of C11_scFv-TAMRA

To generate a C-terminal fluorescence dye-labeled C11_scFv-TAMRA probe representing a traditional immunofluorescence reagent, the pET26-G3-C11_scFv was used as a template to make pET26-G3-C11_scFv-Cys plasmid. The G3-V_HV_L(C11)-DO-1-Cys gene fragment attached with a cysteine at the C-terminal of VL was amplified by PCR using primers VH(DO-1)-AgeI-Back and VL(DO-1)-Cys-Xho-For. The PCR product was inserted into RE AgeI and XhoI digested pET26b vector via an In-Fusion HD cloning kit to produce pET26-G3-C11_scFv-Cys plasmid. As aforementioned, the product was sequenced to obtain the pET26-G3-C11_scFv-Cys plasmid.

Maleimide thiol reaction was employed to prepare single-labeled C11_scFv-TAMRA. The His-tag purified C11_scFv-Cys protein (250 μL 2 μM) in a 1.5 mL Eppendorf was mixed with tris (2-carboxyethyl) phosphine -hydrochloride (TCEP-HCl) (final concentration, 2.5 mM) and rotated at RT for 30 min with aluminum foil wrapped to reduce the possible disulfide bond formed at the C-terminal cysteine. Then the excess TCEP was inactivated by adding 4-azidobenzoic acid (ABA), pH 7.0, at a final concentration of 10 mM, and the reaction mixture was kept on ice for 10 min. Afterward, 5-TAMRA C6 was added (the molar ratio of 5-TAMRA C6 to protein is 20:1) and rotated at RT for 2 h avoiding light. Next, FLAG-tag purification was performed as aforementioned. The FLAG-tag purified C11_scFv-TAMRA was stored with 15% glycerol at −30 °C. The concentration C11_scFv-TAMRA was determined by SDS-PAGE as described in Section 3.2.6.

4.2.4 Cell culture

Five cell lines, including HCT116 $p53^{+/+}$, HCT116 $p53^{-/-}$, SK-BR-3, and WiDr were used in this study. HCT116 is a human colon cancer cell line, HCT116 $p53^{+/+}$ cells harbor wild-type p53 while the p53 genes in HCT116 $p53^{-/-}$ cells are knocked-out. SK-BR-3 (HTB30), a human breast adenocarcinoma cell line harboring mutant p53 (R175H) was purchased from ATCC (American Type Culture Collection). WiDr (JCRB0224), a human colon cancer cell line harboring mutant p53 (R273H) was obtained from the JCRB (Japanese Collection of Research Bioresources) cell bank. The former two cell lines were grown in McCoy's 5A (Modified) Medium supplemented with 10% heat-inactivated fetal bovine serum, 100 units/mL penicillin, and 100 μg/mL streptomycin and incubated in a humidified incubator with 5% CO_2 at 37 °C. The other two cell lines were cultured in a DMEM medium containing the same supplementary and in an incubator with the same settings. Cells were seeded at a density of 1.2×10^5 cells/mL in 100 mm, 60 mm, or tiple-well glass base dishes. The cells were harvested using 0.25% trypsin-EDTA (Sigma) and divided into fractions used for sub-culture or experiments once reached 70–90% confluence.

4.2.5 Immunofluorescence assay for fixed cells

4.2.5.1 Conventional immunofluorescence assay for fixed cells

For conventional IF fixed cell staining assay, HCT116 $p53^{+/+}$ and HCT116 $p53^{-/-}$ cells were cultured in a triple-well glass-based ø11 mm dish (Iwaki Technoglass, Tokyo, Japan) as aforementioned. After the cells reached 70–90% confluence, the cells were gently washed twice with PBS and fixed with 4% PFA (paraformaldehyde, in PBS) at RT for 15 min. To remove the trace of PFA, the cells were washed three times (5 min/wash) with 0.1% PBST (containing 0.1% Triton-X100). After washing, the cells were exposed to 0.5% PBST (containing 0.5% Triton-X100) and kept at RT for 10 min to make the cell membrane permeable. Next, 5% BSA 0.1% PBST was added as a blocking reagent to block the well at RT for 1 h. Afterwards, the cells were incubated with the primary antibody [mouse DO-1 IgG diluted in blocking buffer (1:500)] at RT for 1 h. Then the cells were exposed to the secondary antibody [goat anti-mouse IgG FITC diluted in blocking buffer (1:1000)] at RT for 1 h after washing with 0.1% PBST. At the last 10 min of the one-hour treatment, 1 μg/mL Hoechst 33342 was added to stain the cell nucleus. To compare the importance of last washing (after treated with secondary antibody), the images of the cells both before (without washing off secondary antibody) and after (washed with 0.1% PBST three times, 5 min/wash) washing were taken by a fluorescence microscope [(Olympus IX71, lens: UPlanSApo 100X/1.4 Oil ∞/0.17/FN26.5, camera: maGEM EM-CCD (Hamamatsu Photonics, Japan), Cube name: U-MWIY2/Ex. filter: 545-580 nm/Em. Fil-ter: 610IF]

4.2.5.2 One-step immunofluorescence assay using Q-body for fixed cells

For the corresponding fixed cell Q-body staining assay, the indicated cells were cultured as the same as described in Section 4.2.4. For "visualization of p53 levels under different treatment conditions in fixed HCT116 $p53^{+/+}$ cells using C11_Fab Q-body", the cells were first treated with 12 μM nutlin-3a or 0.06% ethanol for 16 h after reaching 60% confluence. Then, they were treated with 6 μM cisplatin (dissolved in PBS, 1 mg/mL) or vehicle for 12 h. In the one-step IF Q-body assay, the cells were washed twice with PBS. Then, 100% methanol stored at -30°C was used to fix and permeabilize cells at 4°C for 15 min. Followed by washing three times with PBS, the cells were then treated with 40 nM C11_Fab Q-body or C11_scFv-TAMRA which were diluted in PBS containing 1% BSA, 0.1% Triton-X100 at RT for 1 h. Hoechst 33342 at 1 μg/mL was used to stain the cell nucleus. The fluorescence signals of cells were observed by microscope (Olympus IX71) without washing unbound fluorescence probes out.

4.2.6 Western blotting

Cells were seeded in a 100 mm tissue culture dish. Two dishes were prepared for each cell type. After cell confluence reached 70%, they were treated with 12 μM of nutlin-3a or 0.06% ethanol for 16 h. Cells were harvested with 0.25% trypsin/EDTA and washed with ice-cold PBS twice. The radioimmunoprecipitation assay lysis buffer (Santa Cruz, USA) was added to extract cellular protein. After centrifugation, supernatants were collected, and Bradford Protein Assay (Bio-Rad) was performed to determine total protein concentrations.

Proteins (40 μg) were denatured in 4× SDS loading buffer at 95 °C for 5 min and separated via a 12% SDS-PAGE gel. Then the proteins were transferred to nitrocellulose membranes (Bio-Rad, Tokyo, Japan). The membranes were blocked with Tris Buffer Saline Tween (TBST, containing 0.1% Tween 20) containing 5% skimmed milk (Fujifilm-Wako) at RT for 2 h, following incubation for 2 h at 25 °C with mouse monoclonal DO-1 (1:1000) in 5% skimmed milk- TBST. After washing three times (5 min each) with TBST, the membranes were incubated with secondary antibody HRP-conjugated goat anti-mouse Ig's (BioSource, Thermo-Fisher, Camerillo, CA) in 5% BSA TBST at RT with gentle shaking for 1 h. Unbound secondary antibodies were removed by washing as aforementioned before visualization using the Amersham^{TM} ECL^{TM} Prime Western Blotting Detection Reagent (GE Healthcare, UK) according to its manual.

4.3 Results and discussion

4.3.1 Evaluation of the expression pattern of p53 in HCT116 cell line

To evaluate the expression pattern of p53 in HCT116 $p53^{+/+}$ and HCT116 $p53^{-/-}$ cells, the conventional IF staining assay was performed using mouse DO-1 IgG and goat anti-mouse IgG-FITC as the primary and secondary antibodies, respectively. The cells both with and without washing were observed and their images were shown in Figure 4-1. As shown in these results, a high background signal was observed in the cells without washing. After washing, the background signal was clearly reduced. In HCT116 $p53^{-/-}$ cells, almost no signals can be observed. While in HCT116 $p53^{+/+}$ cells, the fluorescent signals predominately resided in the nucleus and showed various intensities of cells dependently. These results indicate that in the traditional IF assay, washing steps for removing secondary antibodies are necessary to improve the S/B ratio, and the expression levels of p53 in HCT116 $p53^{+/+}$ cells are various cells dependently.

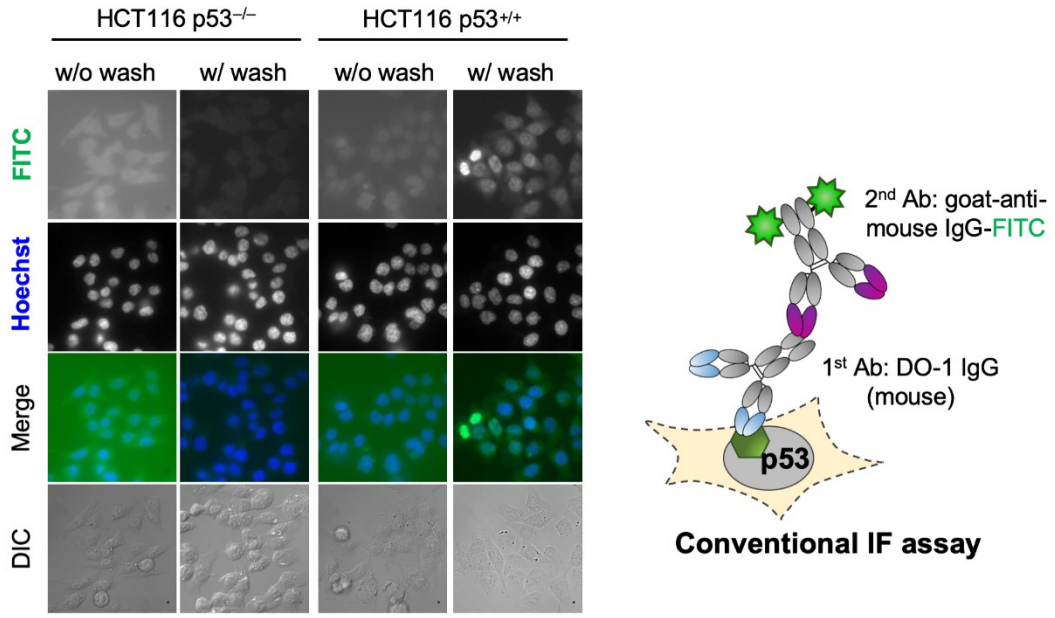

Figure 4-1. Visualization of p53 in fixed cells using conventional immunofluorescence assay. The cells were fixed using 4% PFA and permeabilizated using 0.5% PBST (containing 0.5%). Mouse DO-1 IgG, and goat anti-moues IgG FITC were used as the primary and secondary antibodies, respectively. w/o wash, cells were not washed after being treated with the secondary antibody. w/ wash, cells were washed with PBST three times after being treated with the secondary antibody. FITC, p53. Hoechst, nucleus stained with Hoechst 33342 (1 μg/mL); Merge, overlapped FITC channel with Hoechst channel. DIC, differential interference contrast channel. Microscope: Olympus IX71. Scale bar, 10 μm.

4.3.2 Performance of C11_Fab Q-body in fixed cells staining assay

After obtaining a high-performance Fab Q-body, we first applied it to the visualization of p53 in fixed cells as a direct immunofluorescence (DIF) probe in IF imaging in a more time-saving manner. We expected that the Q-body would be in an "On" status only in the presence of p53. To verify this, all IF assays were performed without blocking (before probe treatment to prevent non-specific binding of probes) and washing (after probe treatment to remove unbound probes). A human colon cancer cell line, HCT116 $p53^{+/+}$ and its subtype HCT116 $p53^{-/-}$ (p53 gene was knocked out) were used to verify our assumption. Nutlin-3a, an MDM2 inhibitor, was used to increase the p53 levels. An outline of this experiment is shown in Figure 4-2a. As indicated in Figure 4-2b and 4-2c, negligible signals were observed in HCT116 $p53^{-/-}$ cells stained with Fab Q-bodies no matter treated with or without nutlin-3a. Notably, the fluorescence signals in HCT116 $p53^{+/+}$ cells were significantly higher than those in $p53^{-/-}$ cells (2.4-fold) and showed a remarkable improvement upon nutlin-3a treatment (8.3-fold). Fluorescence signals were observed in the nucleus, where p53 predominantly resides which were consistent with the results using the traditional IF assay (Figure 4-1).

However, when the cells were stained with C11_scFv-TAMRA (a representative of a traditional IF probe that shows no signal switching function because TAMRA was labeled at

the C-terminus of the light chain far from the antigen-binding site), a high background signal was observed even in $p53^{-/-}$ cells. The difference in the mean F.I. of nuclei between $p53^{+/+}$ and $p53^{-/-}$ cells stained with C11_scFv-TAMRA (3.8-fold) was lower than that of the C11_Fab Q-body (8.3-fold). These results verify that the C11_Fab Q-body displays an antigen-dependent signal on fixed human colon cancer cells and shows a higher S/B ratio than the traditional IF probe (C11_scFv-TAMRA).

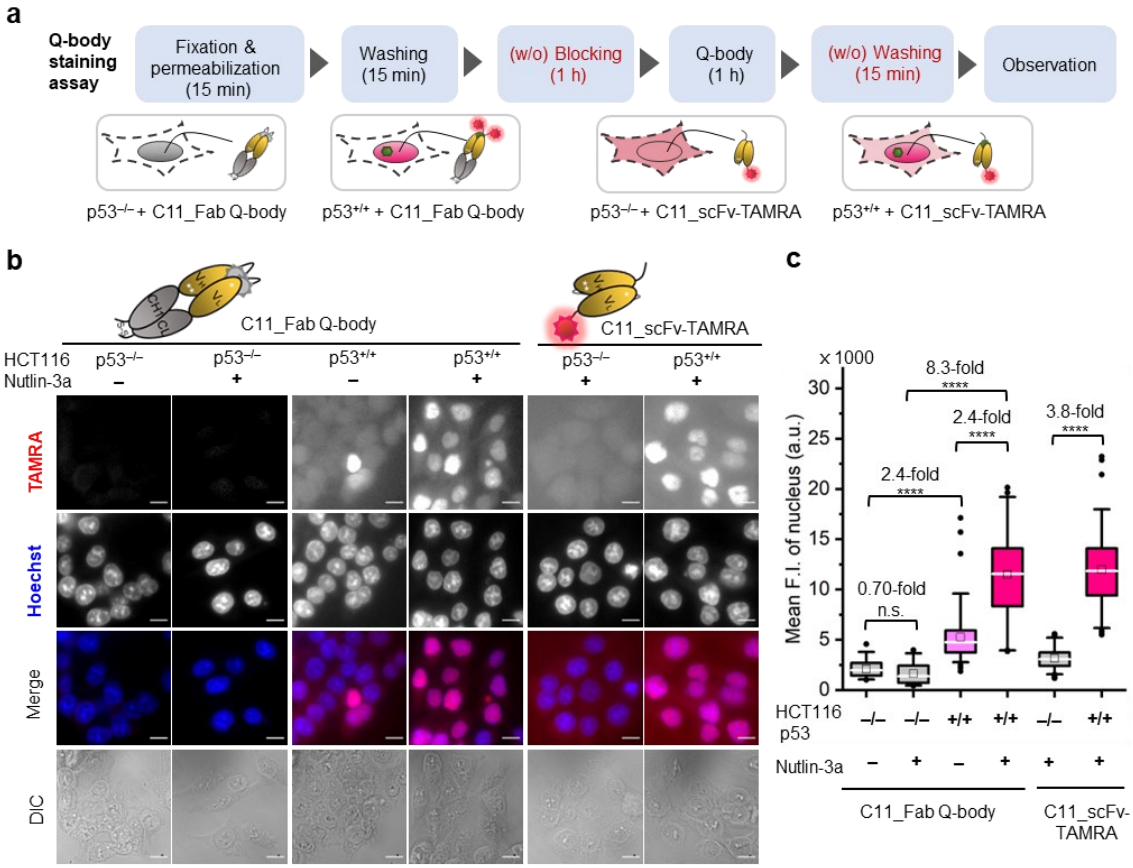

Figure 4-2. Wash-free visualization of p53 in fixed human cancer cells using C11_Fab Q-body. HCT116 $p53^{-/-}$ or $p53^{+/+}$ are human colon cancer cell lines. A representative of a traditional direct immunofluorescence probe C11_scFv-TAMRA was applied as a control to compare the performance of the C11_Fab Q-body. Nutlin-3a, an MDM2 inhibitor, was used to stabilize the p53 protein and improve p53 levels. a) Schematic of wash-free fixed cell staining assay by C11_Fab Q-body andC11_ scFv-TAMRA in a time-saving manner. b) Representative images showing 40 nM C11_Fab Q-body or C11_scFv-TAMRA staining of p53 in HCT116 $p53^{-/-}$ or $p53^{+/+}$ cells after being treated with 12 μM nutlin-3a or 0.06% ethanol for 16 h. TAMRA (red), C11_Fab Q-body or C11_scFv-TAMRA; Hoechst (blue), 1 μg/mL Hoechst 33342; Merge, overlapped TAMRA with Hoechst; DIC, differential interference contrast. Microscope: Olympus IX71. Scale bar, 10 μm. c) Box plot of mean TAMRA intensities in the nucleus subtracted to minimum fluorescence intensities (F.I.) of TAMRA channel. The median F.I. was used to calculate their fluorescence changes between groups. The first four boxes: one-way ANOVA test; the last two boxes: Welch's *t*-test.

****p<0.0001; n.s., not significant; from left to right, n=39, 36, 78, 53, 83, 79 cells. For the box plot, the white line indicates the median, the box indicates 25–75% range, whiskers indicate 1.5 interquartile range, and the black dot indicates outliers.

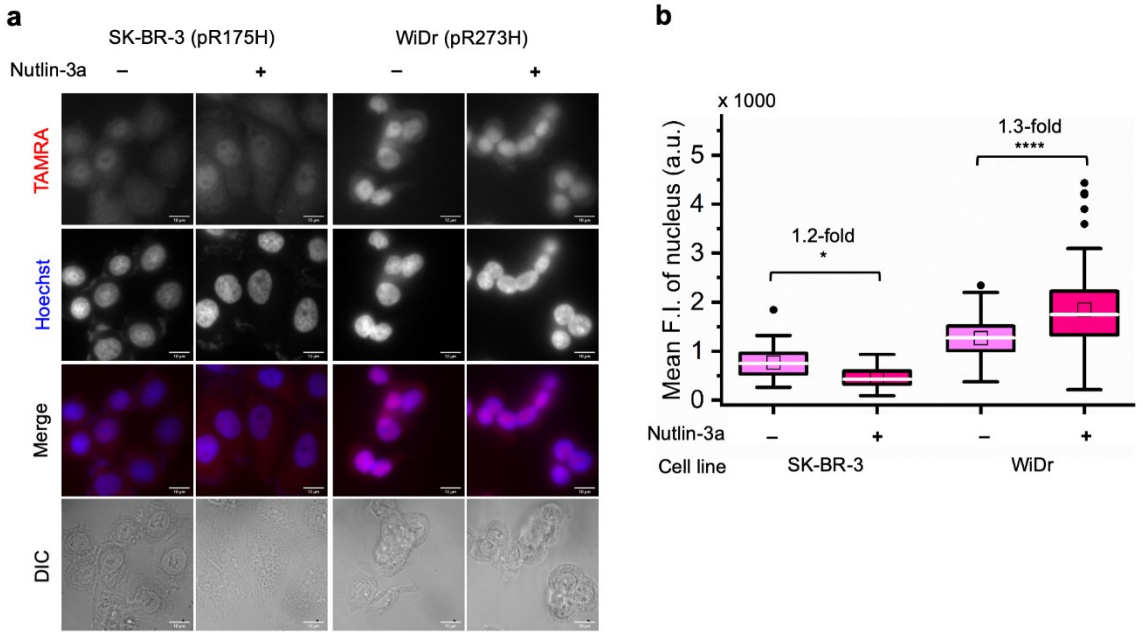

Figure 4-3. Wash-free visualization of p53 in fixed cancer cells using the C11_Fab Q-body. SK-BR-3 is a human breast cancer cell line that expresses mutant p53 (pR175H). WiDr is a colon adenocarcinoma cell line harboring mutant p53 (pR273H). Nutlin-3a, an MDM2 inhibitor, inhibits MDM2-p53 interactions to stabilize the p53 protein and increase p53 levels. a) Representative images showing 40 nM C11_Fab Q-body staining of fixed human cancer cell lines after being treated with 12 μM nutlin-3a or 0.06% ethanol for 16 h. TAMRA channel, the signal from C11_Fab Q-body or C11_scFv-TAMRA. Hoechst, nucleus stained with Hoechst 33342 (1 μg/mL). Merge, overlapped TAMRA channel with Hoechst channel. DIC, differential interference contrast channel. Microscope: Olympus IX71. Scale bar,10 μm. c) Box plot of mean TAMRA intensities in the nucleus subtracted by minimum fluorescence intensities (F.I.) of TAMRA channel. The median F.I. was used to calculate their fluorescence changes between groups. Welch's t-test. *0.01< p <0.05, ****p <0.0001; from left to right, n = 71, 48, 57, 52 cells. For the box plot, the white line indicates the median, the box indicates 25–75% range, whiskers indicate 1.5 interquartile range and the black dot indicates outliers.

I further investigated the efficacy of the Fab Q-body in the detection of mutant p53 in fixed samples. SK-BR-3 human breast cancer cells (p53, pR175H) and WiDr human colon adenocarcinoma cells (p53, pR273H) were used in the IF assay. As shown in Figure 4-3, in Fab Q-body-treated SK-BR-3 and WiDr cells, the fluorescence signal was observed and showed no significant differences with or without nutlin-3a treatment. As expected, the Fab Q-body showed no fluorescence enhancement in mouse cell lines. These results are

consistent with previous publications stating that nutlin-3a does not affect p53 levels in cells harboring mutant p53 (pR273H) (Miyachi et al., 2009). It demonstrated that the Fab Q-body was able to specifically visualize both human WT and mutant p53 in a time-saving manner.

4.3.3 Western blotting

The western blot is a golden analytical technique that is widely used in molecular biology to detect specific proteins. To evaluate the performance of the Q-body staining assay, the western blot assay was performed using DO-1 IgG as the primary antibody to detect p53 levels expressed in HCT116 $p53^{-/-}$, HCT116 $p53^{+/+}$, SK-BR-3, and WiDr cells under the treatment with or without nutlin-3a. As shown in Figure 4-4, obviously, no band was observed in HCT116 $p53^{-/-}$ cells irrespective of nutlin-3a. In HCT116 $p53^{+/+}$ cells, nutlin-3a treatment increased the blot intensity (2.9-fold). While the blot intensity was almost no changes after treatment with the nutlin-3a in both SK-BR-3 (1.1-fold) and WiDr (0.9-fold) cells. These results indicate that the nutlin-3a increases the p53 expressing levels in HCT116 $p53^{+/+}$ cells, but it does not affect p53 levels in SK-BR-3 and WiDr cells and the DO-1 antibody does not recognize murine p53, which is consistent with the conclusion from Q-body staining assay.

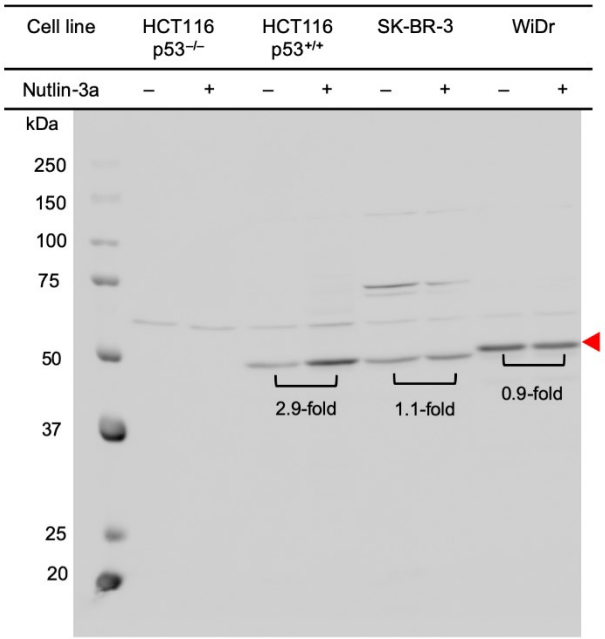

Figure 4-4. Evaluation of p53 levels of different cell lines treated with or without nutlin-3a by western blot assay. The cells were treated with 12 μM nutlin-3a or vehicle ethanol for 16 h before extracting total proteins. Protein loading for each sample is 40 μg. A mouse anti-p53 (Human) mAb DO-1 IgG2a (1:1000) was added as a primary antibody. A goat anti-mouse Ig's HRP (1:3000) was used as a secondary antibody. The gray value of bands was semi-quantified using CSA analyzer software. The fold changes between with and without nutlin-3a treatment of each cell line were calculated as shown in this figure.

4.4 Summary of Chapter 4

In this chapter, to evaluate the performance of the double-labeled C11_Fab Q-body as

a wash-free DIF probe in the visualization of p53 in fixed cells, the one-step fixed cell IF assay was performed. A corresponding single-labeled C11_scFv-TAMRA was used as a representative of a traditional DIF probe. Compared with the C11_scFv-TAMRA probe (3.8-fold), the C11_Fab Q-body (8.3-fold) showed a higher S/B ratio in detecting WT p53 levels in fixed HCT116 cells. And this Q-body was verified to visualize mutant p53 in the SK-BR-3 and WiDr cells. These results indicated that the high specificity of the C11_Fab Q-body in detecting DO-1 epitope p53. The golden protein detection method, western blot, was also performed and it identified the reliability of C11_Fab Q-body in detecting p53 expression levels. To sum up, the C11_Fab Q-body, a new generation of IF probes, could be successfully applied to specifically visualize both human WT and mutant p53 in a time-saving manner.

4.5 References

Bonini, P., Cicconi, S., Cardinale, A., Vitale, C., Serafino, A.L., Ciotti, M.T., and Marlier, L.N. (2004). Oxidative stress induces p53-mediated apoptosis in glia: p53 transcription-independent way to die. J Neurosci Res *75*, 83-95.

Chene, P. (2003). Inhibiting the p53-MDM2 interaction: an important target for cancer therapy. Nat Rev Cancer *3*, 102-109.

Cutilli, T., Leocata, P., Dolo, V., and Altobelli, E. (2016). p53 as a prognostic marker associated with the risk of mortality for oral squamous cell carcinoma. Oncol Lett *12*, 1046-1050.

Fadare, O., Roma, A.A., Parkash, V., Zheng, W., and Walavalkar, V. (2018). Does a p53 "Wild-type" Immunophenotype Exclude a Diagnosis of Endometrial Serous Carcinoma? Adv Anat Pathol *25*, 61-70.

Henchal, E.A., Mccown, J.M., Seguin, M.C., Gentry, M.K., and Brandt, W.E. (1983). Rapid Identification of Dengue Virus Isolates by Using Monoclonal-Antibodies in an Indirect Immunofluorescence Assay. American Journal of Tropical Medicine and Hygiene *32*, 164-169.

Hernandez Borrero, L.J., and El-Deiry, W.S. (2021). Tumor suppressor p53: Biology, signaling pathways, and therapeutic targeting. Biochim Biophys Acta Rev Cancer *1876*, 188556.

Miyachi, M., Kakazu, N., Yagyu, S., Katsumi, Y., Tsubai-Shimizu, S., Kikuchi, K., Tsuchiya, K., Iehara, T., and Hosoi, H. (2009). Restoration of p53 Pathway by Nutlin-3 Induces Cell Cycle Arrest and Apoptosis in Human Rhabdomyosarcoma Cells. Clinical Cancer Research *15*, 4077-4084.

Stiernstedt, G.T., Granstrom, M., Hederstedt, B., and Skoldenberg, B. (1985). Diagnosis of Spirochetal Meningitis by Enzyme-Linked Immunosorbent-Assay and Indirect Immunofluorescence Assay in Serum and Cerebrospinal-Fluid. Journal of Clinical Microbiology *21*, 819-825.

Timofeev, O., Klimovich, B., Schneikert, J., Wanzel, M., Pavlakis, E., Noll, J., Mutlu, S., Elmshäuser, S., Nist, A., Mernberger, M*., et al.* (2019). Residual apoptotic activity of a tumorigenic p53 mutant improves cancer therapy responses. Embo j *38*, e102096.

Zhang, L., Li, M., Wu, Y.F., Hao, F., Wang, C., Han, W.X., Niu, D., and Zheng, W. (2022). Classification of renal biopsy direct immunofluorescence image using multiple attention convolutional neural network. Computer Methods and Programs in Biomedicine *214*.

Chapter 5. Visualization of p53 in living cells using C11_Fab Q-body

5.1 Introduction

Visualization of intracellular proteins in living cells is valuable for understanding the biological principles of cellular homeostasis, dysfunction, and protein dynamics. Fluorescent labeling of the POIs is crucial. Over the past decades, intrinsic probes such as genetically encoded FPs and self-labeling enzyme tags, such as SNAP-tag (Keppler et al., 2003) and HaloTag (Los et al., 2008), have been widely used for the localization of POIs in living cells. However, the fusion of bulky FPs or enzyme tags can result in protein misfolding, mistargeting, imprecise localization, or other artifacts. Currently, small epitope tags (such as split-GFP (Anson et al., 2021) and ultraviolet-photoswitchable protein-fluorophore tags (Sheng et al., 2018)) and modified amino acids (such as unnatural amino acid-mediated bio-orthogonal click reactions (Werther et al., 2021)) for specific labeling have been developed for precise visualization of endogenous proteins. Nevertheless, the difficulty of controlling overexpression, fluorescence non-switchable, and time-consuming protein expression (It usually takes 1–2 days for protein expression after DNA transfection) have limited their biological applications.

Alternatively, extrinsic probes, such as fluorescent dye(s)-conjugated antibody fragments, which include Fab, scFv, and Nb, are prominent tools for tracing intrinsic POIs owing to their high specificities and small sizes (12–55 kDa) (de Beer and Giepmans, 2020). Numerous high-quality antibody-based probes have been successfully developed and extensively applied to fixed and permeabilized cells, along with the cell surface imaging of live cells for many years (Liu et al., 2020b). However, their broad applicability for imaging intracellular analytes in living cells remains limited for two reasons: (i) fluorescent probes are always “On”, resulting in potentially high background signals, and (ii) these probes are not intrinsically cell membrane permeable. In recent decades, intracellular delivery approaches, such as laser-induced photoporation (Liu et al., 2020b), cell-squeezing permeabilization (DiTommaso et al., 2018; Klein et al., 2018), electroporation (Wilbie et al., 2019), lipid nanoparticles (Lim et al., 2017), and the phase-separating peptides (Sun et al., 2022), have been investigated to overcome this obstacle (Klein et al., 2018; Lino et al., 2018; Liu et al., 2020a). Several fluorescent dye-labeled nanobodies (de Beer and Giepmans, 2020), such as anti-fascin nanobodies (Liu et al., 2020b), have been developed and delivered to living cells to detect target antigens. In proof-of-concept experiments, these probes were capable of detecting highly expressed targets, albeit with low signal-to-background (S/B) ratios. However, their sensitivity for the detection of less abundant clinically relevant targets is compromised because of an intracellular excess of unbound or non-specific probes. This excess can reduce the S/B ratio and confound the identification of target proteins since the probes are always “On”.

The p53 tumor suppressor is a key transcription factor that is crucial in DNA repair, cell cycle arrest, and apoptosis under cellular stress (Kastan et al., 1991; Kuerbitz et al., 1992). Normally, p53 is maintained at low levels by mouse double minute 2 homolog (MDM2), an E3 ubiquitin-protein ligase that targets p53 for proteasomal degradation. Cellular stress signals result in p53 stabilization by post-translational modifications, such as

phosphorylation of Ser-20 (Chehab et al., 1999) and/or inhibition of the MDM2-p53 interaction (Chene, 2003). Overexpression of mutant and/or wild-type (WT) p53 is often detected in human cancers and has been used as an important biomarker for cancer diagnostics/therapeutics (Bykov et al., 2018; El-Deiry et al., 2006; Elghetany, 2000; Kobayashi et al., 2017; Wang et al., 2005). Several genetically encoded biosensors have been developed for imaging p53 (Amaral et al., 2013; Zhan et al., 2018). However, difficulties in controlling their *in situ* expression levels, and the need for *in situ* genetic manipulation limit many of their applications. Therefore, robust visualization of endogenous p53, both WT and mutant in living cells using an extrinsic probe would contribute to fundamental cell biology studies, clinical diagnosis, and cancer therapeutics.

I expect that Q-bodies delivered intracellularly by electroporation will reside in a default "Off" status unless triggered to the "On" status in the presence of p53 (Scheme 1-5) while the reduction of p53 levels should result in the Q-bodies being turned "Off". Nutlin-3a was used to improve p53 levels. Cisplatin, an anti-cancer drug, was employed to reduce p53 levels. The fluctuation of p53 levels under the treatment of nutlin-3a or cisplatin was confirmed by western blot assay. Then, to investigate whether the C11_Fab Q-body is able to visualize p53 and monitor the dynamics of p53 in living cells, the C11_Fab Q-body was transfected into live cells by electroporation. The fluorescent signal was observed using a confocal microscope.

5.2 Materials and methods

5.2.1 Materials

10 μL Neon Transfection System (Invitrogen, USA), cisplatin (sc-200896, Santa Cruz Biotechnology, USA). The other materials are the same with the previous chapter.

Other materials were the same as described above unless otherwise indicated.

5.2.2 Cell culture

The cultivation method for HCT116 $p53^{-/-}$, HCT116 $p53^{+/+}$, SK-BR-3, and WiDr cell lines were the same as described in Section 4.2.4.

5.2.3 Live-cell immunofluorescence imaging assay for intracellular target

For the live-cell imaging assay, a total of 2×10^5 cells were seeded into a ø60 × 15 mm tissue culture dish. Cells were cultured and treated with nutlin-3a as aforementioned (Section 4.2.5.2). The 10 μL Neon Transfection System was used to deliver 200 nM C11_Fab Q-body or 1 μM human p53 peptide-preactivated C11_Fab Q-body into live cells according to the company's protocol. Briefly, the cells were treated with 0.25% trypsin-EDTA. Subsequently, the cells were pelleted in a complete growth medium by centrifugation at 100 *g* for 5 min at RT and then resuspended in a 1 mL complete culture medium. The cells were then counted and aliquoted to $1–2 \times 10^5$ cells/tube. The aliquoted cells were washed once with PBS. For each transfection, cells were resuspended in 10 μL of Resuspension Buffer R with a final concentration of 200 nM C11_Fab Q-body. The electroporation setting for HCT116 and SK-

BR-3 is 1530 V, 20 ms, 1 pulse (Spiegel et al., 2019). That for WiDr is 1250 V, 20 ms, 2 pulses, which was recommended by Neon company. After electroporation, cells were gently transferred into a triple-well glass-based well containing a corresponding medium (w/ 10 % FBS, w/o phenol red and penicillin-streptomycin) which was prewarmed in an incubator and cultured for 4 h to recover cells. The cell nucleus was stained by 1 μg/mL Hoechst 33342 for 10 min before observation by a fluorescence microscope (Olympus IX71).

5.2.4 Time-lapse imaging assay for intracellular target

To evaluate whether the C11_Fab Q-body shows p53 level-dependent fluorescence changes and is stable for a longer period in living cells, time-lapse confocal microscopy imaging was performed. For this purpose, the HCT116 $p53^{+/+}$ cell line was employed in this experiment. Nutlin-3a was used to improve p53 levels, while cisplatin was added to reduce p53 levels. In this experiment, cells were separated into three groups, A1 (black), A2 (red), and A3 (blue). Cells in A1 and A2 groups were treated with 0 and 12 μM nutlin-3a during the whole imaging period, respectively, while the cells in the A3 group were firstly treated with 12 μM nutlin-3a for 16 h, then treated with 6 μM cisplatin for 9 h following twice washing. After electroporation, to wait for the cells' adhesion and recovery, they were incubated for 9 h. Then time-lapse imaging commenced. Cells in these three groups were treated as mentioned above during this imaging assay. To investigate the stability of Q-body in living cells, HCT116 $p53^{-/-}$ cells under the treatment of nutlin-3a were also time-lapsed imaged.

5.2.5 Western blot

The western blot assay was performed as described in Section 4.2.6. The differences in this experiment were cell treatment conditions and the primary and secondary antibodies. In this experiment, the cells were treated almost the same as described in Section 5.2.4. The cells were treated as indicated. HCT 116 $p53^{-/-}$ cells without treatment were used as a control to see the unspecific bands in western blot. The primary antibodies, anti-β-Actin mAb (M177-3, 6D1) (mouse) (1:2000), DO-1 IgG (mouse) (1:2000) and p53 monoclonal antibody (mouse) (60283-2Ig, 1:8000) were used. The secondary antibodies, HRP-conjugated goat anti-mouse IgG, (H+L) (31430, 1:5000) was used. Precision Protein™ StrepTactin-HRP (1:8000) was used to stain the protein marker.

5.3 Results and discussion

5.3.1 Visualization of p53 in living cells at nanomolar concentrations using C11_Fab Q-body

Currently, almost all the extrinsic antibody-based probes are always in an "On" state, which could result in a low S/B ratio in the visualization of intracellular targets. This is due to excess and/or non-specifically bound probes that generate fluorescence irrespective of target engagement. Furthermore, it is extremely difficult to remove these probes by washing, which is normally used to remove excess probes in IF staining assays because most probes are impermeable to the cell membrane. Having established that the C11_Fab Q-body

displays antigen-dependent signal turn-On in fixed cell imaging, we next evaluated its applicability to live-cell imaging.

Since Q-bodies are membrane-impermeable, electroporation was employed to intracellularly deliver Q-bodies. After electroporation, temporary pores will form on the cell membrane through which the Q-body can pass into the cytosol then diffuse into the nucleus. Electroporation is a physical delivery approach (Shi et al., 2018). It will not promote the formation of endocytosis which take in the delivered protein and degrade them. HCT116 (p53, WT or null), SK-BR-3 (p53, pR175H), and WiDr (p53, pR273H) cells were incubated for 3–4 h to recover after electroporation with 200 nM C11_Fab Q-body. The expected mechanism of this Q-body in living cells is shown in Figure 5-1a. Imaging under wash-free conditions showed that fluorescence signals colocalizing with nuclear staining (Hoechst) were only observed in p53-positive cell lines HCT116 $p53^{+/+}$, SK-BR-3, and WiDr. Conversely, negligible signals were observed in p53-negative (HCT116 $p53^{-/-}$) cells (Figure 5-1b). The mean F.I. of the nucleus in p53-positive cells was 8.4-fold higher than that in p53-negative cells (Figure 5-1c). Co-transfection of Q-body and p53 peptide into HCT116 $p53^{-/-}$ cells resulted in signals spread over whole cells (Figure 5-2). The result proved on-target engagement of peptides in $p53^{-/-}$ cells. However, the signal was spread out as the peptide does not localize to any particular region. Notably, traditional probes can give a similar phenotype in the absence of the target (i.e., false positive). These results indicate that Q-body shows antigen-dependent fluorescence enhancement in the complex intracellular environment of live cells.

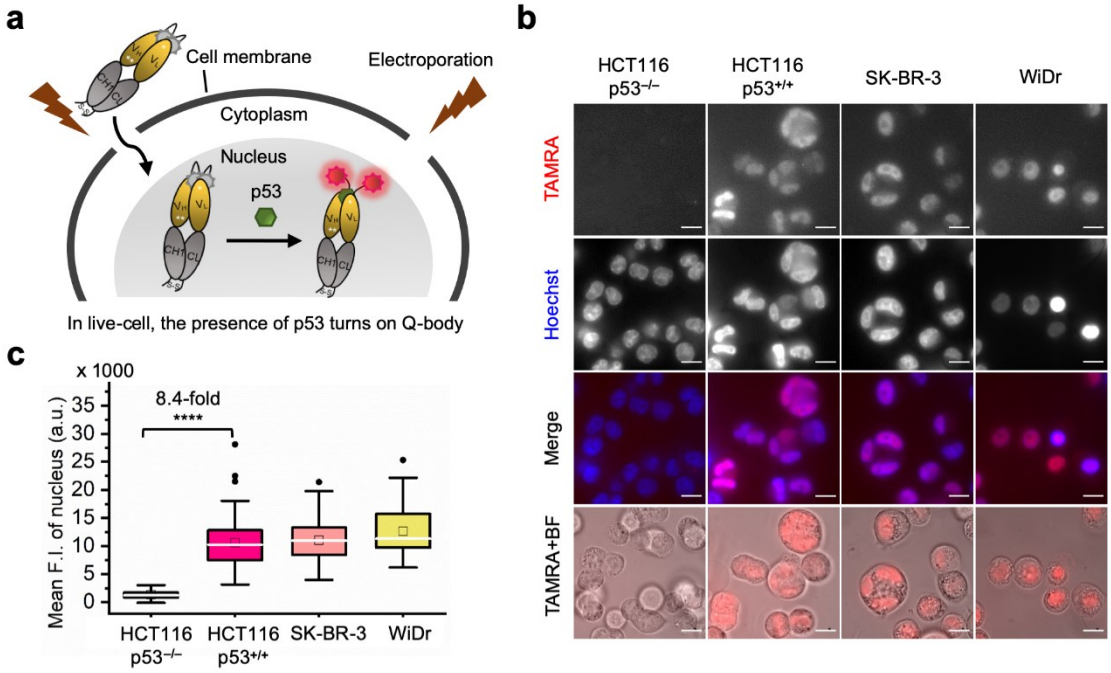

Figure 5-1. Wash-free imaging of intracellular p53 in live-cell using C11_Fab Q-body. Four kinds of cells, including HCT116 $p53^{+/+}$ (WT p53), HCT116 $p53^{-/-}$ (p53 null), SK-BR-3 [mutant p53 (pR175H)], and WiDr [mutant p53 (pR273H)] were employed. a) Scheme of Q-body in live-cell imaging assay. Following treated with 12 μM nutlin-3a for 16 h, cells were electroporated to drive Q-bodies (200 nM) into cells through transiently formed pores at the cell membrane. In p53 expressing cells, Q-body turns on. b) Representative images of live-cell imaging assay. HCT116 $p53^{-/-}$ cells were used as a negative control showing background signals of C11_Fab Q-body in live-cell. The other three cell lines were employed to understand the performance of antigen-dependent fluorescence enhancement of Q-body inside of live-cell. Microscope: Olympus IX71. Scale bar, 10 μm. c) Box plot of mean TAMRA intensities in the nucleus subtracted to minimum fluorescence intensities (F.I.) of TAMRA channel. The median F.I. was used to calculate their fluorescence changes between groups. Welch's *t*-test. ****p<0.0001; from left to right, n=106, 122, 77, 66 cells. For the box plot, the white line indicates the median, the box indicates 25–75% range, whiskers indicate 1.5 interquartile range, and the black dot indicates outliers.

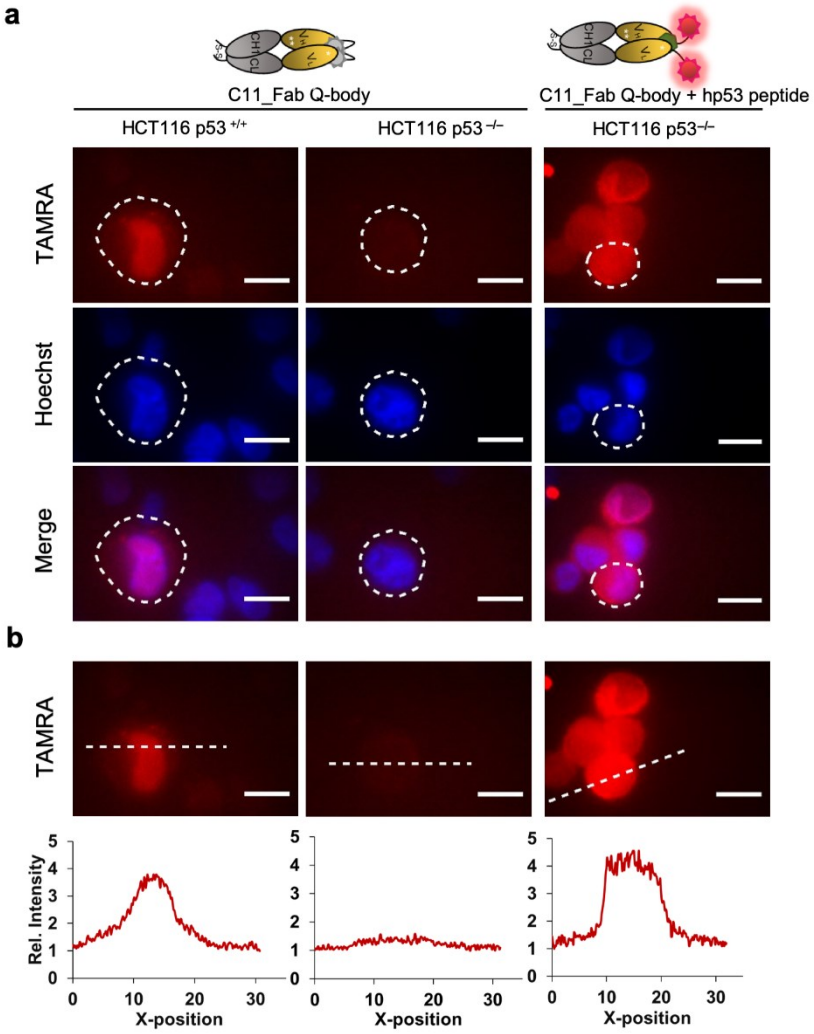

Figure 5-2. Wash-free imaging of p53 in live-cells using C11_Fab Q-body. HCT116 $p53^{+/+}$, a human colon cancer cell line, expresses wild-type p53. In HCT116 $p53^{-/-}$ cells, the p53 gene is knocked out. Cells were not treated with nutlin-3a. a) Representative images of C11_Fab Q-body-transfected live cells. HCT116 $p53^{+/+}$ cells were electroporated with 200 nM C11_Fab Q-body. HCT116 $p53^{-/-}$ were either electroporated with only 200 nM C11_Fab Q-body or with the same amount of Q-body plus 1 μM human p53 (hp53) peptide. The group of human p53 peptide-treated C11_Fab Q-body was performed as a control to see the efficiency of electroporation and the stability and specificity of the C11_Fab Q-body in live cells. The dotted line circles indicate the border of cells. Scale bar, 10 μm. b) The relative fluorescence intensity profiles along the dashed line of the corresponding group in (a). (b) was profiled by Fiji. Microscope: Olympus IX71.

5.3.2 Western blot

To evaluate whether the C11_Fab Q-body is stable for a longer period and shows p53 level-dependent fluorescence changes in living cells, the cells with different levels of p53 time-dependently were prepared. According to the previous results (Figures 4-2 and 4-4), nutlin-3a can improve p53 levels in HCT116 $p53^{+/+}$ cells. Therefore, nutlin-3a was used to

increase p53 levels in the first stage. After checking the references, cisplatin, a chemotherapy drug that has been used for the treatment of different types of cancers (Dasari and Tchounwou, 2014), was chosen as the candidate to reduce p53 levels or DO-1 epitope p53 because the results presented in a previous article (Hernandez-Valencia et al., 2018) showed that cisplatin treatment increased Ser20 phosphorylation of p53 (p53-pSer20) and decreased the DO-1 detectable p53 [Figure 3a in ref. (Hernandez-Valencia et al., 2018)]. I hypothesized that nutlin-3a treatment increases p53 level in HCT116 $p53^{+/+}$ cells in the first stage. While followed by the further treatment of cisplatin, p53 level and/or DO-1 epitope p53 (p53-pSer20) increase.

To verify this hypothesis, the western blot was performed. As shown in Figure 5-3, compared with the HCT116 $p53^{+/+}$ cells without treatment, the cells treated with nutlin-3a showed a higher level of p53. When the cells treated with nutlin-3a subsequently treated with cisplatin, the p53 level decreased dramatically (Lane 4, Figure 5-3a). The HCT116 $p53^{-/-}$ cells were used as a negative control (no corresponding band was observed). The results of western blot using two p53 antibodies (DO-1 and another p53 mAb) clearly showed that nutlin-3a increased p53 level and subsequent treatment with cisplatin reduced p53 level. I don't have direct evidence to prove the change of p53-pS20 protein level. But I postulated that signal decrease of p53 after cisplatin treatment is not result from Ser20 phosphorylation of p53 because another p53 mAb antibody showed the similar results (Figure 5-3b). From this point of view, these results were different as shown in the reference paper. The differences might be due to the difference in the cell line used (In the reference paper, MCF-7, a breast cancer cell line, was used. In this research, HCT116, a colon cancer cell line, was used) or the slight difference of treatment conditions (In the reference paper, the cells were only treated with cisplatin. In this paper, before the cisplatin treatment, the cells were treated with nutlin-3a) which might give rise to the p53 related signal pathways changed. Fortunately, with the further treatment of cisplatin in the nutlin-3a treated cells, the p53 proteins were surprisingly reduced. These results indicated that the cells that could show the fluctuation of p53 levels were successfully constructed.

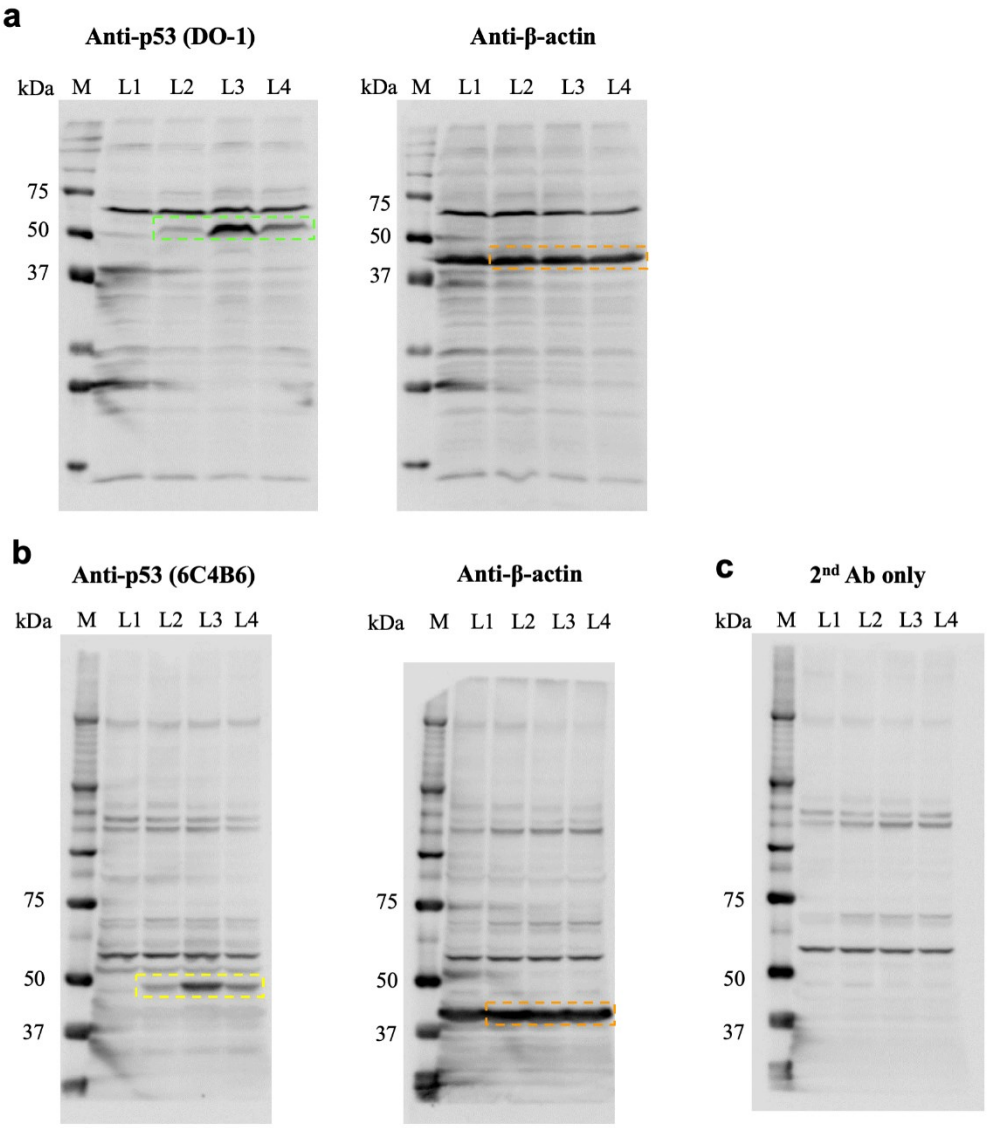

Figure 5-3. Western blot analysis of p53 levels under different treatment conditions using indicated antibodies. Different primary antibodies were used as indicated. Anti-β-actin antibody was used as a loading control. Equal amounts of total proteins were loaded for each lane. Lane 1 (L1): HCT116 $p53^{-/-}$ cells, without treatment; Lane 2 (L2): HCT116 $p53^{+/+}$ cells, without treatment; Lane 3 (L3): HCT116 $p53^{+/+}$ cells, nutlin-3a (12 μM, 16 hours) → wash twice with PBS → nutlin-3a (12 μM, 9 hours). Lane 4 (L4): HCT116 $p53^{+/+}$ cells, nutlin-3a (12 μM, 16 hours) → wash twice with PBS → cisplatin (6 μM, 9 hours). M: protein marker. In (a), 12.5% gel was used. In (b) and (c), 5–12% gradient gel was used. The red and blue boxes indicate p53 blots stained by DO-1 and 6C4B6, respectively. Orange box indicates β-actin (42 kDa) blots.

5.3.3 Visualization of p53 levels under different treatment conditions in fixed cells

After confirming the changes of p53 expression level under nutlin-3a and cisplatin treatment using the western blot, the fixed cell Q-body staining assay was performed to see if the same trend of p53 level can be observed using the C11_Fab Q-body. The cells were treated the same way as in the western blot assay. As shown in Figure 5-4, compared with non-treated cells, the fluorescent signal increased (7.7-fold) under the treatment of the nutlin-3a (16 h) → wash once with the fresh medium → PBS (6 μM, 12 h), while the signal decreased (0.24-fold) dramatically under the treatment of the nutlin-3a (16 h) → wash once with the fresh medium → cisplatin (6 μM, 12 h). These results indicate that cisplatin treatment reduces p53 levels, which is consistent with the western blot results.

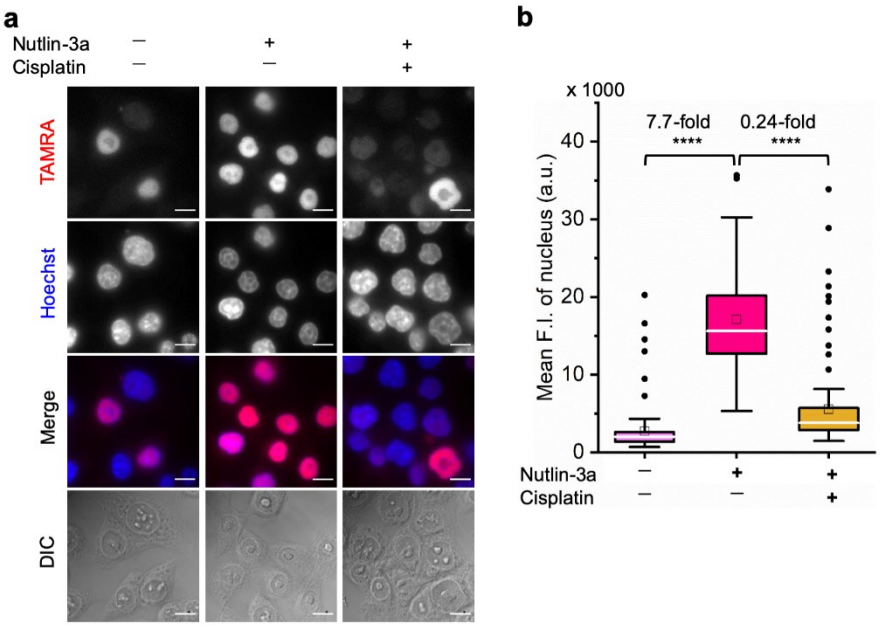

Figure 5-4. Visualization of p53 levels under different treatment conditions in fixed HCT116 $p53^{+/+}$ cells using C11_Fab Q-body. The cells were first treated with 12 μM nutlin-3a or 0.06% ethanol for 16 h after reaching 60% confluency. Then they have treated with 6 μM cisplatin (dissolved in PBS, 1 mg/mL) or vehicle for 12 h. a) Representative fluorescence microscopy images of C11_Fab Q-body staining assay. TAMRA channel, the signal from C11_Fab Q-body. Hoechst, nucleus stained with Hoechst 33342 (1 μg/mL). Merge, overlapped TAMRA channel with Hoechst channel. DIC, differential interference contrast channel. Microscope: Olympus IX71. Scale bar, 10 μm. b) Box plot of mean TAMRA intensities in the nucleus subtracted by minimum fluorescence intensities (F.I.) of TAMRA channel. The median F.I. was used to calculate their fluorescence changes between groups. Welch's *t*-test. ****p<0.0001; from left to right, n=88, 85, 104 cells. For the box plot, the white line indicates the median, the box indicates the 25–75% range, whiskers indicate the 1.5 interquartile range, and the black dot indicates outliers.

5.3.4 Visualization of p53 dynamics in living cells using C11_Fab Q-body

After constructing the cell system, time-lapse confocal microscopy was performed to observe the fluorescent signal changes under the treatment of different combinations of

nutlin-3a and cisplatin as indicated. The same as the western blot, to make HCT116 $p53^{+/+}$ cells with different levels of p53 time-dependently, the cells were treated with nutlin-3a first for 16 h to improve the p53 level followed by treatment with cisplatin for 9 h to reduce p53 level. I hypothesized that nutlin-3a will turn on the C11_Fab Q-body, while cisplatin treatment led to its turn off. In this experiment, after cells reached 70–80% confluency, the cells were electroporated with 200 nM C11_Fab Q-body. Then the transfected HCT116 $p53^{+/+}$ cells were incubated for approximately 9 h to allow cell recovery and attachment (Figure 5-5a). After that, time-lapse imaging commenced under different treatment conditions. As shown in Figures 5-5b and 5-5c, under the treatment of nutlin-3a, the fluorescence signals gradually increased and reached a plateau (2.6-fold) with a slight decrease upon 10 h treatment. The slightly decreased signal might be due to the reduction of DO-1 epitope of p53, and/or the degradation- or cell-division-derived Q-body decreases. When the medium was washed off and replaced with cisplatin after 16 h treatment with nutlin-3a, the signal reduced from 2.4-fold to 1.0-fold within 3 h and kept at low levels. In the non-treated, but electroporated cells, the fluorescent signal was high at the beginning while reduced time-dependently (Figure 5-5c), which might be because the electroporation increased the p53 level (Lepik et al., 2003). After time-dependent recovery, the p53 level gradually went back to normal. Therefore, the fluorescent signals decreased with time. Overall, these were consistent with the results of the corresponding fixed cell Q-body staining assay (Figure 4-2). In HCT116 $p53^{-/-}$ cells, the signals were almost unchanged and kept at a low level (Figure 5-6). These data indicate that the Q-body is stable enough for long-term live-cell imaging and enables visualization of p53 dynamics in live cells. These pilot studies demonstrate that Q-body technology can be utilized to localize intracellular POIs in viable cells, but also allows visualization of the dynamic changes in intracellular targets in living cells.

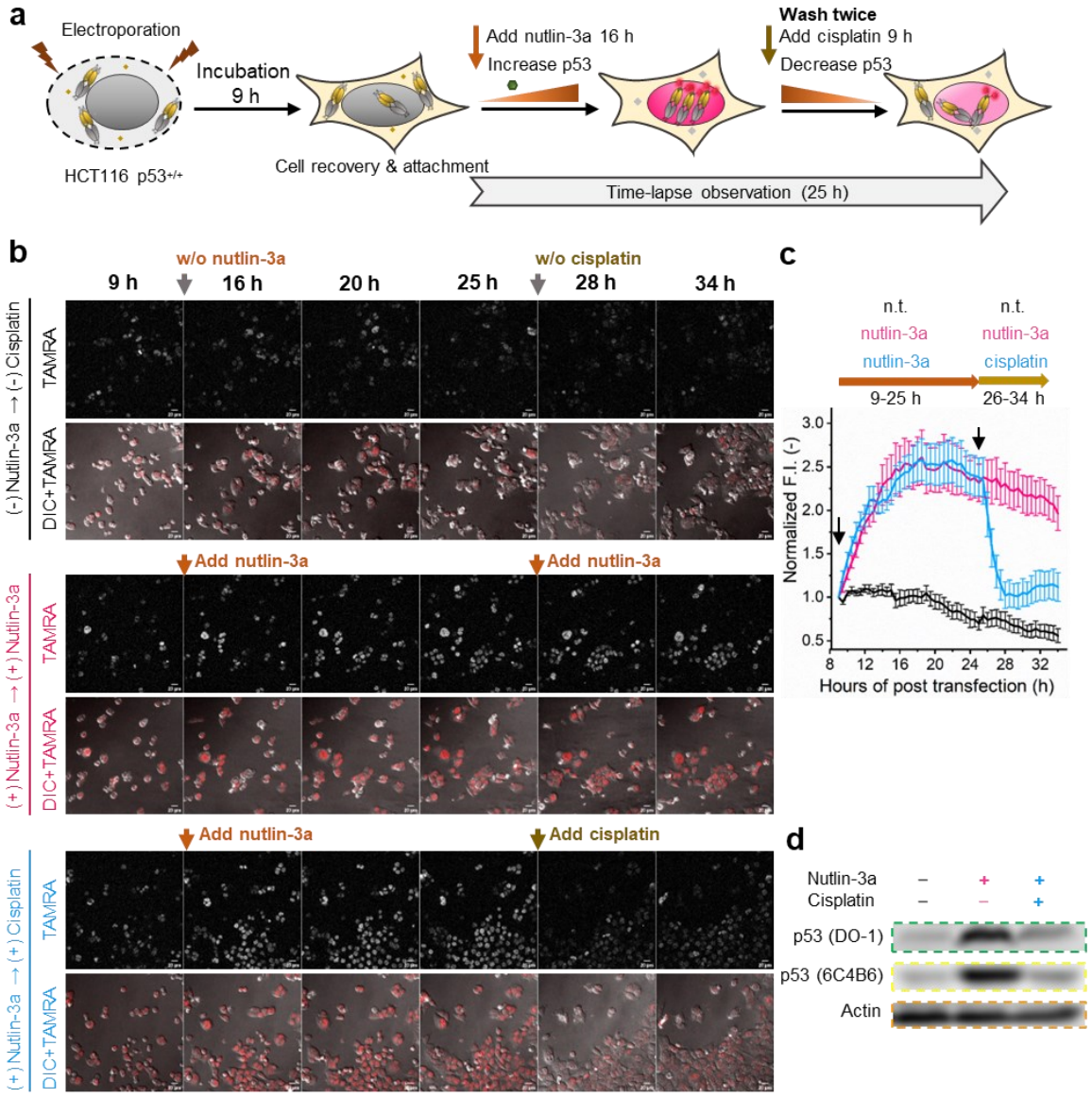

Figure 5-5. Time-lapse observation of p53 dynamics in HCT116 p53$^{+/+}$ using C11_Fab Q-body. a) Schematics of time-lapse imaging assay. The cells were incubated for 9 h to allow cell recovery and adherence following electroporation. After the addition of 12 μM nutlin-3a, time-lapsed observation commenced. After 16 h, the old medium containing nutlin-3a was removed and gently washed twice with the fresh medium, then treated with the fresh medium containing 12 μM nutlin-3a or 6 μM cisplatin. Cisplatin is an anti-cancer chemotherapy drug. b) Representative images of HCT116 p53$^{+/+}$ cells transfected with C11_Fab Q-body after being treated with nutlin-3a, cisplatin, or non-treated as indicated. Red color, TAMRA channel. DIC, differential interference contrast. Scale bar, 20 μm. c) Time-dependent TAMRA intensity changes in nuclei. Normalized F.I. of the nucleus, the mean fluorescence intensity (F.I.) of nucleus areas subtracted to that in the blank area, then normalized to the F.I. of the start point (9 h). Data are presented as the mean ± SEM of 18 cells. All images were acquired as Z-stacks and the most representative Z-stack images were presented and used for F.I. analysis. n.t., non-treated. d) Corresponding western blot results as indicated. Two monoclonal antibodies, DO-1 and 6C4B6, were sued for p53. Actin was

used as a loading control. Lane 1 sample was non-treated. Lane 2 sample was treated with nutlin-3a for 16 h, after washing, continuously treated with nutlin-3a for 9 h. Lane 3 sample was first treated with nutlin-3a for 16 h, after washing, subsequently treated with cisplatin for 9 h. Blots in (d) are derived from Figure 5-3.

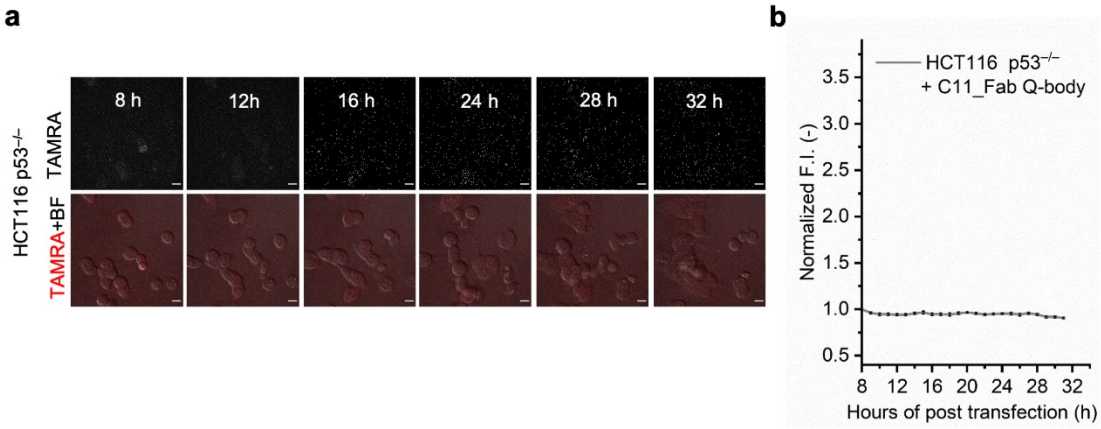

Figure 5-6. Time-lapsed observation of p53 in live-cells using C11_Fab Q-body. HCET116 $p53^{-/-}$ cells were constantly treated with nutlin-3a no matter before or after electroporation. a) Representative images in different time points. Scale bar, 10 μm. b) Time-dependent TAMRA intensity changes in nuclei. Normalized F.I. of nucleus, the mean F.I. of nucleus areas subtracted to that in the blank area, then normalized to the F.I. of the start point (8 h). Data are presented as the mean ± SEM of 8 cells.

5.4 Summary of Chapter 5

In this chapter, to evaluate the feasibility and applicability of the C11_Fab Q-body in the visualization of intracellular p53 in living cells in a wash-free manner, the live-cell imaging of p53 in different cell lines using this Fab Q-body was performed. The results showed that this Q-body only showed fluorescence enhancement in the cells with p53 (WT and mutant) expression. In p53 negative cells, almost no signal was observed. The mean fluorescence intensities in p53 positive cells (HCT116 $p53^{+/+}$) were 8.4-fold higher than that in p53 negative cells (HCT116 $p53^{-/-}$). Most importantly, the C11_Fab Q-body was proved to image the dynamics of p53 in a long period (over 34 h) in living cells. These pilot studies demonstrate that Q-body technology can be utilized to localize intracellular POIs in viable cells, but also allows visualization of the dynamic changes in intracellular targets in living cells.

5.5 References

Amaral, J.D., Herrera, F., Rodrigues, P.M., Dionisio, P.A., Outeiro, T.F., and Rodrigues, C.M. (2013). Live-cell imaging of p53 interactions using a novel Venus-based bimolecular fluorescence complementation system. Biochem Pharmacol *85*, 745-752.

Anson, F., Kanjilal, P., Thayumanavan, S., and Hardy, J.A. (2021). Tracking exogenous intracellular casp-3 using split GFP. Protein Science *30*, 366-380.

Bykov, V.J.N., Eriksson, S.E., Bianchi, J., and Wiman, K.G. (2018). Targeting mutant p53 for efficient cancer therapy. Nat Rev Cancer *18*, 89-102.

Chehab, N.H., Malikzay, A., Stavridi, E.S., and Halazonetis, T.D. (1999). Phosphorylation of Ser-20 mediates stabilization of human p53 in response to DNA damage. Proc Natl Acad Sci U S A *96*, 13777-13782.

Chene, P. (2003). Inhibiting the p53-MDM2 interaction: an important target for cancer therapy. Nat Rev Cancer *3*, 102-109.

Dasari, S., and Tchounwou, P.B. (2014). Cisplatin in cancer therapy: molecular mechanisms of action. Eur J Pharmacol *740*, 364-378.

de Beer, M.A., and Giepmans, B.N.G. (2020). Nanobody-Based Probes for Subcellular Protein Identification and Visualization. Front Cell Neurosci *14*, 573278.

DiTommaso, T., Cole, J.M., Cassereau, L., Bugge, J.A., Hanson, J.L.S., Bridgen, D.T., Stokes, B.D., Loughhead, S.M., Beutel, B.A., Gilbert, J.B.*, et al.* (2018). Cell engineering with microfluidic squeezing preserves functionality of primary immune cells in vivo. Proc Natl Acad Sci U S A *115*, E10907-E10914.

El-Deiry, W.S., Sigman, C.C., and Kelloff, G.J. (2006). Imaging and oncologic drug development. J Clin Oncol *24*, 3261-3273.

Elghetany, M.T. (2000). P53 overexpression in bone marrow biopsies in refractory anemia and aplastic anemia: impact of antibody selection. Leuk Res *24*, 975-977.

Hernandez-Valencia, J., Garcia-Villa, E., Arenas-Hernandez, A., Garcia-Mena, J., Diaz-Chavez, J., and Gariglio, P. (2018). Induction of p53 Phosphorylation at Serine 20 by Resveratrol Is Required to Activate p53 Target Genes, Restoring Apoptosis in MCF-7 Cells Resistant to Cisplatin. Nutrients *10*.

Kastan, M.B., Onyekwere, O., Sidransky, D., Vogelstein, B., and Craig, R.W. (1991). Participation of p53 protein in the cellular response to DNA damage. Cancer Res *51*, 6304-6311.

Keppler, A., Gendreizig, S., Gronemeyer, T., Pick, H., Vogel, H., and Johnsson, K. (2003). A general method for the covalent labeling of fusion proteins with small molecules in vivo. Nat Biotechnol *21*, 86-89.

Klein, A., Hank, S., Raulf, A., Joest, E.F., Tissen, F., Heilemann, M., Wieneke, R., and Tampé, R. (2018). Live-cell labeling of endogenous proteins with nanometer precision by transduced nanobodies. Chem Sci *9*, 7835-7842.

Kobayashi, K., Tomita, H., Shimizu, M., Tanaka, T., Suzui, N., Miyazaki, T., and Hara, A. (2017). p53 Expression as a Diagnostic Biomarker in Ulcerative Colitis-Associated Cancer. Int J Mol Sci *18*, 1284.

Kuerbitz, S.J., Plunkett, B.S., Walsh, W.V., and Kastan, M.B. (1992). Wild-type p53 is a cell cycle checkpoint determinant following irradiation. Proc Natl Acad Sci USA *89*, 7491-7495.

Lepik, D., Jaks, V., Kadaja, L., Varv, S., and Maimets, T. (2003). Electroporation and carrier DNA cause p53 activation, cell cycle arrest, and apoptosis. Analytical Biochemistry *318*, 52-59.

Lim, S.I., Lukianov, C.I., and Champion, J.A. (2017). Self-assembled protein nanocarrier for intracellular delivery of antibody. J Control Release *249*, 1-10.

Lino, C.A., Harper, J.C., Carney, J.P., and Timlin, J.A. (2018). Delivering CRISPR: a review of the challenges and approaches. Drug Deliv *25*, 1234-1257.

Liu, J., Fraire, J.C., De Smedt, S.C., Xiong, R., and Braeckmans, K. (2020a). Intracellular Labeling with Extrinsic Probes: Delivery Strategies and Applications. Small *16*, e2000146.

Liu, J., Hebbrecht, T., Brans, T., Parthoens, E., Lippens, S., Li, C.N., De Keersmaecker, H., De Vos, W.H., De Smedt, S.C., Boukherroub, R.*, et al.* (2020b). Long-term live-cell microscopy with labeled nanobodies delivered by laser-induced photoporation. Nano Research *13*, 485-495.

Los, G.V., Encell, L.P., McDougall, M.G., Hartzell, D.D., Karassina, N., Zimprich, C., Wood, M.G., Learish, R., Ohana, R.F., Urh, M.*, et al.* (2008). HaloTag: a novel protein labeling technology for cell imaging and protein analysis. ACS Chem Biol *3*, 373-382.

Sheng, W., Nick, S.T., Santos, E.M., Ding, X., Zhang, J., Vasileiou, C., Geiger, J.H., and Borhan, B. (2018). A Near-Infrared Photoswitchable Protein-Fluorophore Tag for No-Wash Live Cell Imaging. Angew Chem Int Ed Engl *57*, 16083-16087.

Shi, J., Ma, Y., Zhu, J., Chen, Y., Sun, Y., Yao, Y., Yang, Z., and Xie, J. (2018). A Review on Electroporation-Based Intracellular Delivery. Molecules *23*.

Spiegel, A., Bachmann, M., Jurado Jiménez, G., and Sarov, M. (2019). CRISPR/Cas9-based knockout pipeline for reverse genetics in mammalian cell culture. Methods *164-165*, 49-58.

Sun, Y., Lau, S.Y., Lim, Z.W., Chang, S.C., Ghadessy, F., Partridge, A., and Miserez, A. (2022). Phase-separating peptides for direct cytosolic delivery and redox-activated release of macromolecular therapeutics. Nat Chem *14*, 274-283.

Wang, Y.C., Lin, R.K., Tan, Y.H., Chen, J.T., Chen, C.Y., and Wang, Y.C. (2005). Wild-type p53 overexpression and its correlation with MDM2 and p14ARF alterations: an alternative pathway to non-small-cell lung cancer. J Clin Oncol *23*, 154-164.

Werther, P., Yserentant, K., Braun, F., Grussmayer, K., Navikas, V., Yu, M., Zhang, Z., Ziegler, M.J., Mayer, C., Gralak, A.J.*, et al.* (2021). Bio-orthogonal Red and Far-Red Fluorogenic Probes for Wash-Free Live-Cell and Super-resolution Microscopy. ACS Cent Sci *7*, 1561-1571.

Wilbie, D., Walther, J., and Mastrobattista, E. (2019). Delivery Aspects of CRISPR/Cas for in Vivo Genome Editing. Acc Chem Res *52*, 1555-1564.

Zhan, H.J., Xie, H.B., Zhou, Q., Liu, Y.C., and Huang, W.R. (2018). Synthesizing a Genetic Sensor Based on CRISPR-Cas9 for Specifically Killing p53-Deficient Cancer Cells. Acs Synth Biol *7*, 1798-1807.

Chapter 6. Intracellular antigen-specific live-cell sorting using C11_Fab Q-body

6.1 Introduction

Cell-based therapy plays an important role in the treatment of many diseases (Buzhor et al., 2014), such as Parkinson's disease, autoimmune diseases, and type 1 diabetes. Isolation of high-fidelity antigen-specific cells for cell therapy is crucial for the improvement of treatment performance. Fluorescence-activated cell sorting (FACS) is considered a valuable tool that can be used to sort antigen-specific live cells. However, the isolation of live cells using this approach is only suitable for cell-surface marker-based sorting. For intracellular biomarker-specific cell sorting, there remains limited for two reasons: (i) biosensors for the intracellular POIs are always in a fluorescence "On" state, and (ii) these biosensors are not intrinsically cell membrane permeable. The second obstacle, due to the rapid development of the intracellular delivery approaches in recent decades, such as laser-induced photoporation (Liu et al., 2020), cell-squeezing permeabilization (Kollmannsperger et al., 2016; Sharei et al., 2013), electroporation (Stolwijk and Wegener, 2020; Yamashita et al., 2020), lipid nanoparticle (Dobrowolski et al., 2022; Sanchez et al., 2022; Woo et al., 2022), and phase-separating peptides (Sun et al., 2022), the delivery problem has been gradually overcome. Several fluorescent dye-labeled nanobodies (de Beer and Giepmans, 2020), such as anti-fascin nanobodies (Liu et al., 2020), have been developed and delivered to living cells to detect target antigens. In proof-of-concept experiments, these probes were capable of detecting highly expressed targets, albeit with low S/B ratios. However, their sensitivity for the detection of less abundant clinically relevant targets is compromised because of an intracellular excess of unbound or non-specific probes. This excess can reduce the S/B ratio and confound the identification of target proteins since the probes are always "On" and hard to be removed. As described in the previous chapter, it has been proved that the C11_Fab Q-body shows antigen-dependent fluorescent enhancement in living cells.

In this chapter, to further investigate if the Q-body shows enough fluorescence intensity difference between the cells with and without the target POI and if this difference is high enough to be distinguished by flow cytometry, I performed a proof-of-concept experiment using HCT116 $p53^{-/-}$ and $p53^{+/+}$ as model cells and C11_Fab Q-body as an intracellular biosensor.

6.2 Materials and methods

6.2.1 Materials

Sorting chip-100 μm (Sony, Tokyo, Japan). The other materials are the same with the previous chapter.

Other materials were the same as described above unless otherwise indicated.

6.2.2 Cell culture

The cultivation method for HCT116 $p53^{-/-}$ and HCT116 $p53^{+/+}$ were same as described in the Section 4.2.4.

6.2.3 Flow cytometry analysis and FACS

To investigate the feasibility and applicability of applying Q-body technology in intracellular antigen-specific live-cell sorting, HCT116 $p53^{+/+}$, HCT116 $p53^{-/-}$ cells, and the p53 C11_Fab Q-body were employed to perform a model study. Nutlin-3a-treated HCT116 $p53^{+/+}$ and $p53^{-/-}$ cells were transfected with 200 nM C11_Fab Q-body by electroporation, respectively. As shown in Scheme 6-1, HCT116 $p53^{+/+}$ cells electroporated with Q-body, HCT116 $p53^{-/-}$ cells electroporated with Q-body, and HCT116 $p53^{+/+}$ cells electroporated without Q-body were prepared, respectively. Firstly, flow cytometry analysis was performed to evaluate the fluorescence intensities of each group and determine the sorting gate for FACS. The cell sorting model study was performed by mixing the cells from "$p53^{+/+}$ + C11_Fab Q-body" and "$p53^{-/-}$ + C11_Fab Q-body" groups at a 1:10 ratio according to the cell counter. The collected cells after sorting were incubated for 1 h to recover. Then, the cell mixtures before and after sorting were observed by a confocal microscope. The number of $p53^{+/+}$ cells was counted and the ratio of HCT116 $p53^{+/+}$ cells transfected with C11_Fab Q-body (showing fluorescence in the cell nucleus) was calculated to evaluate the enrichment efficiency of cell sorting. All samples were analyzed and sorted with flow cytometry (SH800, Sony, Tokyo, Japan) using a 100 μm chip. To detect the TAMRA signal, a 561 nm laser was used for excitation, and the 617/30 nm filter (FL3) was used to detect the emission signals. The data were analyzed using the SH800 control software (Sony).

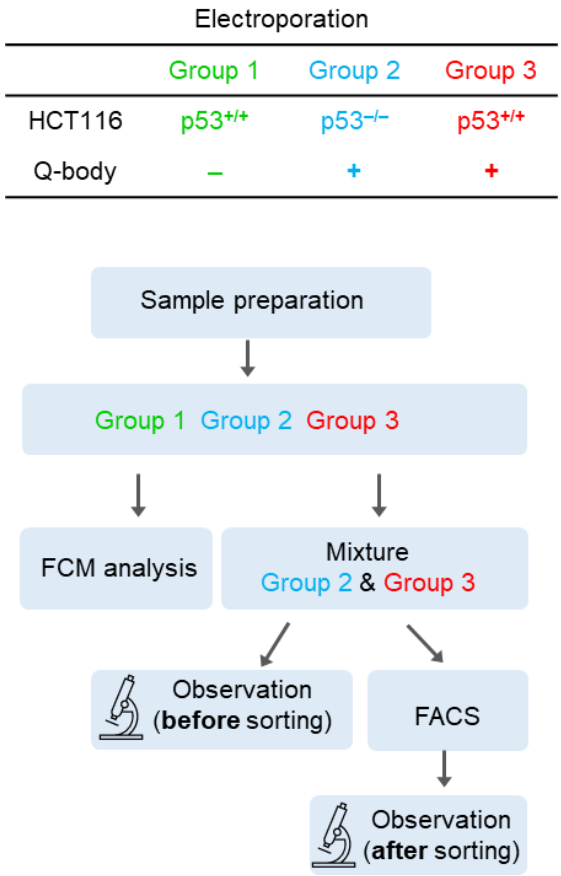

Scheme 6-1. Preparation of live-cell sorting samples and flow chart for live-cell sorting assay. FCM: flow cytometry.

6.2.4 Microscope setting and image analysis

Images were acquired by a confocal microscope [a Ti-E (Nikon; operated by NIS-elements software) with a spinning disk (CSU-W1; Yokogawa Electric, Tokyo, Japan), Plan Apo VC 100× Oil DIC N2 (NA 1.4) lens, and an EM-CCD camera (iXON3 DU888 X-8465, Andor)] with a 555 nm laser setting as 50%, exposure time 500 ms. Fiji software was used to quantify the fluorescence intensity of the nucleus.

6.3 Results and discussion

6.3.1 Performance of C11_Fab Q-body in intracellular antigen-specific live-cell sorting

To investigate the feasibility of applying this technology to intracellular antigen-specific live-cell sorting, a proof-of-concept experiment was performed. Three cell groups, including HCT116 $p53^{+/+}$ cells transfected with or without C11_Fab Q-body, and HCT116 $p53^{-/-}$ cells transfected with C11_Fab Q-body, were used for flow cytometric analysis to evaluate the cell distributions of each group. As shown in Figure 6-1 a, a clear F.I. increment in Q-body-transfected HCT116 $p53^{+/+}$ cells was observed in comparison with the other two groups. Next, a mixture of the positive ($p53^{+/+}$ + C11_Fab Q-body) and negative ($p53^{-/-}$ + C11_Fab Q-body) cells at a 10% proportion (this value was determined as 6.9% by microscope) was used for live-cell sorting. After sorting, the ratio of HCT116 $p53^{+/+}$ cells transfected with the Fab Q-body increased to 94% (Figure 6-1 b), which corresponds to approximately 14-fold (from 6.9% to 94%) enrichment of $p53^{+/+}$ cells. Additionally, the F.I. changes before and after sorting showed a significant increase (4.6-fold) (Figure 6-1 c). Taken together, these results indicate that the application of Q-body technology in intracellular antigen-specific live-cell sorting is possible.

Fulfillment of intracellular antigen-specific live-cell sorting is valuable for improving cell therapies. However, to the best of my knowledge, current approaches used to isolate intracellular antigen-specific live cells are not available. For instance, the isolation of regulatory T cells (Tregs), which are crucial in the treatment of human diseases that include graft-versus-host disease and autoimmune disease (Jeffery et al., 2016) is based on cell surface markers. Although it is clear that Foxp3 (an intracellular protein) is the best and most specific marker of Tregs, people still use cell surface markers (such as CD25, CD4, and CD127) for Treg isolation (Shen et al., 2009; Yu et al., 2012) because current technologies are not able to isolate viable Tregs using Foxp3 directly. In this study, we provide the first demonstration that intracellular antigen-specific live-cell sorting using Q-body technology is possible.

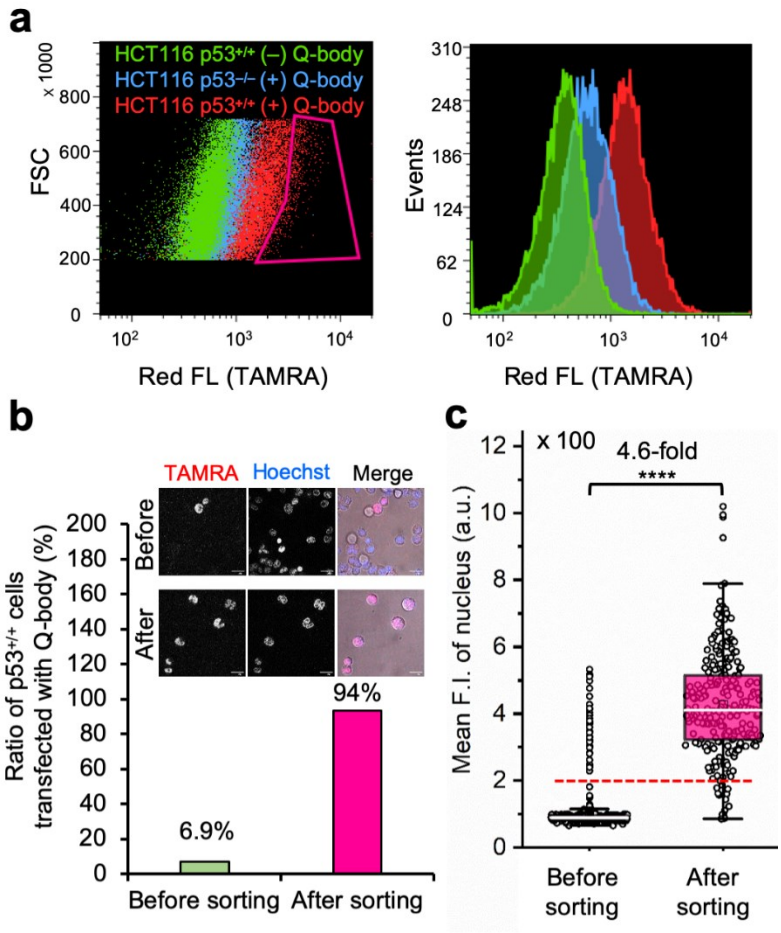

Figure 6-1. Intracellular antigen-specific live-cell sorting using C11_Fab Q-body. a) Flow cytometry analysis of HCT116 $p53^{+/+}$ cells transfected with (red) or without (green) Q-body and HCT116 $p53^{-/-}$ cells with (blue) Q-body. Left figure: density plot (Red box indicates the sorting gate); right figure: histogram plot. b) The ratio of HCT116 $p53^{+/+}$ cells transfected with C11_Fab Q-body before and after sorting. Their ratio was determined based on the mean F.I. of cell nuclei from their fluorescence images. The cells with mean F.I. below the red dotted line in (c) were counted as negative cells. Representative photos before and after sorting are presented. Merge, TAMRA (red) + Hoechst (blue) + Bright field (gray). Scale bar, 20 μm. c) Box plot of mean TAMRA intensities in nuclei subtracted to that in the blank areas (before sorting, n= 535; after sorting, n=246). The median F.I. was used to calculate their fluorescence changes between groups. Welch's t-test. ****p<0.0001. For the box plot, the white line indicates the median, the box indicates 25–75% range, whiskers indicate 1.5 interquartile range, and circles indicate data distributions.

6.4 Summary of Chapter 6

In this chapter, to verify whether the Q-body technology is able to sort live cells based on a specific intracellular POI, a proof-of-concept experiment was performed using the C11_Fab Q-body. In this experiment, the C11_Fab Q-body was transfected into the HCT116

$p53^{-/-}$ and HCT116 $p53^{+/+}$ cells. Then flow cytometry was employed to isolate the p53-positive cells from a mixture of $p53^{-/-}$ and $p53^{+/+}$ cells based on the fluorescence intensity. The results showed that the ratio of $p53^{+/+}$ cells containing Q-bodies enriched 14-fold from 6.9% (before sorting) to 94% (after sorting), indicating that the application of Q-body technology in intracellular antigen-specific live-cell sorting is possible.

6.5 References

Buzhor, E., Leshansky, L., Blumenthal, J., Barash, H., Warshawsky, D., Mazor, Y., and Shtrichman, R. (2014). Cell-based therapy approaches: the hope for incurable diseases. Regenerative Medicine *9*, 649-672.

de Beer, M.A., and Giepmans, B.N.G. (2020). Nanobody-Based Probes for Subcellular Protein Identification and Visualization. Front Cell Neurosci *14*, 573278.

Dobrowolski, C., Paunovska, K., Echeverri, E.S., Loughrey, D., Sanchez, A.J.D., Ni, H.Z., Hatit, M.Z.C., Lokugamage, M.P., Kuzminich, Y., Peck, H.E.*, et al.* (2022). Nanoparticle single-cell multiomic readouts reveal that cell heterogeneity influences lipid nanoparticle-mediated messenger RNA delivery. Nature Nanotechnology.

Jeffery, H.C., Braitch, M.K., Brown, S., and Oo, Y.H. (2016). Clinical Potential of Regulatory T Cell Therapy in Liver Diseases: An Overview and Current Perspectives. Frontiers in Immunology *7*.

Kollmannsperger, A., Sharei, A., Raulf, A., Heilemann, M., Langer, R., Jensen, K.F., Wieneke, R., and Tampe, R. (2016). Live-cell protein labelling with nanometre precision by cell squeezing. Nat Commun *7*, 10372.

Liu, J., Hebbrecht, T., Brans, T., Parthoens, E., Lippens, S., Li, C.N., De Keersmaecker, H., De Vos, W.H., De Smedt, S.C., Boukherroub, R.*, et al.* (2020). Long-term live-cell microscopy with labeled nanobodies delivered by laser-induced photoporation. Nano Research *13*, 485-495.

Sanchez, A.J.D., Dobrowolski, C., Cristian, A., Echeverri, E.S., Zhao, K., Hatit, M.Z.C., Loughrey, D., Paunovska, K., and Dahlman, J.E. (2022). Universal Barcoding Predicts In Vivo ApoE-Independent Lipid Nanoparticle Delivery. Nano Letters *22*, 4822-4830.

Sharei, A., Cho, N., Mao, S., Jackson, E., Poceviciute, R., Adamo, A., Zoldan, J., Langer, R., and Jensen, K.F. (2013). Cell squeezing as a robust, microfluidic intracellular delivery platform. J Vis Exp, e50980.

Shen, L.S., Wang, J., Shen, D.F., Yuan, X.L., Dong, P., Li, M.X., Xue, J., Zhang, F.M., Ge, H.L., and Xu, D. (2009). CD4(+)CD25(+)CD127(low/-) regulatory T cells express Foxp3 and suppress effector T cell proliferation and contribute to gastric cancers progression. Clin Immunol *131*, 109-118.

Stolwijk, J.A., and Wegener, J. (2020). Impedance analysis of adherent cells after in situ electroporation-mediated delivery of bioactive proteins, DNA and nanoparticles in mu L-volumes. Scientific Reports *10*.

Sun, Y., Lau, S.Y., Lim, Z.W., Chang, S.C., Ghadessy, F., Partridge, A., and Miserez, A. (2022). Phase-separating peptides for direct cytosolic delivery and redox-activated release of macromolecular therapeutics. Nat Chem *14*, 274-283.

Woo, C.J., Allawzi, A., Clark, N., Kaushal, N., Efthymiou, T., Thamsen, M., Nguyen, J., Wooster, R., and Sullivan, J.C. (2022). Inhaled delivery of a lipid nanoparticle encapsulated messenger RNA encoding a ciliary protein for the treatment of primary ciliary dyskinesia. Pulmonary Pharmacology & Therapeutics *75*.

Yamashita, S., Kogasaka, Y., Hiradate, Y., Tanemura, K., and Sendai, Y. (2020). Suppression of mosaic mutation by co-delivery of CRISPR associated protein 9 and three-prime repair exonuclease 2 into porcine zygotes via electroporation. Journal of Reproduction and Development *66*, 41-48.

Yu, N., Li, X., Song, W., Li, D., Yu, D., Zeng, X., Li, M., Leng, X., and Li, X. (2012). CD4(+)CD25 (+)CD127 (low/-) T cells: a more specific Treg population in human peripheral blood. Inflammation *35*, 1773-1780.

Chapter 7. Summary and discussion

7.1 Summary of this work

Although intracellular biomarkers can be imaged with fluorescent dye(s)-labeled antibodies, the use of such probes for the precise imaging of intracellular biomarkers in living cells remains challenging due to background noise from unbound probes. The Quenchbody (Q-body) is a newly developed fluorescent immunosensor with the potential to solve this issue. It is a site-specific fluorescent dye(s)-labeled antibody fragment that exhibits antigen-dependent fluorescence signal enhancement (Abe et al., 2014; Abe et al., 2011; Dong et al., 2020b; Inoue et al., 2020). Unlike conventional antibody probes, Q-bodies have the advantage of antigen-dependent signal generation. In this study, to investigate the applicability and feasibility of using Q-body technology in the imaging and dynamics monitoring of intracellular protein of interests (POIs) in living cells and intracellular antigen-specific live-cell sorting, the development of a conditionally active Fab-type Q-body probe derived from a monoclonal antibody (DO-1) (Cohen et al., 1998; Stephen et al., 1995) with the ability to both targets and spatiotemporally visualize intracellular p53 in living cells with low background signal as described.

In Chapter 2, a mutant (C11) of WT_scFv DO-1 with improved secretory productivity was selected by constructing a consensus mutagenesis library and phage display bio-panning. The C11_scFv mutant showed an approximately 7-fold increment of signal in the monoclonal-secreted antibody ELISA assay. To understand the effect of mutation site introduction on the Q-body activity (e.g., LOD, maximum response, and EC_{50}), single-labeled WT_scFv and C11_scFv Q-bodies were prepared. The C11_scFv showed an increased sensitivity (LOD = 0.028 nM) in comparison to WT_scFv Q-body. Their EC_{50} and maximum response were not changed too much. A Q-body (C11_Fab -body) with a maximum response of 27-fold and LOD of 0.78 nM against only human p53 peptide was obtained by labeling the C11_Fab with two TAMRA dyes. And it was verified that the dye labeling showed minimal perturbation to the antigen-binding affinity. Besides the quenching mechanism of the dyes in the C11_Fab Q-body was investigated and suggested that both Trp residues and H-dimer formations contribute to the fluorescent quenching in this Q-body. And the F/P ratio and quantum yield of self-quenched and activated forms of Q-bodies were investigated. The results indicated that C11_Fab was efficiently labeled with TAMRA and the C11_Fab Q-body showed antigen-dependent quantum yield that was consistent with its fluorescence intensity changes.

In Chapter 3, after obtaining a high-performance Q-body, the one-step immunofluorescence assay was performed to investigate the ability to use the C11_Fab Q-body in the visualization of p53 in fixed cells, a representative of traditional immunoprobe C11_scFv-TAMRA was used as a control. The results showed that the C11_Fab Q-body displays an antigen-dependent signal on fixed human cancer cells that either harbor WT p53 or mutant p53 and shows a higher S/B ratio than the traditional IF probe. Besides, this Q-body showed no fluorescent enhancement in mouse cells, indicating that the C11_Fab Q-body specifically recognizes human p53.

In Chapter 4, after confirming that the C11_Fab Q-body displays antigen-dependent

signal turn-on in fixed cell image, next, its applicability to live-cell imaging was evaluated. The ability of visualization of both WT and mutant p53 in living cells was evaluated followed by delivery of the C11_Fab Q-body into the cytosol using electroporation. It showed fluorescence enhancement in the p53 expression cells irrespective of mutation types of p53 in comparison to p53-negative cells, indicating that Q-body shows antigen-dependent fluorescence enhancement in the complex intracellular environment of live cells.

In Chapter 5, the intracellular live-cell imaging assay was performed to further evaluate the stability and performance of the C11_Fab Q-body visualizing the p53 dynamics under the treatment of nutlin-3a (increase p53) and cisplatin (decrease p53). The fluorescent signals fluctuated p53 levels dependently. While in p53-negative cells, the signals were almost unchanged and kept at a low level. These data indicate that the Q-body is stable enough for long-term live-cell imaging and enables visualization of p53 dynamics in live cells. These pilot studies demonstrate that Q-body technology can be utilized to localize intracellular POIs in viable cells, but also allows visualization of the dynamic changes in intracellular targets in living cells.

In Chapter 6, to finally investigate the feasibility of applying this technology to intracellular antigen-specific live-cell sorting, a proof-of-concept experiment was performed using fluorescence-activated cell sorting. The ratio of p53-positive cells was enriched from 6.9% (before sorting) to 94% (after sorting) indicating that the application of Q-body technology in intracellular antigen-specific live-cell sorting is possible.

Taken together, this study provides the first evidence of the feasibility and applicability of Q-body probes for the live-cell imaging of intrinsically intracellular proteins and opens a novel avenue for research and diagnostic applications on intracellular target-based live-cell sorting.

7.2 General discussion

Previously, people changed the incubation time and incubation condition (e.g., pH, temperature, reducibility) during phage bio-panning to screen the proteins with certain characteristics, such as pH resistance, thermal stability, or stability in reducing environment (Amin et al., 2004; Brockmann, 2012; Brockmann et al., 2005). In this study, to obtain enough protein (DO-1) using the *E. coli* system for preparing Q-body, I constructed a combinatorial consensus mutagenesis phagemid library, then performed phage display to screen the mutant with improved secretory productivity. I successfully obtained a variant (C11) with improved expression ability in *E. coli*. To the best of my knowledge, no one using the secreted-antibody ELSIA to screen variants with improved secretory productivity. I developed a new strategy to improve the productivity of antibodies in *E. coli* expression system using phage display. This strategy can also be applied to any other antibodies to improve productivity.

I have improved the antigen-dependent response of the p53 Q-body by changing the single dye-labeling to double dyes-labeling. The double-labeled C11_Fab Q-body (27-fold) showed around 14-fold higher response than the single-labeled C11_scFv Q-body (2.0-fold).

And by detecting the absorbance spectra of the self-quenched and p53-activated forms of C11_Fab Q-bodies and the free TAMRA dye, it has been proved that the H-dimer formation of TAMRA in the C11_Fab Q-body is the main reason for this increase. Although the H-dimer formation in the Fab Q-bodies has been estimated as one of the main quenching mechanisms in previous publications (Abe et al., 2014; Dong et al., 2018; Dong and Ueda, 2021), here I first provided the direct evidence.

Previously, to make Q-body, the antibody fragments can be synthesized and simultaneously labeled with fluorophore-conjugated amino acids using cell-free protein synthesis (Abe et al., 2011; Jeong et al., 2013), or recombinantly expressed by *E. coli* (Jeong et al., 2016) followed by dye-labeling through the thiol-maleimide reaction (Jeong et al., 2016), transamination reaction (Dong et al., 2016) or coiled-coil hetero-assembly (Yasuda et al., 2021). The most cost-effective way to make Q-body is through thiol-maleimide reaction (Cys-tag) and coiled-coil hetero-assembly. However, according to the experience of making Q-body, the formed covalent bond by thiol-maleimide reaction is not stable, especially after a long time of storage. Even though the K_D value of the E4/K4 coiled-coil peptides was estimated as several pM (Gröger et al., 2017; Litowski and Hodges, 2002) and showed robust ability in making Q-body (Yasuda et al., 2021), the stability of coiled-coil Q-body in the intracellular environment is still needed investigation. To ensure the stability of the Q-body in a complex intracellular environment, I used a transpeptidase, sortase A, which has shown robust capability *in vivo* labeling (Wu et al., 2017). Therefore, in this study, I am the first to use this transpeptidase to prepare Q-body. The labeling ratio for C11_Fab Q-body was calculated as 190%–218%, indicating the high labeling efficiency of sortase A. Besides, the stability of the C11_Fab Q-body in an intracellular environment was evaluated in living HCT116 cells.

Although the Q-body technology has been widely used to develop biosensors for various antigens, most of their applications are in the detection of targets in solutions (Abe et al., 2014; Abe et al., 2011; Inoue et al., 2020; Jeong et al., 2018; Jeong et al., 2013; Li et al., 2021) and/or cell-surface markers (Dong et al., 2020b; Jeong et al., 2017). Here, it was the first time to apply the Q-body technology in the imaging of the intracellular antigens and provided the first evidence that the Q-body is stable enough in the highly reductive intracellular environment. Most importantly, it has been confirmed that the C11_Fab Q-body could monitor the dynamics of p53 in live cells. To the best of my knowledge, the Q-body technology might be the first antibody-based extrinsic probe that can use to visualize the dynamic changes of intracellular POIs in the native environment.

Of note, DO-1 has multiple abilities due to the specific location of its epitope and binding specificity. The epitope of DO-1 is a linear peptide (^{20}SDLWKL^{25}) (Stephen et al., 1995) which is located in the transactivation domain of human p53 and is a conserved region. Therefore, this clone can both recognize WT and mutant p53. Besides, it has been reported that DO-1 does not bind to p53 with phosphorylation at Ser-20 (p53-pS20) (Chehab et al., 1999). Thus, DO-1 may be used to detect phosphorylation of p53-pS20. In this study, the C11_Fab Q-body showed specifically visualize WT and mutant p53 protein in both fixed

and living human cells in a wash-free manner with the S/B ratio of approximately 8.3-fold in fixed cells and 8.4-fold in living cells (Figures 4-2, 4-3, and 5-1). Besides, this Q-body can use to monitor the dynamics of p53. As p53 expression levels are closely related to cancer progression (Bouchet et al., 2006; Machado-Silva et al., 2010; Wistuba et al., 1996), the above performance of this Q-body may not only allow it to be used for the detection of p53 levels in patient samples to diagnosis p53 aggregation-related human cancers but also make it available for the fundamental studies of biological processes (e.g., p53 related signal pathway illustrations) as well as for the anti-cancer drug screening in the live-cell level.

Last but not least, as a proof-of-concept study, I have verified that the C11_Fab Q-body can show difference F.I. in the cells with (HCT116 $p53^{+/+}$) or without p53 (HCT116 $p53^{-/-}$). And this difference can be distinguished by Flow cytometry. Most importantly, these two types of cells can be sorted by FACS and exhibited a 14-fold (from 6.9% to 94%) enrichment ratio. Theoretically, the ratio of $p53^{+/+}$ cells was 10%, but when calculating based on the microscope images, this value was determined as 6.9%. One possible reason is the electroporation damaged cells. During FACS, the deeply damaged cells were sorted out as waste (dead cells). When analyzing the images, the dead cells were not counted. Moreover, the viability of the sorted cells was not detected yet. Nevertheless, this research showed the feasibility and applicability of using the Q-body technology to isolate the intracellular antigen-specific live cells by FACS. In the future, to reduce the damage derived from delivery, I plan to introduce a new delivery technology, called phase-separating peptides (Sun et al., 2022). These peptides showed a robust ability to directly deliver molecules (e.g., small peptides, mRNAs, and enzymes) into the cytosol that bypasses endocytosis and showed no damage to the plasma membrane.

7.3 Limitations of the Q-body technology in intracellular POI imaging

In this study, it was verified that the Q-body response is reversible in the inside living cells which means the presence of antigen can turn on the fluorescence of the Q-body and vice versa. But for the visualization of intracellular targets, this technology is closely dependent on the delivery technology due to its cell-membrane impermeability. Besides, not all antibody fragments (e.g., scFvs or Fabs) are stable enough in the reducing intracellular environment. It is necessary to identify the intracellular stability of the antibody before constructing the corresponding Q-body. Although developing a Q-body is not as hard as constructing a flashbody, it also needs a period of time from several months to years. Luckily, a pre-screening technology (termed PM Q-probe) for the estimation of Q-body response was developed and has been successfully applied to screen antibodies with a high potential to be a good Q-body (Dong et al., 2020a).

Compared with genetically encoded probes, the Q-body technology may not be able to visualize the target located inside some organelles, such as mitochondria, endoplasmic reticulum, and Golgi apparatus. Because even though the Q-body is successfully delivered into the cytosol, it is hard to go through the membrane of these organelles. But for the target in the cytosol, the out membrane of the organelles, or the nucleus, the Q-body technology has its superiorities. Besides, the Q-body technology may be difficult to be applied in vivo

studies because it is difficult to pass through the extracellular matrix for Q-body to localize the intracellular targets.

7.4 Concluding remarks

1) A mutant (C11) of scFv DO-1 with improved secretion productivity in the *E. coli* expression system has been selected.

2) C11_Fab Q-body that shows high response and specificity to human p53 was successfully developed.

3) C11 Fab Q-body could visualize p53 in both fixed and live cells with high S/B ratios without washing.

4) C11 Fab Q-body visualized p53 dynamics in live cells.

5) C11 Fab Q-body enabled live-cell sorting based on p53 expression.

6) This study provided the first demonstration of intracellular antigen-specific live-cell sorting using Q-body technology

7.5 References

Abe, R., Jeong, H.J., Arakawa, D., Dong, J., Ohashi, H., Kaigome, R., Saiki, F., Yamane, K., Takagi, H., and Ueda, H. (2014). Ultra Q-bodies: quench-based antibody probes that utilize dye-dye interactions with enhanced antigen-dependent fluorescence. Sci Rep *4*, 4640.

Abe, R., Ohashi, H., Iijima, I., Ihara, M., Takagi, H., Hohsaka, T., and Ueda, H. (2011). "Quenchbodies": Quench-Based Antibody Probes That Show Antigen-Dependent Fluorescence. Journal of the American Chemical Society *133*, 17386-17394.

Amin, N., Liu, A.D., Ramer, S., Aehle, W., Meijer, D., Metin, M., Wong, S., Gualfetti, P., and Schellenberger, V. (2004). Construction of stabilized proteins by combinatorial consensus mutagenesis. Protein Eng Des Sel *17*, 787-793.

Bouchet, B.P., de Fromentel, C.C., Puisieux, A., and Galmarini, C.M. (2006). p53 as a target for anti-cancer drug development. Critical Reviews in Oncology Hematology *58*, 190-207.

Brockmann, E.C. (2012). Selection of stable scFv antibodies by phage display. Methods Mol Biol *907*, 123-144.

Brockmann, E.C., Cooper, M., Strömsten, N., Vehniäinen, M., and Saviranta, P. (2005). Selecting for antibody scFv fragments with improved stability using phage display with denaturation under reducing conditions. J Immunol Methods *296*, 159-170.

Chehab, N.H., Malikzay, A., Stavridi, E.S., and Halazonetis, T.D. (1999). Phosphorylation of Ser-20 mediates stabilization of human p53 in response to DNA damage. Proc Natl Acad Sci U S A *96*, 13777-13782.

Cohen, P.A., Mani, J.C., and Lane, D.P. (1998). Characterization of a new intrabody directed against the N-terminal region of human p53. Oncogene *17*, 2445-2456.

Dong, J., Fujita, R., Zako, T., and Ueda, H. (2018). Construction of Quenchbodies to detect and image amyloid beta oligomers. Anal Biochem *550*, 61-67.

Dong, J., Jeong, H.J., and Ueda, H. (2016). Preparation of Quenchbodies by protein transamination reaction. J Biosci Bioeng *122*, 125-130.

Dong, J., Miyake, C., Yasuda, T., Oyama, H., Morita, I., Tsukahara, T., Takahashi, M., Jeong, H.J., Kitaguchi, T., Kobayashi, N.*, et al.* (2020a). PM Q-probe: A fluorescent binding protein that converts many antibodies to a fluorescent biosensor. Biosens Bioelectron *165*, 112425.

Dong, J., Oka, Y., Jeong, H.J., Ohmuro-Matsuyama, Y., and Ueda, H. (2020b). Detection and destruction of HER2-positive cancer cells by Ultra Quenchbody-siRNA complex. Biotechnol Bioeng *117*, 1259-1269.

Dong, J., and Ueda, H. (2021). Recent Advances in Quenchbody, a Fluorescent Immunosensor. Sensors (Basel) *21*.

Gröger, K., Gavins, G., and Seitz, O. (2017). Strand Displacement in Coiled-Coil Structures: Controlled Induction and Reversal of Proximity. Angew Chem Int Ed Engl *56*, 14217-14221.

Inoue, A., Ohmuro-Matsuyama, Y., Kitaguchi, T., and Ueda, H. (2020). Creation of a Nanobody-Based Fluorescent Immunosensor Mini Q-body for Rapid Signal-On Detection of Small Hapten Methotrexate. ACS Sens *5*, 3457-3464.

Jeong, H.-J., Kojima, T., Dong, J., Ohashi, H., and Ueda, H. (2016). One-pot construction of Quenchbodies using antibody-binding proteins. Analytical Methods *8*, 7774-7779.

Jeong, H.J., Dong, J., and Ueda, H. (2018). Single-Step Detection of the Influenza Virus Hemagglutinin Using Bacterially-Produced Quenchbodies. Sensors (Basel) *19*.

Jeong, H.J., Kawamura, T., Iida, M., Kawahigashi, Y., Takigawa, M., Ohmuro-Matsuyama, Y., Chung, C.I., Dong, J., Kondoh, M., and Ueda, H. (2017). Development of a Quenchbody for the Detection and Imaging of the Cancer-Related Tight-Junction-Associated Membrane Protein Claudin. Anal Chem *89*, 10783-10789.

Jeong, H.J., Ohmuro-Matsuyama, Y., Ohashi, H., Ohsawa, F., Tatsu, Y., Inagaki, M., and Ueda, H. (2013). Detection of vimentin serine phosphorylation by multicolor Quenchbodies. Biosens Bioelectron *40*, 17-23.

Li, H., Li, X., Chen, L., Li, B., Dong, H., Liu, H., Yang, X., Ueda, H., and Dong, J. (2021). Quench-Release-Based Fluorescent Immunosensor for the Rapid Detection of Tumor Necrosis Factor alpha. ACS Omega *6*, 31009-31016.

Litowski, J.R., and Hodges, R.S. (2002). Designing heterodimeric two-stranded alpha-helical coiled-coils. Effects of hydrophobicity and alpha-helical propensity on protein folding, stability, and specificity. J Biol Chem *277*, 37272-37279.

Machado-Silva, A., Perrier, S., and Bourdon, J.C. (2010). p53 family members in cancer diagnosis and treatment. Seminars in Cancer Biology *20*, 57-62.

Stephen, C.W., Helminen, P., and Lane, D.P. (1995). Characterization of Epitopes on Human P53 Using Phage-Displayed Peptide Libraries - Insights into Antibody Peptide Interactions. Journal of Molecular Biology *248*, 58-78.

Sun, Y., Lau, S.Y., Lim, Z.W., Chang, S.C., Ghadessy, F., Partridge, A., and Miserez, A. (2022). Phase-separating peptides for direct cytosolic delivery and redox-activated release of macromolecular therapeutics. Nat Chem *14*, 274-283.

Wistuba, II, Gazdar, A.F., Roa, I., and Albores-Saavedra, J. (1996). p53 protein overexpression in gallbladder carcinoma and its precursor lesions: an immunohistochemical study. Hum Pathol *27*, 360-365.

Wu, Q., Ploegh, H.L., and Truttmann, M.C. (2017). Hepta-Mutant Staphylococcus aureus Sortase A (SrtA(7m)) as a Tool for in Vivo Protein Labeling in Caenorhabditis elegans. ACS Chem Biol *12*, 664-673.

Yasuda, T., Inoue, A., Kitaguchi, T., and Ueda, H. (2021). Rapid construction of fluorescence quenching-based immunosensor Q-bodies using alpha-helical coiled-coil peptides. Chem Commun (Camb) *57*, 8206-8209.

Publications and Presentations

Publication

Yancen Dai, Yuko Sato, Bo Zhu, Hiroshi Kimura, Tetsuya Kitaguchi, Farid. J. Ghadessy, Hiroshi Ueda, "Intra Q-body: an antibody-based fluorogenic probe for intracellular proteins that allows live cell imaging and sorting". *Chemical Science*, **2022**, DOI: 10.1039/d2sc02355e**.**

International conference

1) **Poster presentation: Yancen Dai**, Yuko Sato, Bo Zhu, Hiroshi Kimura, Tetsuya Kitaguchi, Farid. J. Ghadessy, Hiroshi Ueda, Intra Q-body: an antibody-based fluorogenic probe for intracellular proteins that allows live-cell imaging and sorting. Gordon Research Conference on Bioanalytical Sensors, Salve Regina University, RI, USA, Jun. 2022

2) **Poster presentation:** Bo Zhu, Haimei Li, **Yancen Da**i, Akihito Inoue, Yinghui Yang, Kaori Kobayashi, Tetsuya Kitaguchi, Jinhua Dong, Hiroshi Ueda. Rapid construction of homogeneous immunosensors for SARS-CoV-2 nucleocapsid and spike proteins using Quenchbody and Quenchprobe technology, Gordon Research Conference on Bioanalytical Sensors, Salve Regina University, RI, USA, Jun. 2022.

Domestic conference

1) **Oral presentation** (査読有)
Yancen Dai, Bo Zhu, Yuko Sato, Hiroshi Kimura, Farid J. Ghadessy, Tetsuya Kitaguchi, Hiroshi Ueda. Development of an immunofluorescence probe Q-body for the direct visualization of tumor marker p53 in fixed and living cells., The SCEJ 87th Annual Meeting, I219, online, Mar. 2022.

2) **Poster presentation** (査読有)
Yanmin Chen, **Yancen Dai**, Tetsuya Kitaguchi, Hiroshi Ueda, Development of a multicolor Q-body construction method using Escherichia coli., The SCEJ 87th Annual Meeting, PA157, online, Mar. 2022.

3) **Oral presentation** (査読無)
Yancen Dai, Atsushi Izutani, Takanobu Yasuda, Tetsuya Kitaguchi, Hiroshi Ueda. Intracellular detection of tumor suppressor protein p53 by Q-body technology, The SBJ 73rd Annual Meeting, online, G3H4-0311, Oct. 2021.

4) **Poster presentation** (査読有)
Yancen Dai, Atsushi Izutani, Takanobu Yasuda, Tetsuya Kitaguchi, Hiroshi Ueda. Instant detection of tumor suppressor protein p53 by Q-body technology., The SCEJ 86th Annual Meeting, online, PB208, Mar. 2021.

Acknowledgement

First of all, I would like to express my deepest appreciation to my supervisor, Prof. Hiroshi Ueda, for his supportive and invaluable suggestions on my academic studies. Words cannot express my gratitude to him for accepting me as his Ph.D. student. It is my great pleasure to do research under his supervision.

I am also extremely grateful to Assoc. Prof. Tetsuya Kitaguchi, Asst. Prof. Bo Zhu, and Asst. Prof. Takanobu Yasuda for their instructive discussions and guidance.

I also would like to express my special thanks to Prof. Hiroshi Kimura and Asst. Prof. Yuko in the Kimura-Lab of Tokyo Institute of Technology, and Dr. Farid J. Ghadessy in Disease Intervention Technology Laboratory, A*STAR, Singapore, kindly provided experiment platform and materials as well as gave a lot of instructive suggestions for this research.

Special thanks to all the lab members (including Dr. Jiulong Su, Dr. Xuerao Ning, Ryotai Arisaka, Masaki Takahashi, Hiroshi Aihara, Fujimori Takeru, Junqian Wang, Haoxuan Tang, Junetae Park, Ippei Tsujimura, Kaoori Kobayashi, Rinka Tsubaki, Yoshihiro Ito, Akihito Inoue, Kana Sasamoto, Cheng Qian, Yusuke Suchi, Zhirou Qiu, Kaito Iijima, Keisuke Yamashita, Rianto Sato, Tomoko Tsutsumi, Sohei Hiasa, Yanmin Chen, Yinghui Yang, Li Tian, Yoshimitsu Ono, Sae Kazumi, Haruki Kurata, Natsuki Shibukawa, Mai Honjo, Ayumu Ninomiya, Shintaro Mitani, Shuxin Zhao) for their help during daily life and study. They make my laboratory life full of happiness. I will remember all the heart-touching moments forever

Thanks to Junki Kashida for his help to measure the absolute quantum yield.

I acknowledge the “Cross the border! Tokyo Tech pioneering doctoral research program” by JST SPRING, Japan, the “IIR Research Fellow” under the Institute of Innovative Research, Tokyo Institute of Technology, Japan, and the Tsubame Scholarship for Doctoral Students, Tokyo Institute of Technology, Japan, for their financial support during my Ph.D. study.

Finally, I am deeply grateful to my parents for their unselfish love and support, my brother, my sister-in-law, and my aunts who enlighten me with their positive and optimistic attitude toward life whenever I encounter difficulties.

August 2022

Yancen DAI